Title
Discrete Elastic Rods for Simulating Soft Robot Limbs

Author
Novelia, Alyssa

Publication Date
2018

Peer reviewed|Thesis/dissertation

Discrete Elastic Rods for Simulating Soft Robot Limbs

by

Alyssa Novelia

A dissertation submitted in partial satisfaction of the

requirements for the degree of

Doctor of Philosophy

in

Engineering - Mechanical Engineering

in the

Graduate Division

of the

University of California, Berkeley

Committee in charge:

Professor Oliver M. O'Reilly, Chair
Professor James Casey
Professor Per-Olof Persson

Fall 2018

Discrete Elastic Rods for Simulating Soft Robot Limbs

Abstract

Discrete Elastic Rods for Simulating Soft Robot Limbs

by

Alyssa Novelia

Doctor of Philosophy in Engineering - Mechanical Engineering

University of California, Berkeley

Professor Oliver M. O'Reilly, Chair

Discrete elastic rods (DER) is a recent formulation of a rod theory by Bergou et al. The material curve of the rod is approximated by a discrete set of lines connected at vertices. The formulation originated in the field of computer graphics and uses concepts from the nascent field of discrete differential geometry to characterize bending energies and torsional strains. Specifically, the discrete curvature vector associated with a vertex is used as a measure of bending strain and the length of the edges are used to account for stretching. Additionally, each edge is associated with a reference frame and a material frame, where the angle difference of the latter frame between adjacent edges is a measure of twist. Space- and time- parallel transport operators are introduced to update these frames in space and time respectively, so the torsion of the rod can be efficiently computed.

While DER is an elegant formulation, it is challenging to comprehend. In this dissertation, complete derivations for the expressions for the variations, gradients, and Hessians of kinematic variables induced by changes to the vertices are presented. These gradients are needed to numerically solve the governing equations of motion. The method by which a component of the rotation of the cross section is computed in the discrete elastic rod formulation is exceptional and exploits a phenomenon in differential geometry known as a holonomy. Relevant background from differential geometry and spherical geometry are presented to understand how the reference twist in the rod can be related to a solid angle enclosed by the trace of a unit tangent vector on a sphere and several examples are presented to illuminate the calculation of twist.

The second part of the dissertation is devoted to using the DER formulation to examine the dynamics of soft robots. To this end, a planar formulation of DER (PDER) is derived. Our work allows the governing equations of a discrete rod to be expressed in a canonical using Lagrange's equations. This in turn allows us to use PDER with folded and branched elastic structures which feature in the designs of soft robots. To illustrate our developments, PDER is used to formulate and analyze the equations of motion needed to simulate the locomotion of a caterpillar-inspired soft robot on a rough surface.

Contents

Acknowledgments

First of all I would like to thank Professor Oliver O'Reilly, who I first encountered in my undergraduate course on dynamics at University of California, Berkeley. It was through his lessons and nurturing that I began to become fascinated with the dynamics of mechanical systems, to the point that I took more advanced classes in the series of dynamics courses and further honed my interest in the graduate program. Oliver has helped me tremendously to grow from a curious child to a (hopefully) mature researcher, and thanks to his patience, support, and guidance I could carry on the tasks that were bestowed upon me.

My dissertation is devoted to utilizing the Discrete Elastic Rods (DER) framework pioneered by Miklos Bergou while he was in Eitan Grinspun's Columbia University computer graphics group in the 2000s. I would like to sincerely thank Basile Audoly and Etienne Vouga who were also involved in formulating this framework for their support and guidance as I dove in deeper in their work. Special thanks to M. Khalid Jawed being a very patient coauthor and for helping me to get accustomed to the DER code and for transcribing it to MATLAB.

My thanks to Dr. Samuel Stanton from Army Research Office for facilitating this collaborative project between Berkeley, University of Maryland, and Carnegie Mellon University. I would like to thank Professors Carmel Majidi and Derek Paley for their leadership in their respective fields of manufacturing and controlling the soft robots. I would also like to thank Sean (Xiaonan) Huang for fabricating the SMA actuator samples and Will Scott for his work on control of the state space formulations.

Many, many thanks to Dr. Christopher Daily-Diamond for the early work in modeling the actuator using elastica theory and for his support during difficult times. I would also like to thank fellow graduate students Evan Hemingway and Nathaniel Goldberg for their careful proof reading of my work and for working on the motion capture experiments.

I would not be able to make it this far without the wonderful friendships that began in Berkeley and which continue to keep me afloat until this day - Selina Pan, Alexandra Daily-Diamond, Andreas Hansen, Eugen Solowjow, Robert Luan, Ben Yee, Dennis Wai, Jared Porter, and Chris Meissen.

My most heartfelt thanks towards both the faculties and staff of the Department of Mechanical Engineering at Berkeley. I would like to thank Professor James Casey for sparking my interest in differential geometry, and also to Shareena Samson and Donna Craig for their sincere interest in the graduate students' well beings and for arranging generous financial supports. I am proud to be supported by the department by being a graduate student instructor in my first three years and, in addition to ARO grant number W911NF-16-1-0242, partially support by the block grants awards from the graduate division and the J. K. Zee fellowship during my final two years in Berkeley.

Finally, I would like to thank my sister Jennifer for always being my comrade and my parents for providing the best education one could ever ask for and for their continual hard work and persistence.

Chapter 1

Introduction

In contrast to their conventional rigid counterparts, soft machines and robots are composed of deformable bodies capable of extreme changes in shape and functionality [28, 32]. Despite their potential advantages, the deformability of soft bio-inspired robots yields an infinite degree-of-freedom system that is significantly more difficult to model and control than a discrete system (e.g. piecewise rigid). Up to this point, the design of soft machines have been done by "morphological computation" [49, 52] where the forgiving nature of mechanical and elastic properties of the soft bodies are taken advantage of to simplify the control algorithm to perform specific tasks and to negate the margins of error in computations. However we believe that progress in the nascent field of soft robotics depends on the ability to rapidly and faithfully model the dynamical state of a soft robot and incorporate this model into a feedback control for real time path planning and locomotion just like its rigid counterparts. The difficulty in achieving that goal is obviously due to the lack of tools in the field of continuum mechanics to look into dynamic deformations that are computationally simple and robust enough to tackle a class of problems.

A subclass of continuum mechanics is the theory of rods. Rod theory is a good starting point in modeling a variety of problems in engineering because of its simplicity and generality. By restricting the geometry of the body to be slender and to have a length much greater than its width and height, the equations of motion of the centerline and other lengthwise properties depending on the extent of the model may be found by a set of balance laws. In a seminal work published in 1859, Gustav Kirchhoff (1824-1887) proposed a rod theory capable of modeling bending and torsion and his treatment was refined by the Cosserat brothers Eugéne (1866-1931) and François (1852-1914) by introducing orthogonal frames along the length of the rod known as directors. Consequently, rod theory is also considered as an example of a Cosserat rod theory. Kirchhoff's rod theory is arguably the most popular three-dimensional rod theory in use and has been the subject of a large number of works since the mid-1950s. This rod theory is also used in computer graphics to model strands of hair [4, 48, 63] and in engineering to develop soft robots [62].

A formulation of a Kirchoff rod theory which exploits recent developments in discrete differential geometry was developed by Bergou et al. [3, 4]. In their formulation, the rod

is modeled as a collection of points (vertices or nodes) connected by stretchable edges. Associated with each edge are a pair of directors (or material vectors) and either a Bishop frame or a reference frame. Later works by Jawed et al. [23, 24] found excellent agreement between the numerical results produced by the formulation and experiments on slender rod-like bodies. The formulation is a novel, computationally efficient, discretized version of the celebrated Kirchhoff rod theory. In a historical context, the formulation is arguably among the most significant additions to the literature since the numerical formulation of Kirchhoff's rod theory by Simo and Vu-Quoc [56] in 1988 and the introduction of Cosserat rod theories to the computer graphics community by Pai [48] in 2002. The discrete elastic rod formulation is computationally cheap and, as a result, is used in computer graphics to render images of hairs and trees and is the technical underpinning behind the *Bristle Brush* feature in Adobe Illustrator and Adobe Photoshop.

Bergou et al.'s discrete elastic rod (DER) formulation uses ideas from the nascent field of discrete differential geometry and concepts such as holonomy from classic differential geometry. As a result, understanding the DER formulation can be very challenging and is addressed in the core of this dissertation. We discuss a discretized space curve and three frames that can be associated with it. Next, derivations of gradients and variations for various kinematical quantities that have appeared in the literature are discussed. One unusual feature of the DER formulation is the use of holonomy to help determine the twist of the rod. We devote an entire chapter to discussing results from differential geometry of spherical triangles and spherical quadrilaterals that are used to determine the twist of the rod. The next chapter synthesizes the kinematical results and shows how they are used to formulate a set of ordinary differential equations for the position vectors of the nodes of the rod and the twisting of the edges, and the equations of the rods in a state space form for the planar case. The final chapter comprises the result of simulating a soft robot using the DER framework and comparison with a testbed built by the Soft Machines Laboratory at Carnegie Mellon University.

1.1 Remarks on Vector and Tensor Notation

In the present paper, a tensor notation for the rotation is employed following [46]. All vectors in Euclidean three-space $\mathbb{E}^3$ are denoted by bold-faced letters. A tensor can be considered as a linear operator which transforms a vector in $\mathbb{E}^3$ to another vector in $\mathbb{E}^3$. For example, $\mathbf{a}\otimes\mathbf{b}$ transforms $\mathbf{c}$ to the vector $(\mathbf{b}\cdot\mathbf{c})\mathbf{a}$: $(\mathbf{a}\otimes\mathbf{b})\mathbf{c} = (\mathbf{b}\cdot\mathbf{c})\mathbf{a}$. The Euclidean norm of a vector $\mathbf{a}$ is denoted by $\|\mathbf{a}\| = \sqrt{(\mathbf{a}\cdot\mathbf{a})}$.

Chapter 2

The Kinematics of Discretized Curves

2.1 Introduction

In the discrete elastic rod formulation of Kirchhoff's rod theory, the material curve $\mathcal{L}$ is discretized into a set of $n-1$ segments (cf. Figure 2.1). The edges of the segments are defined by a pair of vertices. We use the widely adopted notational convention that quantities associated with a vertex are labelled with a subscript and those associated with an edge are labelled with a superscript (cf. [2, 3]).

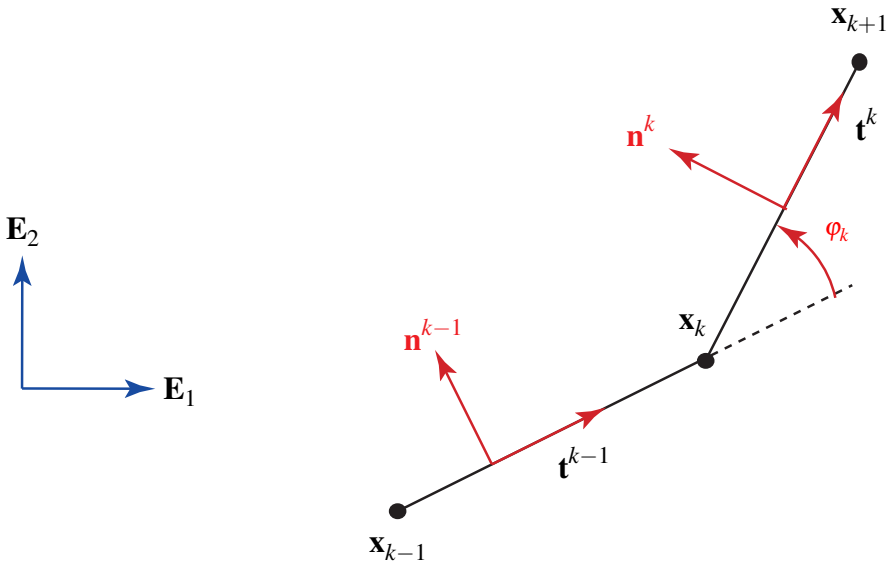

Fig. 2.1 *Three vertices $\mathbf{x}_{k-1}$, $\mathbf{x}_k$, and $\mathbf{x}_{k+1}$ of a planar discrete elastic rod. This figure also illustrates the pairs of unit vectors $\{\mathbf{t}_k, \mathbf{n}_k\}$ associated with the edges.*

As shown in Figure 2.1, the curve of interest is discretized into n vertices

$$\mathbf{x}_0, \quad \mathbf{x}_1, \quad \ldots, \quad \mathbf{x}_{n-1}. \tag{2.1}$$

Edges (or bond vectors) can be defined using this collection of points:

$$\mathbf{e}^0 = \mathbf{x}_1 - \mathbf{x}_0, \quad \mathbf{e}^1 = \mathbf{x}_2 - \mathbf{x}_1, \quad \ldots, \quad \mathbf{e}^{n-2} = \mathbf{x}_{n-1} - \mathbf{x}_{n-2}. \tag{2.2}$$

The associated unit tangent vectors are

$$\mathbf{t}^0 = \frac{\mathbf{e}^0}{\left\|\mathbf{e}^0\right\|}, \qquad \mathbf{t}^1 = \frac{\mathbf{e}^1}{\left\|\mathbf{e}^1\right\|}, \qquad \ldots, \qquad \mathbf{t}^{n-2} = \frac{\mathbf{e}^{n-2}}{\left\|\mathbf{e}^{n-2}\right\|}. \tag{2.3}$$

The arc-length parameters at the vertices are

$$\begin{aligned} &s_0 = 0, \qquad s_1 = \left\|\mathbf{e}^0\right\| + s_0, \quad s_2 = \left\|\mathbf{e}^1\right\| + s_1, \quad \ldots, \\ &s_j = \left\|\mathbf{e}^{j-1}\right\| + s_{j-1}, \quad \ldots, \quad s_{n-1} = \left\|\mathbf{e}^{n-2}\right\| - s_{n-2}. \end{aligned} \tag{2.4}$$

The length ℓ_k of the Voronoi region (or cell) associated with a vertex $\mathbf{x}_k$ is

$$\begin{aligned} \ell_0 &= \frac{1}{2}\left\|\mathbf{e}^0\right\|, \\ \ell_k &= \frac{1}{2}\left(\left\|\mathbf{e}^{k-1}\right\| + \left\|\mathbf{e}^k\right\|\right), \qquad (k = 1, \ldots, n-2), \\ \ell_{n-1} &= \frac{1}{2}\left\|\mathbf{e}^{n-2}\right\|. \end{aligned} \tag{2.5}$$

This length scale is used to define the curvature and elastic energies.

2.2 The Turning Angle and Curvatures

One also defines the angle φ_k between the edges of the discretized curve at $\mathbf{x}_k$:

$$\varphi_k = \arccos\left(\mathbf{t}^{k-1} \cdot \mathbf{t}^k\right). \tag{2.6}$$

That is,

$$\cos(\varphi_k) = \mathbf{t}^{k-1} \cdot \mathbf{t}^k, \qquad |\sin(\varphi_k)| = \left\|\mathbf{t}^{k-1} \times \mathbf{t}^k\right\|. \tag{2.7}$$

The angle φ_k, which is known as the turning angle, can be used to define a discrete pointwise curvature $\hat{\kappa}_k$ at $\mathbf{x}_k$:

$$\frac{1}{R_k} = \hat{\kappa}_k = \frac{2}{\ell_k}\tan\left(\frac{\varphi_k}{2}\right) = \frac{2\sin(\varphi_k)}{\ell_k(1+\cos(\varphi_k))}, \tag{2.8}$$

where ℓ_i is the length of the Voronoi domain of the vertex at $\mathbf{x}_i$. As shown in Figure 2.2, the curvature $\hat{\kappa}_k$ is the inverse of the radius R_k of the osculating circle to the edges emanating from a vertex $\mathbf{x}_k$.

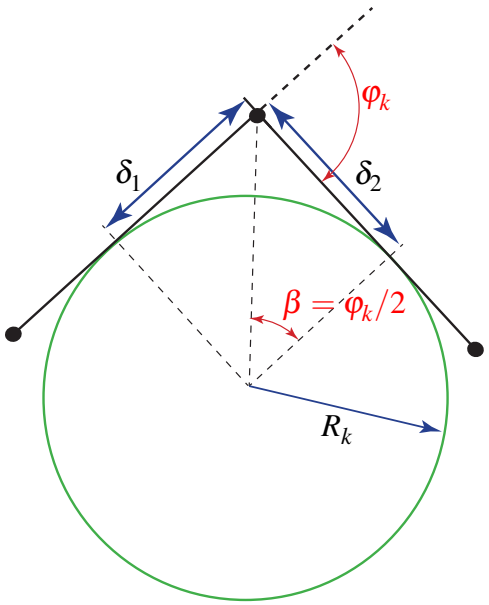

Fig. 2.2 *The osculating circle of radius R_k is constructed by projecting perpendicular lines from the edges with $\delta_1 = \delta_2 = \frac{\ell_k}{2}$. Elementary geometry is all that is needed to show that $R_k = \frac{\ell_k}{2}\cot\left(\frac{\varphi_k}{2}\right)$.*

As lucidly discussed in [5, Page 15], the definition (2.8) of the discrete curvature follows from the continuous case by considering curvature as a measure of the change in arc-length of a plane curve when it is moved along the normal direction. For instance, if an arc of radial extent $1/R$ of a circle of radius R is deformed into an arc of a circle of radius $R+\varepsilon$, then the arc length will have changed by an amount ε/R. Thus, κ can be considered as the rate of change of the arc length with respect to ε. For discretized curves, the only change in arc length is achieved at a vertex $\mathbf{x}_k$ and the change in length is directly related to the angle φ_k subtended by $\mathbf{t}^{k-1}$ and $\mathbf{t}^k$.

The discrete integrated curvature κ_i is related to the discrete pointwise curvature $\hat{\kappa}_i$ using the length ℓ_i:

$$\begin{aligned}\kappa_i &= \hat{\kappa}_i \ell_i \\ &= \frac{2\sin(\varphi_i)}{1+\cos(\varphi_i)} \\ &= 2\tan\left(\frac{\varphi_i}{2}\right).\end{aligned} \tag{2.9}$$

Furthermore, the discrete binormal vector to the curve at the ith vertex can be defined as

$$\mathbf{b}_i = \frac{\mathbf{t}^{i-1}\times\mathbf{t}^i}{\left\|\mathbf{t}^{i-1}\times\mathbf{t}^i\right\|} = \frac{\mathbf{t}^{i-1}\times\mathbf{t}^i}{\sqrt{1-\left(\mathbf{t}^{i-1}\cdot\mathbf{t}^i\right)^2}}. \tag{2.10}$$

Combining the expression for κ_i with the expression for $\mathbf{b}_i$, we find the pair of commonly used expressions for the discrete integrated curvature vector $(\kappa\mathbf{b})_i$ at the vertex $\mathbf{x}_i$:

$$(\kappa\mathbf{b})_i = \kappa_i\mathbf{b}_i = \frac{2\mathbf{t}^{i-1}\times\mathbf{t}^i}{1+\mathbf{t}^{i-1}\cdot\mathbf{t}^i} = \frac{2\mathbf{e}^{i-1}\times\mathbf{e}^i}{\left\|\mathbf{e}^{i-1}\right\|\left\|\mathbf{e}^i\right\|+\mathbf{e}^{i-1}\cdot\mathbf{e}^i}. \tag{2.11}$$

Although this vector has parallels to the component $\kappa\mathbf{e}_b$ of the Darboux vector, it is important to note that it is dimensionless unlike $\kappa\mathbf{e}_b$ which has the dimensions of $1/L$. In addition, as the discretization of a curve becomes finer the vector $(\kappa\mathbf{b})_i$ and the discrete integrated curvature κ_i both tend to approach zero while the discrete pointwise curvature $\hat{\kappa}_i \to \kappa$.

As discussed in Section 2.7, the components of the discrete integrated curvature vector $(\kappa\mathbf{b})_i$ at the vertex $\mathbf{x}_i$ are used to measure the bending strains in the rod. In addition, the length $\left\|\mathbf{e}^k\right\|$ is used to measure stretching of the centerline of the rod.

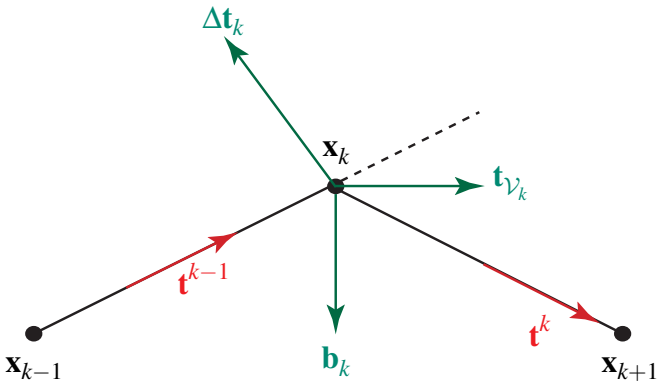

Fig. 2.3 *The triad $\left\{\Delta\mathbf{t}_k, \mathbf{b}_k, \mathbf{t}_{\mathcal{V}_k}\right\}$ of vectors at a vertex $\mathbf{x}_k$. Although $\Delta\mathbf{t}_k$ and $\mathbf{t}_{\mathcal{V}_k}$ are not necessarily unit vectors, this triad can be considered as a discrete analog of the Frenet triad.*

2.3 An Orthogonal Triad at a Vertex

As shown in Figure 2.3, an orthogonal triad of vectors at a vertex $\mathbf{x}_k$ can be defined using the discrete binormal vector and the edge tangent vectors:

$$\left\{\Delta\mathbf{t}_k, \mathbf{b}_k, \mathbf{t}_{\mathcal{V}_k}\right\}, \tag{2.12}$$

where

$$\Delta\mathbf{t}_k = \mathbf{t}^k - \mathbf{t}^{k-1}, \qquad \mathbf{t}_{\mathcal{V}_k} = \frac{1}{2}\left(\mathbf{t}^k + \mathbf{t}^{k-1}\right). \tag{2.13}$$

The vector $\mathbf{t}_{\mathcal{V}_k}$ is known as the discrete vertex tangent. It is the average of the edge tangent vectors at a vertex. Closely related vectors appear in the literature, most notably $\tilde{\mathbf{t}}$ in [3, 4] and $\nabla^h \boldsymbol{\gamma}$ in Hoffman [21, Definition 2.7]:

$$\tilde{\mathbf{t}} = \nabla^h \boldsymbol{\gamma} = \frac{\mathbf{t}^{i-1} + \mathbf{t}^i}{1 + \mathbf{t}^{i-1} \cdot \mathbf{t}^i}. \tag{2.14}$$

The vectors $\left\{\Delta \mathbf{t}_k, \mathbf{b}_k, \mathbf{t}_{\mathcal{V}_k}\right\}$ lead to an appealing discrete analogue of the Serret-Frenet relation $\mathbf{e}_t^{'} = \kappa \mathbf{e}_b \times \mathbf{e}_t$:

$$\Delta \mathbf{t}_i = (\kappa \mathbf{b})_i \times \mathbf{t}_{\mathcal{V}_i}. \tag{2.15}$$

We also note that

$$\tilde{\mathbf{t}} \times \Delta \mathbf{t}_i = (\kappa \mathbf{b})_i. \tag{2.16}$$

The triad $\left\{\Delta \mathbf{t}_k, \mathbf{b}_k, \mathbf{t}_{\mathcal{V}_k}\right\}$ can be considered as a discrete analog of the Frenet triad.

2.4 Bishop Frames and Reference Frames

Associated with the 0th edge, we can define a pair of vectors that are orthogonal to the tangent vector $\mathbf{t}^0$ (cf. Figure 2.7). The pair of vectors and $\mathbf{t}^0$ constitute a (right-handed) Bishop triad[1]:

$$\left\{\mathbf{t}^0, \mathbf{u}^0, \mathbf{v}^0 = \mathbf{t}^0 \times \mathbf{u}^0\right\}. \tag{2.17}$$

By associating the midpoint of the 0th edge with this triad, we are able to define the Bishop frame associated with the 0th edge. To compute the Bishop frame on subsequent edges, we use the operator $P^{\mathbf{t}^k}_{\mathbf{t}^{k-1}}$ to define the Bishop frame on the edge $\mathbf{e}^k$ given the Bishop frame on the previous edge:

$$\mathbf{u}^k = P^{\mathbf{t}^k}_{\mathbf{t}^{k-1}} \mathbf{u}^{k-1}, \qquad \mathbf{v}^k = P^{\mathbf{t}^k}_{\mathbf{t}^{k-1}} \mathbf{v}^{k-1}. \tag{2.18}$$

Exploiting the fact that the Bishop frame vectors form an orthonormal triad, we can conclude that $P^{\mathbf{t}^k}_{\mathbf{t}^{k-1}}$ has the representation

$$P^{\mathbf{t}^k}_{\mathbf{t}^{k-1}} = \mathbf{u}^k \otimes \mathbf{u}^{k-1} + \mathbf{v}^k \otimes \mathbf{v}^{k-1} + \mathbf{t}^k \otimes \mathbf{t}^{k-1}. \tag{2.19}$$

Referring to $P^{\mathbf{t}^k}_{\mathbf{t}^{k-1}}$ as a parallel transport operator is also consistent with the fact that the Bishop frame associated with a continuous curve is parallel-propagated along the curve. As with its continuous counterpart, the Bishop frame is also known as a twist-free frame.

[1] For further discussion of the Bishop frame, see [25].

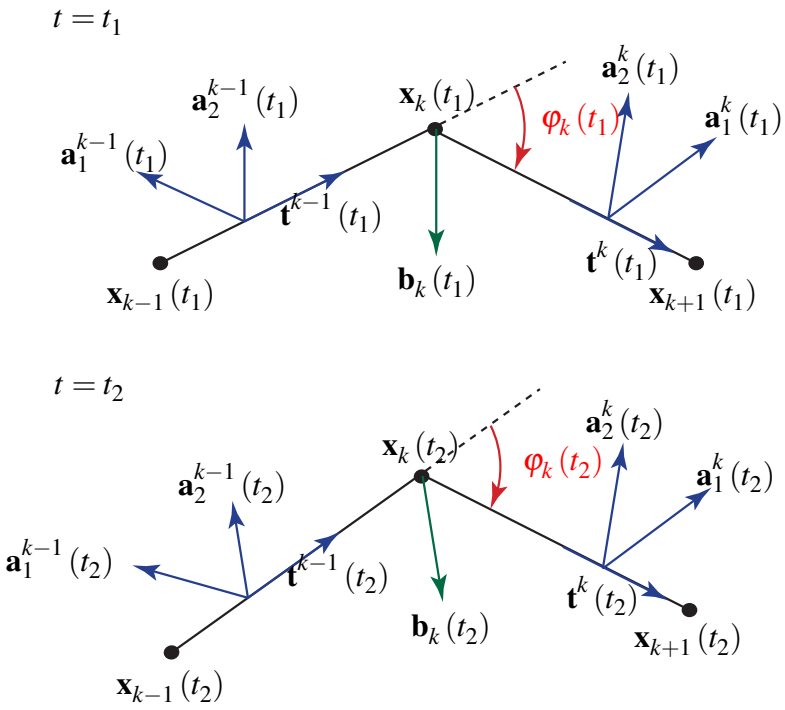

Fig. 2.4 *Defining the reference frame vectors at time $t_2 = t + \Delta t$ by a time-parallel transport (2.21) from the configuration at time $t_1 = t$. For example, $\mathbf{a}_1^k(t_2) = \bar{P}^k(t_1, t_2 - t_1)\,\mathbf{a}_1^k(t_1)$ and $\mathbf{a}_1^{k-1}(t_2) = \bar{P}^{k-1}(t_1, t_2 - t_1)\,\mathbf{a}_1^{k-1}(t_1)$. For the instance shown in this figure, the turning angles have negative values.*

The Bishop frame we have just discussed features prominently in Bergou et al. [4]. Later works, such as Bergou et al. [3] and Kaldor et al. [26], use a frame that is parallel-transported in time on an edge. The notation for the basis vectors associated with this orthonormal reference frame varies in the literature. Here, we denote the triad of vectors on the kth edge associated with this frame as $\left\{\mathbf{t}^k, \mathbf{a}_1^k, \mathbf{a}_2^k\right\}$.[2] Referring to Figure 2.4, the (right-handed) frame is assigned to each edge initially and then propagated in time:

$$\mathbf{a}_1^k(t + \Delta t) = \bar{P}^k(t, \Delta t)\,\mathbf{a}_1^k(t), \qquad \mathbf{a}_2^k(t + \Delta t) = \bar{P}^k(t, \Delta t)\,\mathbf{a}_2^k(t). \tag{2.20}$$

We can also conclude that $\bar{P}^k(t, \Delta t)$ has the representation

$$\bar{P}^k(t, \Delta t) = \mathbf{a}_1^k(t + \Delta t) \otimes \mathbf{a}_1^k(t) + \mathbf{a}_2^k(t + \Delta t) \otimes \mathbf{a}_2^k(t) + \mathbf{t}^k(t + \Delta t) \otimes \mathbf{t}^k(t). \tag{2.21}$$

We invite the reader to compare Eqns. (2.20) and (2.21) to Eqns. (2.18) and (2.19).

Unlike the Bishop frame, the reference frame is not space-parallel propagated along the discretized curve. That is,

$$\mathbf{a}_1^{k+1}(t) \neq P_{\mathbf{t}^k}^{\mathbf{t}^{k+1}}(t)\mathbf{a}_1^k(t), \qquad \mathbf{a}_2^{k+1}(t) \neq P_{\mathbf{t}^k}^{\mathbf{t}^{k+1}}(t)\mathbf{a}_2^k(t). \tag{2.22}$$

[2] In Bergou et al. [3], the triad is denoted by $\left\{\mathbf{t}^k, \underline{\mathbf{d}}_1^k, \underline{\mathbf{d}}_2^k\right\}$ while the triad is denoted by $\left\{\mathbf{t}^k, \mathbf{u}^k, \mathbf{v}^k\right\}$ in Kaldor et al. [26].

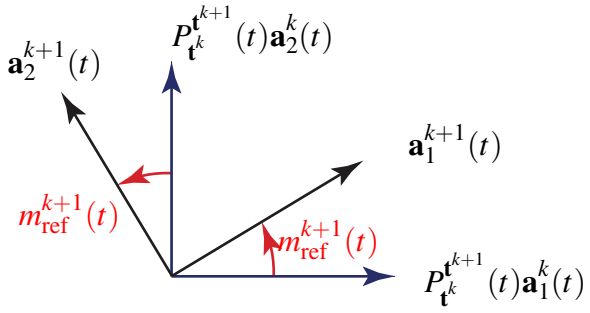

Fig. 2.5 *The reference twist m_{ref}^{k+1} on the $(k+1)$th edge at time t is defined by comparing the reference frame on an edge with its space-parallel transported counterpart from the adjacent edge.*

However both of these pairs of vectors lie on a plane, and so we can define an angle m_{ref}^{k+1} that captures the difference between $\mathbf{a}_1^{k+1}$ and its counterpart computed using the space-parallel transport operator $P_{\mathbf{t}^k}^{\mathbf{t}^{k+1}}$. Here, $\mathbf{a}_1^{k+1}$, $\mathbf{a}_2^{k+1}$, $\mathbf{t}^k$, $\mathbf{t}^{k+1}$, $P_{\mathbf{t}^k}^{\mathbf{t}^{k+1}}$, $\mathbf{a}_1^k$, and $\mathbf{a}_2^k$ are each evaluated at the same instant in time. Referring to Figure 2.5:

$$\begin{bmatrix} \mathbf{a}_1^{k+1}(t) \\ \mathbf{a}_2^{k+1}(t) \end{bmatrix} = \begin{bmatrix} \cos\left(m_{\text{ref}}^{k+1}(t)\right) & \sin\left(m_{\text{ref}}^{k+1}(t)\right) \\ -\sin\left(m_{\text{ref}}^{k+1}(t)\right) & \cos\left(m_{\text{ref}}^{k+1}(t)\right) \end{bmatrix} \begin{bmatrix} P_{\mathbf{t}^k}^{\mathbf{t}^{k+1}}(t)\mathbf{a}_1^k(t) \\ P_{\mathbf{t}^k}^{\mathbf{t}^{k+1}}(t)\mathbf{a}_2^k(t) \end{bmatrix}. \tag{2.23}$$

The angle m_{ref}^k is known as the referential discrete (integrated) twist associated with the kth edge. For the 0th edge, $m_{\text{ref}}^0 = 0$. We refer to m_{ref}^k as the reference twist in the sequel.

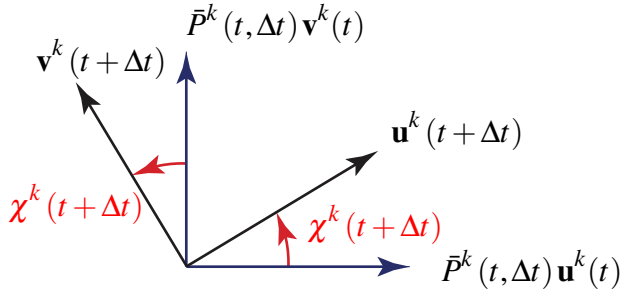

Fig. 2.6 *The angle $\chi^k(t+\Delta t)$ relating the Bishop frame to its time-parallel propagated values on the kth edge at time $t+\Delta t$.*

Complementing the angle m_{ref}^{k+1}, a related angle χ^k can be defined for the Bishop vectors and their time-parallel propagated counterparts. Referring to Figure 2.6,

$$\begin{bmatrix} \mathbf{u}^k(t+\Delta t) \\ \mathbf{v}^k(t+\Delta t) \end{bmatrix} = \begin{bmatrix} \cos\left(\chi^k(t+\Delta t)\right) & \sin\left(\chi^k(t+\Delta t)\right) \\ -\sin\left(\chi^k(t+\Delta t)\right) & \cos\left(\chi^k(t+\Delta t)\right) \end{bmatrix} \begin{bmatrix} \bar{P}^k(t,\Delta t)\mathbf{u}^k(t) \\ \bar{P}^k(t,\Delta t)\mathbf{v}^k(t) \end{bmatrix}. \tag{2.24}$$

The angle χ^k and its space-parallel propagated counterpart are distinct. Indeed, because the Bishop frame vectors are space-parallel propagated, the latter angle is 0. An angle denoted $\psi_k(\varepsilon)$ that is closely related to χ^k features in the work by Bergou et al. [4, Section 6]. The angle $\psi_k(\varepsilon)$ represents the holonomy of a connection induced by parallel transporting $\mathbf{t}^k$ around a closed circuit. We shall discuss this holonomy in further detail in Section 4.4.

The initial values of the Bishop vectors $\mathbf{u}^0(t_0)$ and $\mathbf{v}^0(t_0)$ at time $t = t_0$ are prescribed modulo a rotation about $\mathbf{t}^0(t_0)$. Once the initial values for this pair of vectors is selected, then the parallel propagation operators $P_{\mathbf{t}^0}^{\mathbf{t}^1}(t_0), \ldots, P_{\mathbf{t}^{n-2}}^{\mathbf{t}^{n-1}}(t_0)$ define the Bishop triads throughout the rod at time $t = t_0$. By way of contrast, the initial values of the vectors $\mathbf{a}_1^k(t_0)$ and $\mathbf{a}_2^k(t_0)$ at time $t = t_0$ are prescribed modulo a rotation about $\mathbf{t}^k(t_0)$ for each edge and the operators $\bar{P}^k(t_0, \Delta t)$ are used to define the reference frame on the kth edge at time $t = t_0 + \Delta t$.

2.5 Space-Parallel and Time-Parallel Transport Operators

Central components in the theory of discrete elastic rods are the notions of an operator that transforms a tangent vector from one edge to its adjacent neighbor and another operator which transforms the tangent vector at an edge at time t to its counterpart at time $t + \Delta t$. These operators are denoted by $P_{\mathbf{t}^{k-1}}^{\mathbf{t}^k}$ and $\bar{P}^k(t, \Delta t)$, respectively. Understanding these operators is a crucial step towards comprehending the discrete elastic rod formulation.

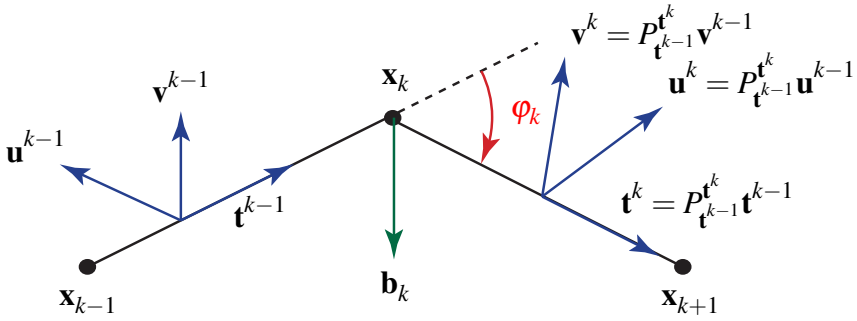

Fig. 2.7 *Three vertices $\mathbf{x}_{k-1}$, $\mathbf{x}_k$, and $\mathbf{x}_{k+1}$, and the unit vectors associated with the edges. The frames $\left\{\mathbf{t}^{k-1}, \mathbf{u}^{k-1}, \mathbf{v}^{k-1} = \mathbf{t}^{k-1} \times \mathbf{u}^{k-1}\right\}$ and $\left\{\mathbf{t}^k, \mathbf{u}^k, \mathbf{v}^k = \mathbf{t}^k \times \mathbf{u}^k\right\}$ are Bishop frames. The frame on one edge is computed from the frame on the adjacent edge using the operator $P_{\mathbf{t}^{k-1}}^{\mathbf{t}^k}$: $\mathbf{t}^k = P_{\mathbf{t}^{k-1}}^{\mathbf{t}^k}\mathbf{t}^{k-1}$, $\mathbf{u}^k = P_{\mathbf{t}^{k-1}}^{\mathbf{t}^k}\mathbf{u}^{k-1}$, and $\mathbf{v}^k = P_{\mathbf{t}^{k-1}}^{\mathbf{t}^k}\mathbf{v}^{k-1}$ (cf. Eqn. (2.18)).*

2.5.1 The Operator $P_{\mathbf{t}^{k-1}}^{\mathbf{t}^k}$ and its Associated Darboux Vector $\kappa_k \mathbf{b}_k$

Because $\mathbf{t}^k$ and $\mathbf{t}^{k-1}$ are unit vectors, an operator, which is denoted by $P_{\mathbf{t}^{k-1}}^{\mathbf{t}^k}$, can be defined as the rotation that transforms $\mathbf{t}^{k-1}$ to $\mathbf{t}^k$ by rotating it about a unit vector $\mathbf{b}_k$ that is parallel to $\mathbf{t}^k \times \mathbf{t}^{k-1}$ (i.e., the discrete version of the binormal vector):

$$P_{\mathbf{t}^{k-1}}^{\mathbf{t}^k} = \mathbf{R}(\varphi_k, \mathbf{b}_k). \tag{2.25}$$

For the reader's convenience, we recall that

$$\mathbf{b}_k = \frac{\mathbf{t}^{k-1} \times \mathbf{t}^k}{\left\| \mathbf{t}^{k-1} \times \mathbf{t}^k \right\|}, \qquad \cos(\varphi_k) = \mathbf{t}^k \cdot \mathbf{t}^{k-1}, \tag{2.26}$$

and note that the rotation operator $\mathbf{R}(\varphi_k, \mathbf{b}_k)$ represents a counterclockwise rotation through an angle φ_k about an axis $\mathbf{b}_k$ (cf. Figure 2.7). Indeed, using the definition (2.11) of the discrete integrated curvature vector,

$$(\kappa \mathbf{b})_k = \kappa_k \mathbf{b}_k = \frac{2\mathbf{t}^{k-1} \times \mathbf{t}^k}{1 + \mathbf{t}^{k-1} \cdot \mathbf{t}^k}, \tag{2.27}$$

we can associate a relative Darboux vector $\kappa_k \mathbf{b}_k$ with $P_{\mathbf{t}^{k-1}}^{\mathbf{t}^k}$. On a related intriguing note,

$$\kappa_k \mathbf{b}_k = 2 \tan\left(\frac{\varphi_k}{2}\right) \mathbf{b}_k \tag{2.28}$$

is twice the Rodrigues or Gibbs vector associated with the rotation $\mathbf{R}(\varphi_k, \mathbf{b}_k)$ (cf. Shuster [55, Page 469]).

The tensor $P_{\mathbf{t}^{k-1}}^{\mathbf{t}^k}$ is known as a space-parallel transport operator. A possible motivation for this terminology is provided by imagining the transformation of a vector $\mathbf{t}$ from $\mathbf{t}^{k-1}$ to $\mathbf{t}^k$ as a continuous process performed at constant speed. Then, the path traced by the vector $\mathbf{t}$ as it transforms from $\mathbf{t}^{k-1}$ to $\mathbf{t}^k$ will be an arc of a great circle on a unit sphere. The axis of rotation $\mathbf{b}_k$ will be normal to the plane formed by the arc of the circle and the associated angular velocity vector will be constant. As discussed in great detail in [43], such rotational motions are geodesics of the rotation group $SO(3)$.[3] The operator $P_{\mathbf{t}^{k-1}}^{\mathbf{t}^k}$ will be a function of time but in the interests of keeping notation as compact as possible, this dependency is not explicitly emphasized in the sequel.

2.5.2 The Operator $\bar{P}^k(t, \Delta t)$ and its Associated Angular Velocity Vector ${}_P\bar{\boldsymbol{\omega}}^k(t)$

.

[3] Our remarks here complement comments in [2, Appendix C].

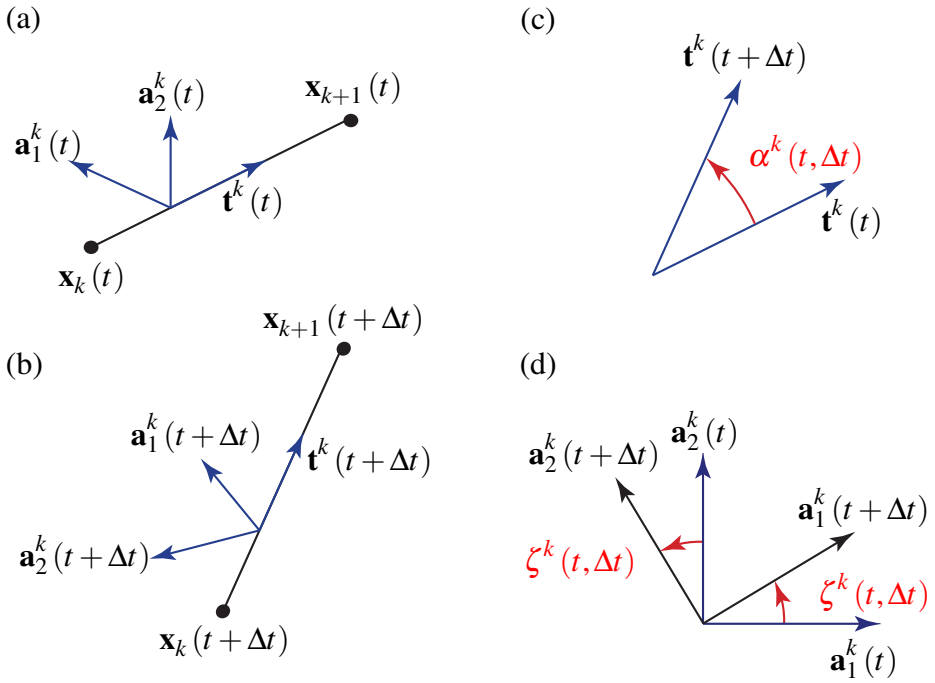

Fig. 2.8 *Features of the time-parallel transport operator $\bar{P}^k(t,\Delta t)$. (a), The kth edge at time t. (b) The kth edge at time $t+\Delta t$. (c) The angle $\alpha^k(t,\Delta t)$ associated with the rotation $\bar{P}^k(t,\Delta t)$. (d) The rotation of the reference frame vectors. The angles of rotation ζ^k and α^k are distinct.*

An alternative parallel transport operator can be defined by considering the configuration of an edge at time t.

As shown in Figures 2.8 and 2.4, consider the kth edge at time t and its evolved counterpart at time $t+\Delta t$. Given the tangent vectors $\mathbf{t}^k(t)$ and $\mathbf{t}^k(t+\Delta t)$, we can define a rotation $\bar{P}^k(t,\Delta t)$. This rotation transforms $\mathbf{t}^k(t)$ to $\mathbf{t}^k(t+\Delta t)$:

$$\bar{P}^k(t,\Delta t) \equiv P_{\mathbf{t}^k(t)}^{\mathbf{t}^k(t+\Delta t)} = \mathbf{R}\left(\alpha^k(t,\Delta t),\mathbf{h}^k(t,\Delta t)\right), \tag{2.29}$$

where the axis and angle of rotation are

$$\mathbf{h}^k(t,\Delta t) = \frac{\mathbf{t}^k(t)\times\mathbf{t}^k(t+\Delta t)}{\left\|\mathbf{t}^k(t)\times\mathbf{t}^k(t+\Delta t)\right\|}, \qquad \cos\left(\alpha^k(t,\Delta t)\right) = \mathbf{t}^k(t)\cdot\mathbf{t}^k(t+\Delta t). \tag{2.30}$$

It is convenient to substitute for $\mathbf{h}^k(t,\Delta t)$ and $\alpha^k(t,\Delta t)$ into Euler's representation of rota-

tion. After some manipulations, we find that

$$\begin{aligned}\bar{P}^k(t,\Delta t) &= \cos\left(\alpha^k(t,\Delta t)\right)\mathbf{I} + \text{skewt}\left(\mathbf{t}^k(t)\times\mathbf{t}^k(t+\Delta t)\right)\\ &+ \frac{1}{1+\cos\left(\alpha^k(t,\Delta t)\right)}\left(\left(\mathbf{t}^k(t)\times\mathbf{t}^k(t+\Delta t)\right)\otimes\left(\mathbf{t}^k(t)\times\mathbf{t}^k(t+\Delta t)\right)\right).\end{aligned} \tag{2.31}$$

This representation is well defined for all values of Δt and so it can be used to verify that

$$\bar{P}^k(t,0) = \mathbf{I}. \tag{2.32}$$

For future purposes an angular velocity vector associated with $\bar{P}^k(t,\Delta t)$ will be of use. To compute this angular velocity vector, we define

$$\dot{\bar{P}}^k(t) = \lim_{\Delta t\to 0}\frac{\bar{P}^k(t,\Delta t)-\bar{P}^k(t,0)}{\Delta t}. \tag{2.33}$$

With the help of the representation (2.31) and the identities

$$\begin{aligned}\cos\left(\alpha^k(t,\Delta t)\right)-1 &= \mathbf{t}^k(t+\Delta t)\cdot\mathbf{t}^k(t)-\mathbf{t}^k(t+\Delta t)\cdot\mathbf{t}^k(t+\Delta t)\\ &= -\left(\mathbf{t}^k(t+\Delta t)-\mathbf{t}^k(t)\right)\cdot\mathbf{t}^k(t+\Delta t),\\ \lim_{\Delta t\to 0}\frac{1}{\Delta t}\left(\cos\left(\alpha^k(t,\Delta t)\right)-1\right) &= -\dot{\mathbf{t}}^k(t)\cdot\mathbf{t}^k(t)=0,\end{aligned} \tag{2.34}$$

and

$$\begin{aligned}&\lim_{\Delta t\to 0}\frac{1}{\Delta t}\left(\left(\mathbf{t}^k(t)\times\mathbf{t}^k(t+\Delta t)\right)\otimes\left(\mathbf{t}^k(t)\times\mathbf{t}^k(t+\Delta t)\right)\right)\\ &= \left(\mathbf{t}^k(t)\times\dot{\mathbf{t}}^k(t)\right)\otimes\left(\mathbf{t}^k(t)\times\mathbf{t}^k(t)\right)=0,\end{aligned} \tag{2.35}$$

it can quickly be shown that

$$\dot{\bar{P}}^k(t) = \text{skewt}\left(\mathbf{t}^k(t)\times\dot{\mathbf{t}}^k(t)\right). \tag{2.36}$$

The angular velocity vector of interest is the following axial vector:

$${}_P\bar{\boldsymbol{\omega}}^k(t) = \text{ax}\left(\dot{\bar{P}}^k(t)\left(\bar{P}^k(t,0)\right)^T\right). \tag{2.37}$$

As $\bar{P}^k(t,0)=\mathbf{I}$, it immediately follows from Eqn. (2.36) that

$${}_P\bar{\boldsymbol{\omega}}^k(t) = \mathbf{t}^k(t)\times\dot{\mathbf{t}}^k(t). \tag{2.38}$$

The angular velocity ${}_P\bar{\boldsymbol{\omega}}^k(t)$ can be expressed in terms of the motion of the vertices. To elaborate, differentiating

$$\mathbf{t}^k(t) = \frac{\mathbf{x}_{k+1}(t) - \mathbf{x}_k(t)}{\|\mathbf{x}_{k+1}(t) - \mathbf{x}_k(t)\|}, \tag{2.39}$$

and performing some minor rearranging we find that

$$\dot{\mathbf{t}}^k(t) = \left(\mathbf{I} - \mathbf{t}^k(t) \otimes \mathbf{t}^k(t)\right) \frac{\dot{\mathbf{x}}_{k+1}(t) - \dot{\mathbf{x}}_k(t)}{\|\mathbf{x}_{k+1}(t) - \mathbf{x}_k(t)\|}. \tag{2.40}$$

Whence one can substitute Eqns. (2.39) and (2.40) into Eqn. (2.38) to obtain an expression for ${}_P\bar{\boldsymbol{\omega}}^k(t)$ in terms of the motion of the vertices.

2.5.3 An Additional Representation for the Operator $P_{\mathbf{t}^{k-1}}^{\mathbf{t}^k}$

It is useful for future purposes to consider different representations of the space-parallel transport and time-parallel transport operators. First, we recall, from Eqn. (2.19), the representation

$$P_{\mathbf{t}^{k-1}}^{\mathbf{t}^k} = \mathbf{u}^k \otimes \mathbf{u}^{k-1} + \mathbf{v}^k \otimes \mathbf{v}^{k-1} + \mathbf{t}^k \otimes \mathbf{t}^{k-1}. \tag{2.41}$$

After noting that the reference triad vectors and Bishop triad vectors are related by results of the form

$$\begin{aligned} \mathbf{a}_1^{k-1} &= \cos\left(\beta^{k-1}\right)\mathbf{u}^{k-1} + \sin\left(\beta^{k-1}\right)\mathbf{v}^{k-1}, \\ \mathbf{a}_2^{k-1} &= \cos\left(\beta^{k-1}\right)\mathbf{v}^{k-1} - \sin\left(\beta^{k-1}\right)\mathbf{u}^{k-1}, \end{aligned} \tag{2.42}$$

some straightforward manipulations can be used to show the representations

$$\begin{aligned} P_{\mathbf{t}^{k-1}}^{\mathbf{t}^k} &= \mathbf{u}^k \otimes \mathbf{u}^{k-1} + \mathbf{v}^k \otimes \mathbf{v}^{k-1} + \mathbf{t}^k \otimes \mathbf{t}^{k-1} \\ &= \cos\left(m_{\text{ref}}^k\right)\left(\mathbf{a}_1^k \otimes \mathbf{a}_1^{k-1} + \mathbf{a}_2^k \otimes \mathbf{a}_2^{k-1}\right) \\ &\quad + \sin\left(m_{\text{ref}}^k\right)\left(\mathbf{a}_1^k \otimes \mathbf{a}_2^{k-1} - \mathbf{a}_2^k \otimes \mathbf{a}_1^{k-1}\right) + \mathbf{t}^k \otimes \mathbf{t}^{k-1}, \end{aligned} \tag{2.43}$$

where

$$m_{\text{ref}}^k = \beta^k - \beta^{k-1}. \tag{2.44}$$

The representations (2.43) for $P_{\mathbf{t}^{k-1}}^{\mathbf{t}^k}$ enable a ready contrast between $P_{\mathbf{t}^{k-1}}^{\mathbf{t}^k}\mathbf{a}_1^{k-1}$ and $P_{\mathbf{t}^{k-1}}^{\mathbf{t}^k}\mathbf{u}^{k-1}$. They also show the privileged role occupied by the Bishop frame vectors $\mathbf{u}^{k-1}$ and $\mathbf{v}^{k-1}$ and how m_{ref}^k can be viewed as a rotation induced by the operator $P_{\mathbf{t}^{k-1}}^{\mathbf{t}^k}$.

As discussed previously, the rotation $\bar{P}^k(t,\Delta t)$ has the representation

$$\bar{P}^k(t,\Delta t) = \mathbf{a}_1^k(t+\Delta t)\otimes\mathbf{a}_1^k(t) + \mathbf{a}_2^k(t+\Delta t)\otimes\mathbf{a}_2^k(t) + \mathbf{t}^k(t+\Delta t)\otimes\mathbf{t}^k(t). \tag{2.45}$$

This tensor can be represented using the Bishop frame vectors $\mathbf{u}^k(t+\Delta t)$, $\mathbf{u}^k(t)$, $\mathbf{v}^k(t+\Delta t)$, and $\mathbf{v}^k(t)$ along with the angles $\beta^k(t+\Delta t)$ and $\beta^k(t)$ but the representation does not appear to be very illuminating.

2.5.4 Computation of Reference Twist in a Simple Rod

To illustrate many of the concepts introduced in this chapter, we consider a rod which has three vertices. The rod is subject to a motion parameterized by a scalar ε. This motion induces a reference twist m^1_{ref} in the rod. Due to the simplicity of the model, the twist m^1_{ref} along with the concomitant parallel transport operators can be explicitly computed. An alternative method of computing m^1_{ref} for this rod, which exploits the Gauss-Bonnet theorem, will be discussed in Section 4.6.

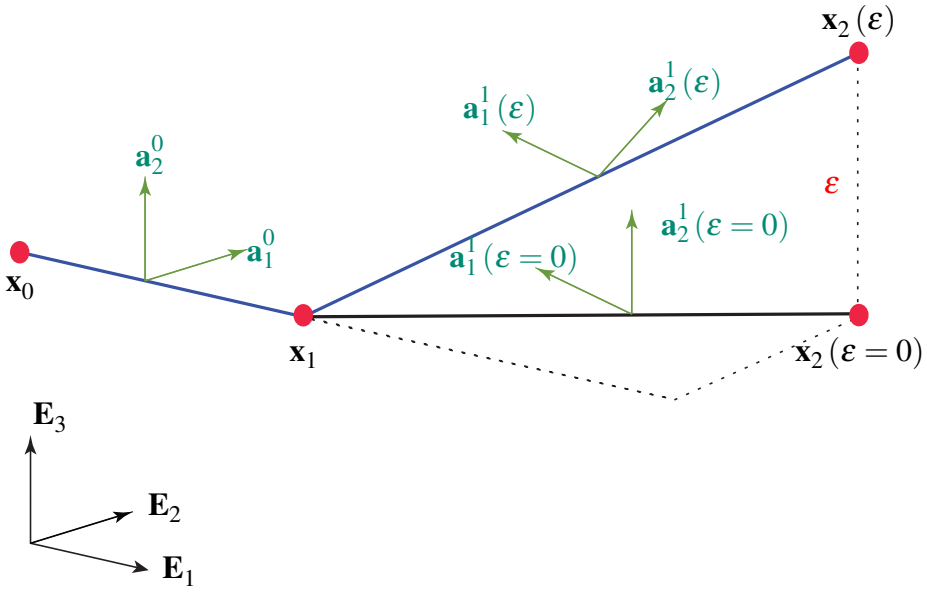

Fig. 2.9 *The configurations of a rod which has three vertices. When $\varepsilon = 0$, all of the vertices lie on a horizontal plane. As ε is increased from 0, the third vertex rises above this plane and a reference twist is induced in the second edge.*

Referring to Figure 2.9, the initial configuration of the rod is defined by the vertices:

$$\mathbf{x}_0(\varepsilon=0) = 0, \qquad \mathbf{x}_1(\varepsilon=0) = \mathbf{E}_1, \qquad \mathbf{x}_2(\varepsilon=0) = 2\mathbf{E}_1 + \mathbf{E}_2. \tag{2.46}$$

During the deformation of the rod, the first edge remains stationary, while the second edge is stretched as its end node is raised upwards:

$$\mathbf{x}_0(\varepsilon) = 0, \qquad \mathbf{x}_1(\varepsilon) = \mathbf{E}_1, \qquad \mathbf{x}_2(\varepsilon) = 2\mathbf{E}_1 + \mathbf{E}_2 + \varepsilon\mathbf{E}_3. \tag{2.47}$$

It is straightforward to compute the edge and tangent vectors for this rod:

$$\begin{aligned}
&\mathbf{e}^0(\varepsilon) = \mathbf{E}_1, \qquad \mathbf{e}^1(\varepsilon) = \mathbf{E}_1 + \mathbf{E}_2 + \varepsilon\mathbf{E}_3. \\
&\mathbf{t}^0(\varepsilon) = \mathbf{E}_1, \qquad \mathbf{t}^1(\varepsilon) = \frac{1}{\sqrt{2+\varepsilon^2}}(\mathbf{E}_1 + \mathbf{E}_2 + \varepsilon\mathbf{E}_3).
\end{aligned} \tag{2.48}$$

We note for completeness that the discrete integrated curvature vector is

$$(\kappa\mathbf{b})_1 = \frac{2}{1+\sqrt{2+\varepsilon^2}}(\mathbf{E}_3 - \varepsilon\mathbf{E}_2). \tag{2.49}$$

Observe that as ε increases from zero, the discrete curvature κ_1 increases from a value $\frac{2}{1+\sqrt{2}}$.

The space-parallel transport operator can be defined as a function of the parameter ε:

$$P_{\mathbf{t}^0}^{\mathbf{t}^1}(\varepsilon) = \mathbf{R}(\varphi_1(\varepsilon), \mathbf{b}_1(\varepsilon)). \tag{2.50}$$

With the help of Eqn. (2.26), the turning angle φ_1 and axis of rotation $\mathbf{b}_1$ can be computed using the tangent vectors associated with the edges:

$$\begin{aligned}
&\cos(\varphi_1(\varepsilon)) = \frac{1}{\sqrt{2+\varepsilon^2}}, \qquad \sin(\varphi_1(\varepsilon)) = \sqrt{\frac{1+\varepsilon^2}{2+\varepsilon^2}}, \\
&\mathbf{b}_1(\varepsilon) = \frac{1}{\sqrt{1+\varepsilon^2}}(\mathbf{E}_3 - \varepsilon\mathbf{E}_2).
\end{aligned} \tag{2.51}$$

The time-parallel transport operators for the edges can be computed using Eqn. (2.29):

$$\bar{P}^0(0,\varepsilon) = \mathbf{I}, \qquad \bar{P}^1(0,\varepsilon) = \mathbf{R}\left(\alpha^1(\varepsilon), \mathbf{h}^1(\varepsilon)\right), \tag{2.52}$$

where

$$\begin{aligned}
&\mathbf{h}^1(0,\varepsilon) = \frac{1}{\sqrt{2}}(\mathbf{E}_1 - \mathbf{E}_2), \\
&\cos\left(\alpha^1(0,\varepsilon)\right) = \sqrt{\frac{2}{2+\varepsilon^2}}, \qquad \sin\left(\alpha^1(0,\varepsilon)\right) = \frac{\varepsilon}{\sqrt{2+\varepsilon^2}}.
\end{aligned} \tag{2.53}$$

In the definition of the time-parallel transport operators $\bar{P}^k(t,\Delta t)$, we have taken time $t = 0$ and used ε in place of Δt. When $\varepsilon = 0$, both of these operators simplify to the identity tensor.

The reference frame vectors on the first edge when $\varepsilon = 0$ are chosen to be

$$\mathbf{a}_1^0(\varepsilon = 0) = \mathbf{E}_2, \qquad \mathbf{a}_2^0(\varepsilon = 0) = \mathbf{E}_3. \tag{2.54}$$

Because the time-parallel operator for the first edge is the identity tensor, these vectors remain constant:

$$\mathbf{a}_1^0(\varepsilon) = \mathbf{E}_2, \qquad \mathbf{a}_2^0(\varepsilon) = \mathbf{E}_3. \tag{2.55}$$

The reference frame vectors on the second edge at $\varepsilon = 0$ are computed using the space-parallel transport operator $P_{\mathbf{t}^0}^{\mathbf{t}^1}(\varepsilon = 0)$:

$$\begin{aligned}
\mathbf{a}_1^1(\varepsilon = 0) &= P_{\mathbf{t}^0}^{\mathbf{t}^1}(\varepsilon = 0)\,\mathbf{a}_1^0(\varepsilon = 0) \\
&= P_{\mathbf{t}^0}^{\mathbf{t}^1}(\varepsilon = 0)\,\mathbf{E}_2 \\
&= \frac{1}{\sqrt{2}}(\mathbf{E}_2 - \mathbf{E}_1), \\
\mathbf{a}_2^1(\varepsilon = 0) &= P_{\mathbf{t}^0}^{\mathbf{t}^1}(\varepsilon = 0)\,\mathbf{a}_2^0(\varepsilon = 0) \\
&= P_{\mathbf{t}^0}^{\mathbf{t}^1}(\varepsilon = 0)\,\mathbf{E}_3 \\
&= \mathbf{E}_3.
\end{aligned} \tag{2.56}$$

It is important to observe that the initial values of the reference vectors $\mathbf{a}_1^k$ and $\mathbf{a}_2^k$ are obtained by specifying $\mathbf{a}_1^0$ and $\mathbf{a}_2^0$ and then using the initial space-parallel transport operators to determine the initial values of $\mathbf{a}_1^k$ and $\mathbf{a}_2^k$. At later instances of time, $\mathbf{a}_1^k$ and $\mathbf{a}_2^k$ are updated using the time-parallel transport operator.

For $\varepsilon \neq 0$, the reference frame vectors on the second edge are computed using the time-parallel transport operator associated with the second edge:

$$\begin{aligned}
\mathbf{a}_1^1(\varepsilon) &= \bar{P}^1(0,\varepsilon)\,\mathbf{a}_1^1(\varepsilon = 0) \\
&= \frac{1}{\sqrt{2}}(\mathbf{E}_2 - \mathbf{E}_1), \\
\mathbf{a}_2^1(\varepsilon) &= \bar{P}^1(0,\varepsilon)\,\mathbf{a}_2^1(\varepsilon = 0) \\
&= \cos\left(\alpha^1(0,\varepsilon)\right)\mathbf{E}_3 - \frac{\sin\left(\alpha^1(0,\varepsilon)\right)}{\sqrt{2}}(\mathbf{E}_2 + \mathbf{E}_1).
\end{aligned} \tag{2.57}$$

The computation of $\mathbf{a}_1^1(\varepsilon)$ is greatly simplified by noting that this vector is parallel to the axis of rotation of $\bar{P}^1(0,\varepsilon)$.

The reference twist m_{ref}^0 for the first edge is identically 0. As shown in Figure 2.10, for

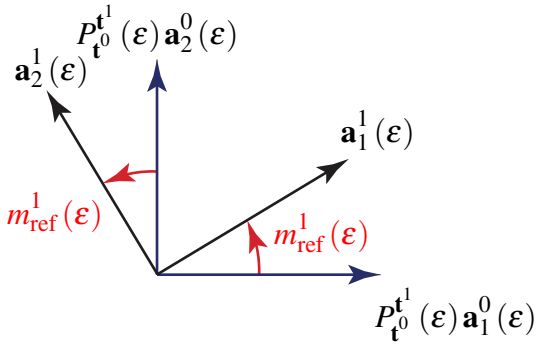

Fig. 2.10 *The angle m_{ref}^1 relating the reference frame vectors to their space-parallel propagated values on the second edge. When $\varepsilon = 0$ for the example of interest in this section of the Brief, $m_{ref}^1 = 0$.*

the second edge, the reference twist m_{ref}^1 is the angle between $P_{\mathbf{t}^0}^{\mathbf{t}^1}(\varepsilon)\,\mathbf{a}_1^0(\varepsilon)$ and $\mathbf{a}_1^1(\varepsilon)$:

$$\begin{aligned} c^1(\varepsilon) \equiv \cos\left(m_{\text{ref}}^1\right) &= \left(P_{\mathbf{t}^0}^{\mathbf{t}^1}(\varepsilon)\,\mathbf{a}_1^0(\varepsilon)\right)\cdot\mathbf{a}_1^1(\varepsilon) \\ &= \left(P_{\mathbf{t}^0}^{\mathbf{t}^1}(\varepsilon)\,\mathbf{E}_2\right)\cdot\mathbf{a}_1^1(\varepsilon), \\ s^1(\varepsilon) \equiv \sin\left(m_{\text{ref}}^1\right) &= \left(P_{\mathbf{t}^0}^{\mathbf{t}^1}(\varepsilon)\,\mathbf{a}_2^0(\varepsilon)\right)\cdot\mathbf{a}_1^1(\varepsilon) \\ &= \left(P_{\mathbf{t}^0}^{\mathbf{t}^1}(\varepsilon)\,\mathbf{E}_3\right)\cdot\mathbf{a}_1^1(\varepsilon). \end{aligned} \tag{2.58}$$

Computing the dot products and expanding the resulting expressions, we find the following representations for the respective functions $\cos\left(m_{\text{ref}}^1\right)$ and $\sin\left(m_{\text{ref}}^1\right)$:

$$\begin{aligned} c^1(\varepsilon) &= \frac{\sin(\varphi_1(\varepsilon))}{\sqrt{2}\sqrt{1+\varepsilon^2}} + \frac{1}{\sqrt{2}}\left(\cos(\varphi_1(\varepsilon)) + \frac{\varepsilon^2(1-\cos(\varphi_1(\varepsilon)))}{1+\varepsilon^2}\right) \\ &= \frac{2+\varepsilon^2\left(1+\sqrt{2+\varepsilon^2}\right)}{\sqrt{2}\left(1+\varepsilon^2\right)\sqrt{2+\varepsilon^2}}, \end{aligned} \tag{2.59}$$

and

$$\begin{aligned} s^1(\varepsilon) &= \varepsilon\cos(\alpha_1(0,\varepsilon))\left(\frac{1-\cos(\varphi_1(\varepsilon))}{1+\varepsilon^2}\right) \\ &+ \frac{\sin(\alpha_1(0,\varepsilon))}{\sqrt{2}}\left(\cos(\varphi_1(\varepsilon)) + \frac{\varepsilon^2(1-\cos(\varphi_1(\varepsilon)))}{1+\varepsilon^2}\right) \\ &- \frac{\sin(\alpha_1(0,\varepsilon))}{\sqrt{2}}\left(\frac{\sin(\varphi_1(\varepsilon))}{\sqrt{2}\sqrt{1+\varepsilon^2}}\right). \end{aligned} \tag{2.60}$$

In contrast to the expression for $c^1(\varepsilon)$, the explicit expression for $s^1(\varepsilon)$ is lengthy and not very illuminating and so it is omitted.

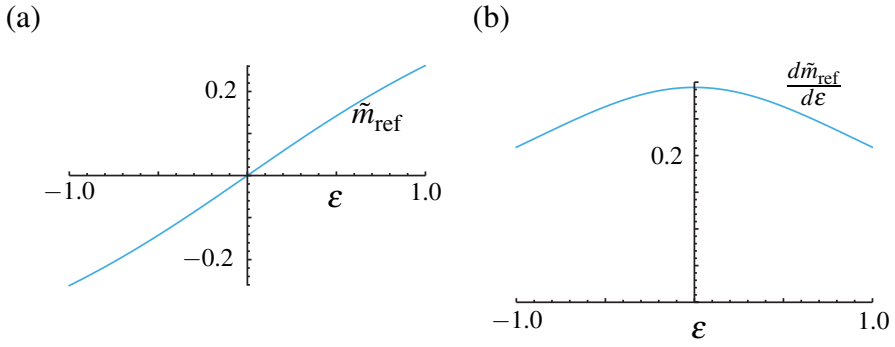

Fig. 2.11 *(a) The reference twist $m^1_{ref} = \tilde{m}_{ref}$ as a function of ε computed using Eqn. (2.61) for the rod with two edges shown in Figure 2.9. (b) The corresponding value of $\frac{d\tilde{m}_{ref}}{d\varepsilon}$ computed by differentiating the lengthy expression for the function $\tilde{m}_{ref}$.*

Using the functions $c^1(\varepsilon)$ and $s^1(\varepsilon)$, the reference twist as a function of ε can be determined. We denote the resulting function by $\tilde{m}_{\text{ref}}(\varepsilon)$:

$$m^1_{\text{ref}} = \tilde{m}_{\text{ref}}(\varepsilon). \tag{2.61}$$

The graph of $\tilde{m}_{\text{ref}}(\varepsilon)$ is shown in Figure 2.11(a). We observe that

$$\tilde{m}_{\text{ref}}(-1) = -\frac{\pi}{12}, \qquad \tilde{m}_{\text{ref}}(0) = 0, \qquad \tilde{m}_{\text{ref}}(1) = \frac{\pi}{12}, \tag{2.62}$$

and note that $m_{\text{ref}}(\varepsilon)$ is a monotonically increasing function of ε. Thus, the simple motion of lifting one of the edges of the rod induces a reference twist in the rod.

In Section 4.6 of this Brief, the reference twist and its derivative will be computed using a construction from spherical trigonometry. As can be seen by comparing Figure 2.11 and Figure 4.9, the results from the two distinct methods are equivalent when $\varepsilon \geq 0$.

2.6 The Material Triad

The most popular nonlinear rod theory that captures three-dimensional motions of the centerline, torsion of the cross-sections, and a pair of flexures of the centerline, dates to Kirchhoff [29] in 1859. In modern formulations of this theory, a pair of unit vectors, known as directors, $\mathbf{d}_1$ and $\mathbf{d}_2$, are associated with each point on the centerline of the rod. These vectors are assumed to remain normal to the unit tangent vector to the centerline of the rod (cf. [1, 47]). Kirchhoff's rod theory assumes that the cross-sections of the rod remain plane and normal to the centerline while the rod is deforming. Thus, the deformation of the triad $\{\mathbf{d}_1, \mathbf{d}_2, \mathbf{d}_3 = \mathbf{e}_t\}$ can be modeled using a rotation tensor and three strains can be

defined with the help of the rotation and its partial derivative with respect to s. This trio of strains are related to the curvature κ and geometric torsion τ of the centerline, and the twist of the cross-section relative to the Frenet frame. It is important to keep in mind that while the behavior of the Bishop and Frenet triads do not generally capture the three strains in Kirchhoff's rod theory, the director triad $\{\mathbf{d}_1, \mathbf{d}_2, \mathbf{d}_3 = \mathbf{e}_t\}$ does.

In the theory of discrete elastic rods, the counterpart to the director triad is a material triad $\left\{\mathbf{t}^k, \mathbf{m}_1^k, \mathbf{m}_2^k\right\}$ associated with an edge. The unit vectors $\mathbf{m}_1^k$ and $\mathbf{m}_2^k$ are coplanar with the Bishop frame vectors $\mathbf{u}^k$ and $\mathbf{v}^k$ and can be related to them by a rotation ϑ^k about $\mathbf{t}^k$ as shown in Figure 2.12(a).[4] The initial prescription for the material vectors at time $t = t_0$ are such that $\left\{\mathbf{t}^k, \mathbf{m}_1^k, \mathbf{m}_2^k\right\}$ form a right-handed orthonormal triad on each edge of the rod.

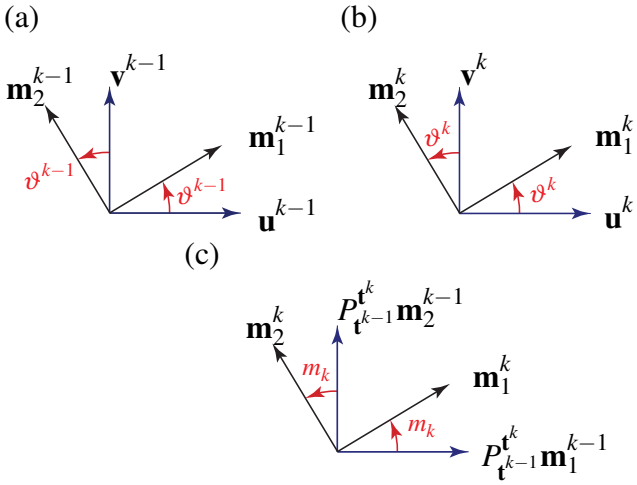

Fig. 2.12 *(a) Schematic of the angle ϑ^{k-1} defining the rotation between the Bishop frame vectors and the material vectors along the edge $\mathbf{e}^{k-1}$. (b) Schematic of the angle ϑ^k defining the rotation between the Bishop frame vectors and the material vectors along the edge $\mathbf{e}^k$. (c) The discrete integrated twist $m_k = \vartheta^k - \vartheta^{k-1}$ and its relation to space-parallel transport.*

2.6.1 The Operators $M_{\mathbf{t}^{k-1}}^{\mathbf{t}^k}$ and $\bar{M}^k(t, \Delta t)$

The rotation of the material triad from one edge to its adjacent counterpart at an instant t can be defined by a rotation tensor:

$$M_{\mathbf{t}^{k-1}}^{\mathbf{t}^k} = \mathbf{m}_1^k \otimes \mathbf{m}_1^{k-1} + \mathbf{m}_2^k \otimes \mathbf{m}_2^{k-1} + \mathbf{t}^k \otimes \mathbf{t}^{k-1}. \tag{2.63}$$

[4] In some works, the material vectors are identified as the discrete directors: $\mathbf{m}_1^k = \mathbf{d}_1^k$ and $\mathbf{m}_2^k = \mathbf{d}_2^k$.

Referring to Figures 2.12(b,c), the tensor $M_{\mathbf{t}^{k-1}}^{\mathbf{t}^k}$ and the parallel transport operator $P_{\mathbf{t}^{k-1}}^{\mathbf{t}^k}$ are related:

$$\begin{aligned} M_{\mathbf{t}^{k-1}}^{\mathbf{t}^k} &= \mathbf{R}\left(\vartheta^k, \mathbf{t}^k\right) P_{\mathbf{t}^{k-1}}^{\mathbf{t}^k} \mathbf{R}^T\left(\vartheta^{k-1}, \mathbf{t}^{k-1}\right) \\ &= \mathbf{R}\left(\vartheta^k, \mathbf{t}^k\right) P_{\mathbf{t}^{k-1}}^{\mathbf{t}^k} \mathbf{R}\left(-\vartheta^{k-1}, \mathbf{t}^{k-1}\right). \end{aligned} \tag{2.64}$$

It should be obvious from Eqn. (2.64) that $\mathbf{t}^k = M_{\mathbf{t}^{k-1}}^{\mathbf{t}^k} \mathbf{t}^{k-1}$. The operator $M_{\mathbf{t}^{k-1}}^{\mathbf{t}^k}$ plays a seminal role in determining the twist of the rod.

Complementing the rotation $M_{\mathbf{t}^{k-1}}^{\mathbf{t}^k}$, we also define an operator that transforms the material frame at an instant t to its counterpart at $t+\Delta t$:

$$\bar{M}^k(t,\Delta t) = \mathbf{m}_1^k(t+\Delta t) \otimes \mathbf{m}_1^k(t) + \mathbf{m}_2^k(t+\Delta t) \otimes \mathbf{m}_2^k(t) + \mathbf{t}^k(t+\Delta t) \otimes \mathbf{t}^k(t). \tag{2.65}$$

Thus, for example, $\mathbf{m}_1^k(t+\Delta t) = \bar{M}^k(t,\Delta t)\mathbf{m}_1^k(t)$. The operator $\bar{M}^k(t,\Delta t)$ will feature in computing the kinetics of the discrete elastic rod and has numerous representations. However, for ease of exposition, we postpone discussion of these representations until Section 2.8.3.

2.7 Bending Strains and Curvatures

The components of the discrete integrated curvature vector $(\kappa \mathbf{b})_k$ at the vertex $\mathbf{x}_k$ are used to quantify the bending strains of the rod. Recalling from Eqn. (2.11) that

$$(\kappa \mathbf{b})_k = \frac{2\mathbf{t}^{k-1} \times \mathbf{t}^k}{1 + \mathbf{t}^{k-1} \cdot \mathbf{t}^k}, \tag{2.66}$$

we observe that $(\kappa \mathbf{b})_k$ is orthonormal to $\mathbf{t}^k$ and $\mathbf{t}^{k-1}$. This implies that we can construct a basis for $\mathbb{E}^3$ where $(\kappa \mathbf{b})_k$ has one zero component. The basis is

$$\left\{ \frac{1}{2}\left(\mathbf{t}^{k-1} + \mathbf{t}^k\right), \frac{1}{2}\left(\mathbf{m}_1^{k-1} + \mathbf{m}_1^k\right), \frac{1}{2}\left(\mathbf{m}_2^{k-1} + \mathbf{m}_2^k\right) \right\}. \tag{2.67}$$

The non-zero components of $(\kappa \mathbf{b})_k$ are used to define the curvatures associated with the material frame at the kth vertex:

$$\begin{aligned} \kappa_{k_1} &= \frac{1}{2}\left(\mathbf{m}_2^{k-1} + \mathbf{m}_2^k\right) \cdot (\kappa \mathbf{b})_k, \\ \kappa_{k_2} &= -\frac{1}{2}\left(\mathbf{m}_1^{k-1} + \mathbf{m}_1^k\right) \cdot (\kappa \mathbf{b})_k. \end{aligned} \tag{2.68}$$

These curvatures were introduced in Bergou et al. [3] and are known as vertex-based material curvatures. The pair of curvatures will be used as the bending strains of the discrete elastic rod (see Section 5.3).

To provide additional motivation for κ_{k_1} and κ_{k_2}, we note that they are discretized versions of the continuous case:

$$\begin{aligned}\kappa_{\mathrm{D}_1} &= \mathbf{e}_t^{'} \cdot \mathbf{d}_1 = \boldsymbol{\nu}_{\mathrm{D}} \cdot \mathbf{d}_2 = \kappa \mathbf{e}_b \cdot \mathbf{d}_2, \\ \kappa_{\mathrm{D}_2} &= \mathbf{e}_t^{'} \cdot \mathbf{d}_2 = -\boldsymbol{\nu}_{\mathrm{D}} \cdot \mathbf{d}_1 = -\kappa \mathbf{e}_b \cdot \mathbf{d}_1. \end{aligned} \tag{2.69}$$

When comparing the discrete and continuous cases, one also needs to be cognizant of the length ℓ_k of the Voronoi region of the vertex $\mathbf{x}_k$ that is used to scale $(\kappa \mathbf{b})_k$.

2.8 Discrete Integrated Twist

As discussed earlier (cf. Eqn. (2.18)), the Bishop triad vectors on an edge can be computed from the previous edge using the rotation (space-parallel transport operator) $P_{\mathbf{t}^{k-1}}^{\mathbf{t}^k}$. Thus, at each instant in time, the propagation of the Bishop frame vectors $\mathbf{u}^{k-1}$ and $\mathbf{v}^{k-1}$ from the $(k-1)$th edge to the vectors $\mathbf{u}^k$ and $\mathbf{v}^k$ on the kth edge using $P_{\mathbf{t}^{k-1}}^{\mathbf{t}^k}$ is known as space-parallel transport. The rotation of the material vectors relative to the Bishop vectors defines a discrete twist. By appropriately accommodating the rotation $P_{\mathbf{t}^{k-1}}^{\mathbf{t}^k}$, the relative rotation of the material vectors between adjacent edges can be computed. The resulting relative rotation is a measure of the torsional strain in the rod.

To elaborate on our previous remarks, we refer the reader to Figure 2.12(c) and observe that

$$\begin{aligned}\mathbf{m}_1^{k-1} &= \cos\left(\vartheta^{k-1}\right)\mathbf{u}^{k-1} + \sin\left(\vartheta^{k-1}\right)\mathbf{v}^{k-1}, \\ \mathbf{m}_2^{k-1} &= \cos\left(\vartheta^{k-1}\right)\mathbf{v}^{k-1} - \sin\left(\vartheta^{k-1}\right)\mathbf{u}^{k-1}. \end{aligned} \tag{2.70}$$

Whence,

$$\begin{aligned}P_{\mathbf{t}^{k-1}}^{\mathbf{t}^k}\mathbf{m}_1^{k-1} &= \cos\left(\vartheta^{k-1}\right)\mathbf{u}^{k} + \sin\left(\vartheta^{k-1}\right)\mathbf{v}^{k}, \\ P_{\mathbf{t}^{k-1}}^{\mathbf{t}^k}\mathbf{m}_2^{k-1} &= \cos\left(\vartheta^{k-1}\right)\mathbf{v}^{k} - \sin\left(\vartheta^{k-1}\right)\mathbf{u}^{k}, \end{aligned} \tag{2.71}$$

and

$$\begin{aligned}\mathbf{m}_1^{k} &= \cos\left(\vartheta^{k} - \vartheta^{k-1}\right)P_{\mathbf{t}^{k-1}}^{\mathbf{t}^k}\mathbf{m}_1^{k-1} + \sin\left(\vartheta^{k} - \vartheta^{k-1}\right)P_{\mathbf{t}^{k-1}}^{\mathbf{t}^k}\mathbf{m}_2^{k-1}, \\ \mathbf{m}_2^{k} &= \cos\left(\vartheta^{k} - \vartheta^{k-1}\right)P_{\mathbf{t}^{k-1}}^{\mathbf{t}^k}\mathbf{m}_2^{k-1} - \sin\left(\vartheta^{k} - \vartheta^{k-1}\right)P_{\mathbf{t}^{k-1}}^{\mathbf{t}^k}\mathbf{m}_1^{k-1}. \end{aligned} \tag{2.72}$$

The latter identity leads to the definition of the discrete integrated twist m_k on the edge $\mathbf{e}^k$:

$$m_k = \vartheta^k - \vartheta^{k-1}. \tag{2.73}$$

As noted in Bergou et al. [4, Section 4.2.2] and summarized in Figure 2.12(c), the twist m_k can be interpreted as the difference between a material frame on the kth edge and the corresponding parallel transported frame from the $(k-1)$th edge.

In the interests of reducing computational cost, use of the relative twist m_k as a measure of torsional strain was modified following the 2008 paper [4]. In later works, such as [3, 26], the Bishop frame vectors $\mathbf{u}^k$ and $\mathbf{v}^k$ are not explicitly used to compute m_k, rather the reference frame vectors $\mathbf{a}_1^k$ and $\mathbf{a}_2^k$ are used. In this case, it is necessary to supplement m_k with a measure known as the referential discrete (integrated) twist (or reference twist) m_{ref}^k. This modification will be discussed in further detail in Section 2.8.2.

2.8.1 Decompositions of the Rotation $M_{\mathbf{t}^{k-1}}^{\mathbf{t}^k}$

As presented in Audoly et al. [2, Equation (C.8), Appendix C.2], the relative twist m_k can be used to provide decompositions of the rotation $M_{\mathbf{t}^{k-1}}^{\mathbf{t}^k}$. The resulting decomposition shows a relationship between the space-parallel transport operator and a rotation through the relative twist about a tangent vector to one of the edges. The resulting decompositions can be useful when computing angular velocity vectors and Darboux vectors.

To establish the decompositions, one starts by noting that

$$\begin{aligned}
P_{\mathbf{t}^{k-1}}^{\mathbf{t}^k}\mathbf{R}\left(m_k,\mathbf{t}^{k-1}\right)\left(P_{\mathbf{t}^{k-1}}^{\mathbf{t}^k}\right)^T\mathbf{t}^k &= \mathbf{t}^k,\\
P_{\mathbf{t}^{k-1}}^{\mathbf{t}^k}\mathbf{R}\left(m_k,\mathbf{t}^{k-1}\right)\left(P_{\mathbf{t}^{k-1}}^{\mathbf{t}^k}\right)^T\mathbf{u}^k &= \cos\left(m_k\right)\mathbf{u}^k+\sin\left(m_k\right)\mathbf{v}^k,\\
P_{\mathbf{t}^{k-1}}^{\mathbf{t}^k}\mathbf{R}\left(m_k,\mathbf{t}^{k-1}\right)\left(P_{\mathbf{t}^{k-1}}^{\mathbf{t}^k}\right)^T\mathbf{v}^k &= -\sin\left(m_k\right)\mathbf{u}^k+\cos\left(m_k\right)\mathbf{v}^k.
\end{aligned} \tag{2.74}$$

These results enable one to find a simple expression for a compound rotation:

$$P_{\mathbf{t}^{k-1}}^{\mathbf{t}^k}\mathbf{R}\left(m_k,\mathbf{t}^{k-1}\right)\left(P_{\mathbf{t}^{k-1}}^{\mathbf{t}^k}\right)^T=\mathbf{R}\left(m_k,\mathbf{t}^k\right). \tag{2.75}$$

Examining the action of $P_{\mathbf{t}^{k-1}}^{\mathbf{t}^k}\mathbf{R}\left(m_k,\mathbf{t}^{k-1}\right)$ on $\mathbf{m}_1^{k-1}$ and $\mathbf{m}_2^{k-1}$ results in the conclusion that

$$M_{\mathbf{t}^{k-1}}^{\mathbf{t}^k}=P_{\mathbf{t}^{k-1}}^{\mathbf{t}^k}\mathbf{R}\left(m_k,\mathbf{t}^{k-1}\right)=\mathbf{R}\left(m_k,\mathbf{t}^k\right)P_{\mathbf{t}^{k-1}}^{\mathbf{t}^k}, \tag{2.76}$$

where the rotation $M_{\mathbf{t}^{k-1}}^{\mathbf{t}^k}$ was defined previously by Eqn. (2.64).

2.8.2 Discrete Integrated Twist and Induced Reference Twist

In later versions of the discrete elastic rod formulation, the reference frame vectors $\mathbf{a}_1^k$ and $\mathbf{a}_2^k$ are used to compute the twist of the rod. As shall be elaborated upon below, the

resulting formulation introduces a so-called reference twist into the measure of torsional strain. In our examination of the literature on discrete elastic rods, we found the notion of induced reference twist to be exceptionally difficult to comprehend. We hope the explanation provided below contributes to clarifying the concept of induced reference twist.

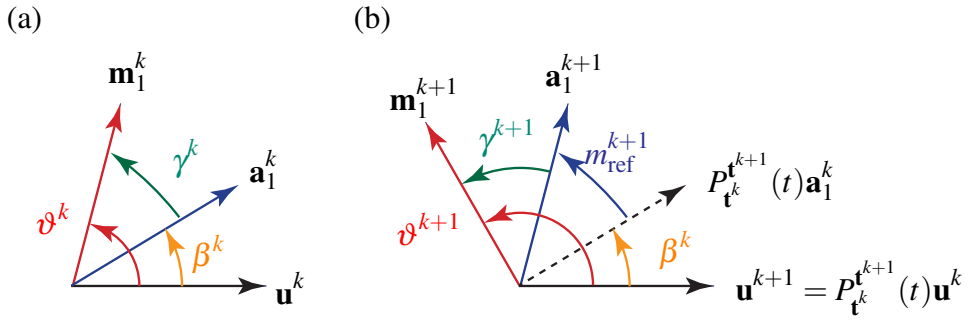

Fig. 2.13 *The angles and unit vectors employed in the definition of the discrete reference twist m_{ref}^{k+1}. (a) The vectors on the kth edge. (b) The vectors associated with the $(k+1)$th edge. It is important to observe that the angle β^k between $\mathbf{a}_1^k$ and $\mathbf{u}^k$ is identical to the angle between $P_{\mathbf{t}^k}^{\mathbf{t}^{k+1}}(t)\mathbf{a}_1^k$ and $\mathbf{u}^{k+1} = P_{\mathbf{t}^{k-1}}^{\mathbf{t}^k}(t)\mathbf{u}^k$. The angle $\beta^{k+1} = \beta^k + m_{ref}^{k+1}$ is not explicitly shown.*

To discuss the formulation of twist featuring the reference frame, it is convenient to assume that the reference frame and the Bishop frame are both being computed for the deformed discrete curve. Consider the kth edge. The vectors $\mathbf{m}_1^k$, $\mathbf{u}^k$, and $\mathbf{a}_1^k$ can be used to define the three angles ϑ^k, γ^k, and β^k shown in Figure 2.13(a):

$$\vartheta^k = \beta^k + \gamma^k. \tag{2.77}$$

Each of these angles can be associated with a measure of twisting of the rod. The angle β^k is the signed angle formed by $\mathbf{a}_1^k$ and $\mathbf{u}^k$, is identical to the angle formed by $\mathbf{a}_2^k$ and $\mathbf{v}^k$, and can be considered as the twist angle of the reference frame. The angles γ^k and ϑ^k are the signed angles formed by $\mathbf{m}_1^k$ and $\mathbf{a}_1^k$ and $\mathbf{m}_1^k$ and $\mathbf{u}^k$, respectively. The change in the angle β^k from one edge to the preceding edge is the induced reference twist:

$$m_{\text{ref}}^{k+1} = \beta^{k+1} - \beta^k. \tag{2.78}$$

This interpretation of the induced reference twist is consistent with our earlier discussion on Page 9 (cf. Eqn. (2.23)). The reference twist m_{ref}^k in [3] and [26] is denoted by $\underline{m}_k$ and $\hat{\vartheta}^k$, respectively.

If we next consider the $(k+1)$th edge, then it is straightforward to argue that the angle between $\mathbf{u}^{k+1}$ and $P_{\mathbf{t}^k}^{\mathbf{t}^{k+1}}(t)\mathbf{a}_1^k$ will be β^k. The argument relies on the facts that for any pair of vectors $\mathbf{a}$ and $\mathbf{b}$ and a rotation tensor $\mathbf{R}$, the following identities hold:

$$\begin{aligned}(\mathbf{Ra})\cdot(\mathbf{Rb}) &= \mathbf{a}\cdot\mathbf{b},\\ (\mathbf{Ra})\times(\mathbf{Rb}) &= \mathbf{R}(\mathbf{a}\times\mathbf{b}).\end{aligned} \tag{2.79}$$

Referring to Figure 2.5 and Eqn. (2.23), we observe that

$$\vartheta^{k+1} = \beta^k + \gamma^{k+1} + m_{\text{ref}}^{k+1}, \qquad \beta^{k+1} = \beta^k + m_{\text{ref}}^{k+1}. \tag{2.80}$$

With the added help of Eqn. (2.73), we note that the discrete integrated twist on the $(k+1)$th edge has the representations

$$\begin{aligned} m_{k+1} &= \vartheta^{k+1} - \vartheta^k \\ &= \left(\gamma^{k+1} + m_{\text{ref}}^{k+1} + \beta^k\right) - \left(\gamma^k + \beta^k\right) \\ &= \gamma^{k+1} - \gamma^k + m_{\text{ref}}^{k+1}. \end{aligned} \tag{2.81}$$

The final representation $m_{k+1} = \gamma^{k+1} - \gamma^k + m_{\text{ref}}^{k+1}$ features in works by Bergou et al. [3] and Kaldor et al. [26] where the reference triad is parallel transported in time. We observe also from the relation $m_{k+1} = \gamma^{k+1} - \gamma^k + m_{\text{ref}}^{k+1}$ that it is not necessary to compute the Bishop frame in order for m_{k+1} to be computed. Indeed, the Bishop frame is not explicitly needed in the most recent discrete elastic rod formulations.

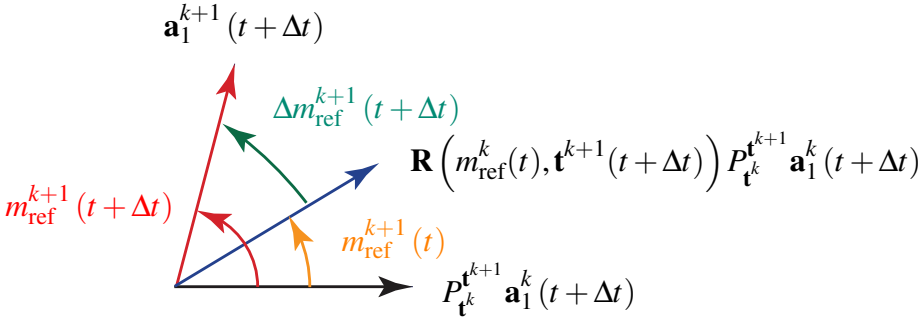

Fig. 2.14 *Schematic of the angle* $\Delta m_{ref}^{k+1}(t+\Delta t)$ *between* $\mathbf{a}_1^{k+1}(t+\Delta t)$ *and* $\mathbf{R}\left(m_{ref}^k(t), \mathbf{t}^{k+1}(t+\Delta t)\right) P_{\mathbf{t}_k}^{\mathbf{t}^{k+1}} \mathbf{a}_1^k(t+\Delta t)$.

In the code for the discrete elastic rod formulation, $m_{\text{ref}}^{k+1}(t+\Delta t)$ is computed using a recursive scheme which assumes that $m_{\text{ref}}^{k+1}(t)$ is known:

$$m_{\text{ref}}^{k+1}(t+\Delta t) = m_{\text{ref}}^{k+1}(t) + \Delta m_{\text{ref}}^{k+1}(t+\Delta t). \tag{2.82}$$

To compute the increment $\Delta m_{\text{ref}}^{k+1}(t+\Delta t)$, the angle $m_{\text{ref}}^{k+1}(t)$ is used to rotate $P_{\mathbf{t}_k}^{\mathbf{t}^{k+1}} \mathbf{a}_1^k(t+\Delta t)$ about $\mathbf{t}^{k+1}(t+\Delta t)$ to define the vector $\mathbf{R}\left(m_{\text{ref}}^k(t), \mathbf{t}^{k+1}\right) P_{\mathbf{t}_k}^{\mathbf{t}^{k+1}} \mathbf{a}_1^k(t+\Delta t)$. Then, the angle between $\mathbf{R}\left(m_{\text{ref}}^k(t), \mathbf{t}^{k+1}\right) P_{\mathbf{t}_k}^{\mathbf{t}^{k+1}} \mathbf{a}_1^k(t+\Delta t)$ and $\mathbf{a}_1^{k+1}(t+\Delta t)$ is computed. As summarized in Figure 2.14, this angle is $\Delta m_{\text{ref}}^{k+1}(t+\Delta t)$.[5]

[5] In the code, $\Delta m_{\text{ref}}^{k+1}$ is known by the variable name SIGNANG.

2.8.3 Representations for the Operator $\bar{M}^k(t,\Delta t)$ and the Vector $\bar{\boldsymbol{\omega}}^k(t)$

The operator $\bar{M}^k(t,\Delta t)$ was defined previously as an operator that transformed the material frame on the kth edge from a time t to a later instant $t+\Delta t$ (cf. Eqn. (2.65)). Recalling the representation (2.21) from Page 8,

$$\bar{P}^k(t,\Delta t) = \mathbf{a}_1^k(t+\Delta t)\otimes\mathbf{a}_1^k(t) + \mathbf{a}_2^k(t+\Delta t)\otimes\mathbf{a}_2^k(t) + \mathbf{t}^k(t+\Delta t)\otimes\mathbf{t}^k(t), \tag{2.83}$$

and then paralleling the developments for $M^{\mathbf{t}^k}_{\mathbf{t}^{k-1}}$ in Section 2.8.1, it is straightforward to show that the operator $\bar{M}^k(t,\Delta t)$ has the following representations:

$$\begin{aligned}\bar{M}^k(t,\Delta t) &= \mathbf{m}_1^k(t+\Delta t)\otimes\mathbf{m}_1^k(t) + \mathbf{m}_2^k(t+\Delta t)\otimes\mathbf{m}_2^k(t) + \mathbf{t}^k(t+\Delta t)\otimes\mathbf{t}^k(t)\\ &= \bar{P}^k(t,\Delta t)\,\mathbf{R}\left(\gamma^k(t+\Delta t)-\gamma^k(t),\mathbf{t}^k(t)\right)\\ &= \mathbf{R}\left(\gamma^k(t+\Delta t)-\gamma^k(t),\mathbf{t}^k(t+\Delta t)\right)\bar{P}^k(t,\Delta t).\end{aligned} \tag{2.84}$$

The angle γ^k in these representations is the angle between $\mathbf{a}_1^k$ and $\mathbf{m}_1^k$ at an instant in time (cf. Figure 2.13).

An angular velocity vector $\bar{\boldsymbol{\omega}}^k(t)$ associated with $\bar{M}^k(t,\Delta t)$ will be of use later in computing expressions for the variations of the material vectors, mechanical power of moments, and the kinetic energy of the discrete elastic rod. To compute $\bar{\boldsymbol{\omega}}^k(t)$, we define

$$\dot{\bar{M}}^k(t) = \lim_{\Delta t\to 0}\frac{\bar{M}^k(t,\Delta t)-\bar{M}^k(t,0)}{\Delta t}. \tag{2.85}$$

The angular velocity vector of interest is the following axial vector:

$$\bar{\boldsymbol{\omega}}^k(t) = \mathrm{ax}\left(\dot{\bar{M}}^k(t)\left(\bar{M}^k(t,0)\right)^T\right). \tag{2.86}$$

It is straightforward to compute a representation for this angular velocity vector using Eqns. (2.38) and $(2.84)_3$:[6]

$$\bar{\boldsymbol{\omega}}^k(t) = \dot{\gamma}^k(t)\,\mathbf{t}^k(t) + \mathbf{t}^k(t)\times\dot{\mathbf{t}}^k(t). \tag{2.87}$$

$\dot{\gamma}^k(t)\,\mathbf{t}^k(t)$ can be interpreted as the angular velocity vector of $\mathbf{R}\left(\gamma^k(t),\mathbf{t}^k(t)\right)$ relative to $\bar{P}^k(t)$ while $\mathbf{t}^k(t)\times\dot{\mathbf{t}}^k(t)$ is the angular velocity vector associated with $\bar{P}^k(t)$.

[6] The easiest method to compute this representation is to use the relative angular velocity vector proposed in Casey and Lam [7]. This relative angular velocity vector was discussed earlier in Section 2.5.2.

2.8.4 Velocity Vectors of the Material Vectors $\mathbf{m}_1^k$ and $\mathbf{m}_2^k$

To compute expressions for $\dot{\mathbf{m}}_1^k$ and $\dot{\mathbf{m}}_2^k$, we recall that

$$\mathbf{m}_1^k(t+\Delta t) = \bar{M}^k(t,\Delta t)\,\mathbf{m}_1^k(t), \qquad \mathbf{m}_2^k(t+\Delta t) = \bar{M}^k(t,\Delta t)\,\mathbf{m}_2^k(t), \tag{2.88}$$

and

$$\bar{\boldsymbol{\omega}}^k(t) = \mathrm{ax}\left(\dot{\bar{M}}^k(t)\left(\bar{M}^k(t,0)\right)^T\right) = \dot{\gamma}^k(t)\,\mathbf{t}^k(t) + \mathbf{t}^k(t)\times\dot{\mathbf{t}}^k(t). \tag{2.89}$$

Whence,

$$\begin{aligned}
\dot{\mathbf{m}}_1^k(t) &= \bar{\boldsymbol{\omega}}^k(t)\times\mathbf{m}_1^k(t)\\
&= \dot{\gamma}^k(t)\,\mathbf{m}_2^k(t) - \left(\mathbf{m}_1^k(t)\cdot\dot{\mathbf{t}}^k(t)\right)\mathbf{t}^k(t),\\
\dot{\mathbf{m}}_2^k(t) &= \bar{\boldsymbol{\omega}}^k(t)\times\mathbf{m}_2^k(t)\\
&= -\dot{\gamma}^k(t)\,\mathbf{m}_1^k(t) - \left(\mathbf{m}_2^k(t)\cdot\dot{\mathbf{t}}^k(t)\right)\mathbf{t}^k(t).
\end{aligned} \tag{2.90}$$

Observe that the velocity vectors $\dot{\mathbf{m}}_1^k$ and $\dot{\mathbf{m}}_2^k$ each have two components: one due to the twist $\dot{\gamma}^k$ and the other due to the motion of the edge vector $\mathbf{e}^k$ (i.e., bending). As discussed earlier, the latter component is determined by the motion of the vertices (cf. Eqns. (2.39) and (2.40)).

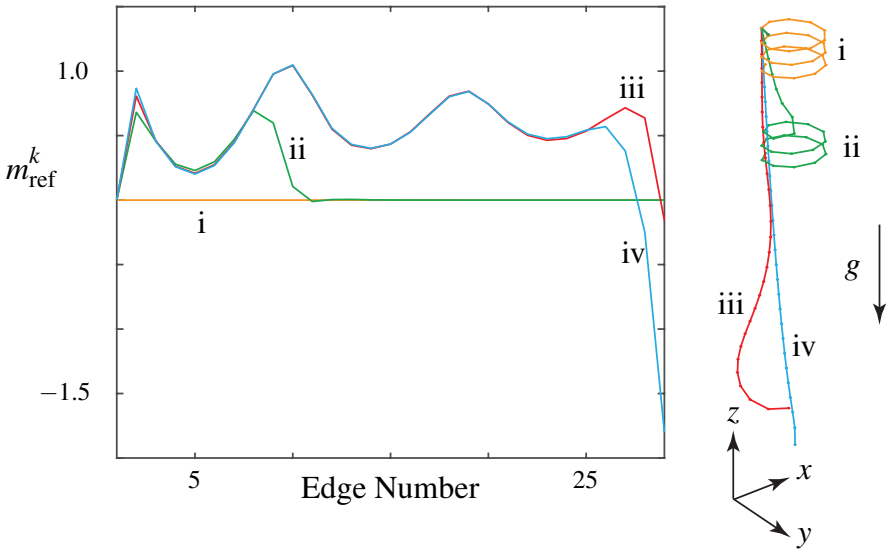

Fig. 2.15 *Evolution of the reference twist m^k_{ref} in a coiled rod which is released from rest at time $t = 0$ and unwinds due to a gravitational force: i, $t = 0$; ii, $t = 0.2$ s; iii, $t = 0.5$ s; and iv, $t = 10$ s.*

2.8.5 Uncoiling of a Twisted Rod

To illustrate the evolution of the reference twist m^k_{ref}, we consider a uniform rod whose centerline is bent into a helical space curve and cantilevered at one of its ends to a fixed point O. The rod is then released from rest and falls under gravity as shown in the inset images in Figure 2.15. This example was inspired by a study on the mechanics of the self-burial of the seeds of a small flowering plant known as a filaree published by Evangelista et al. [13].

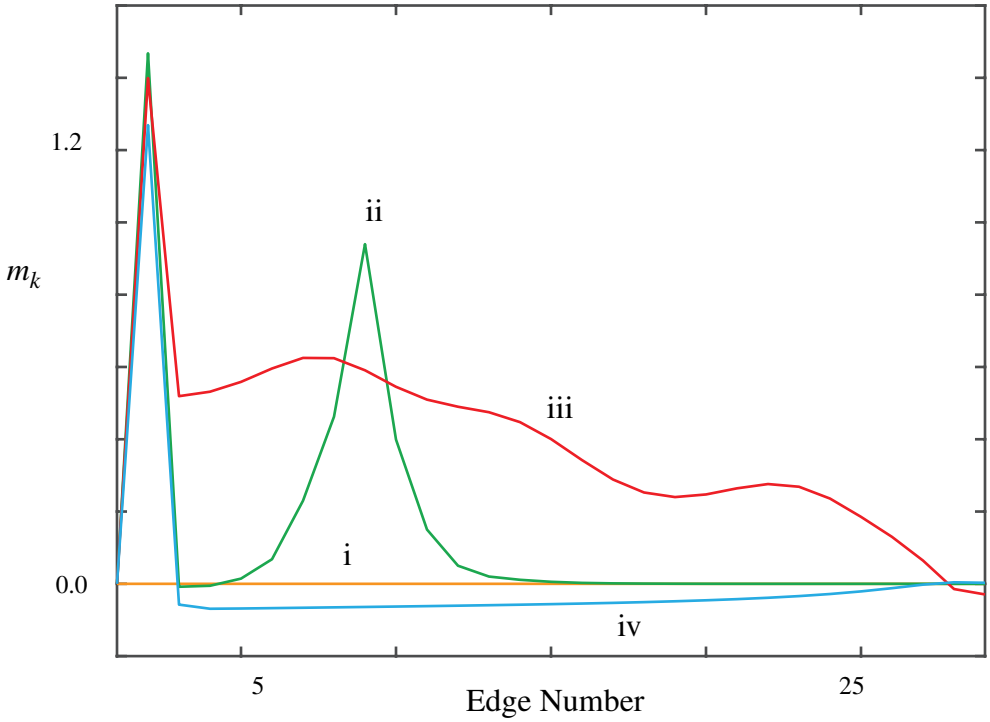

Fig. 2.16 *Evolution of the twist $m_k = \gamma^k - \gamma^{k-1} + m^k_{ref}$ in a coiled rod which is released from rest at time $t = 0$ and unwinds due to a gravitational force: i, $t = 0$; ii, $t = 0.2$ s; iii, $t = 0.5$ s; and iv, $t = 10$ s.*

The rod is assumed to have a length of 1 meter, a circular cross-section of radius 1 mm, a Young's modulus of 1 MPa, a Poisson's ratio of 0.5, and a mass density of 1000 kg/m^3. Initially, the rod is coiled into a right-handed circular helix of radius $R = 5$ cm and pitch angle $\gamma = \tan^{-1}(0.1)$. For the discrete elastic formulation, the rod is modeled as a discrete curve with 30 vertices. To account for the cantilevered boundary conditions, the first two vertices of the rod are fixed: i.e., $\mathbf{x}_0$ and $\mathbf{x}_1$ are constant.

Referring to Figures 2.15 and 2.16, as the rod unwinds, the discrete integrated twist m_k changes as does the reference twist m^k_{ref} in each of the edges. After the transients have died down, the centerline of the rod will be vertical and the rod will be stationary and in a state

of tension. As we shall see later in Chapter 4, the formula used to compute the reference twist can also be established using a concept known as holonomy.

Chapter 3

Variations and Hessians

3.1 Introduction

Expressions for changes to several kinematical quantities, including the discrete integrated curvature vector $\kappa_k \mathbf{b}_k$ and the material frame vectors $\mathbf{m}_1^k$ and $\mathbf{m}_2^k$, as the vertices are varied will be needed both to compute elastic forces in the discrete rod and to compute Hessians for Newton's method. The changes to the position vectors of the vertices are described by the variations $\delta\mathbf{x}_i$:

$$\mathbf{x}_0 \to \mathbf{x}_0 + \delta\mathbf{x}_0, \quad \ldots, \quad \mathbf{x}_k \to \mathbf{x}_k + \delta\mathbf{x}_k, \quad \ldots, \quad \mathbf{x}_{n-1} \to \mathbf{x}_{n-1} + \delta\mathbf{x}_{n-1}. \tag{3.1}$$

Among others, the variations in the vertices induces changes to tangent vectors, edge vectors, turning angles, curvatures, and referential twist m_{ref}^k. For instance, the variations (3.1) result in

$$\mathbf{e}^{k-1} \to \mathbf{e}^{k-1} + \delta\mathbf{e}^{k-1}, \qquad \mathbf{e}^k \to \mathbf{e}^k + \delta\mathbf{e}^k, \tag{3.2}$$

and

$$\mathbf{t}^{k-1} \to \mathbf{t}^{k-1} + \delta\mathbf{t}^{k-1}, \qquad \mathbf{t}^k \to \mathbf{t}^k + \delta\mathbf{t}^k. \tag{3.3}$$

After computing expressions for the variations induced by Eqn. (3.1), we will establish representations for the gradients and Hessians of various kinematical quantities including m_{ref}^k. Our exposition in this chapter provides detailed commentary on several results that are summarized in the papers by Bergou et al. [3, 4] and Kaldor et al. [26].

3.2 Notation for Gradients and Hessians

Given a scalar-valued function A and vectors $\mathbf{w} = \sum_{r=1}^3 w_r \mathbf{E}_r$ and $\mathbf{z} = \sum_{s=1}^3 z_s \mathbf{E}_s$, we use the following representations for the gradient of the scalar-valued function $A(\mathbf{w}, \mathbf{z})$

with respect to $\mathbf{w}$ and the second partial derivative of the scalar-valued function $A(\mathbf{w},\mathbf{z})$ with respect to a pair of vectors:

$$\frac{\partial A}{\partial \mathbf{w}} = \sum_{r=1}^{3} \frac{\partial A}{\partial w_r}\mathbf{E}_r, \qquad \frac{\partial^2 A}{\partial \mathbf{w}\partial \mathbf{z}} = \sum_{r=1}^{3}\sum_{s=1}^{3} \frac{\partial^2 A}{\partial w_s \partial z_r}\mathbf{E}_r \otimes \mathbf{E}_s. \tag{3.4}$$

The Hessian of A is the following 6×6 matrix:

$$\mathcal{H} = \begin{bmatrix} \left(\frac{\partial^2 A}{\partial \mathbf{w}\partial \mathbf{w}}\mathbf{E}_r\right)\cdot\mathbf{E}_s & \left(\frac{\partial^2 A}{\partial \mathbf{z}\partial \mathbf{w}}\mathbf{E}_r\right)\cdot\mathbf{E}_s \\ \left(\frac{\partial^2 A}{\partial \mathbf{w}\partial \mathbf{z}}\mathbf{E}_r\right)\cdot\mathbf{E}_s & \left(\frac{\partial^2 A}{\partial \mathbf{z}\partial \mathbf{z}}\mathbf{E}_r\right)\cdot\mathbf{E}_s \end{bmatrix}. \tag{3.5}$$

In this expression, the indices r and s range from 1 to 3. When computing Hessians, we invoke the facts that $\frac{\partial^2 A}{\partial \mathbf{w}\partial \mathbf{w}}$ and $\frac{\partial^2 A}{\partial \mathbf{z}\partial \mathbf{z}}$ are symmetric while

$$\frac{\partial^2 A}{\partial \mathbf{w}\partial \mathbf{z}} = \left(\frac{\partial^2 A}{\partial \mathbf{z}\partial \mathbf{w}}\right)^T. \tag{3.6}$$

In the interests of brevity, we only record non-zero components of a Hessian.

Consider a vector-valued function $\mathbf{A} = \mathbf{A}(\mathbf{w}) = \sum_{r=1}^{3} A_r\mathbf{E}_r$ where the vector $\mathbf{w} = \sum_{s=1}^{3} w_s\mathbf{E}_s$. The gradient of the vector-valued function $\mathbf{A}(\mathbf{w})$ with respect to $\mathbf{w}$ is a second-order tensor with the representation

$$\nabla_{\mathbf{w}}\mathbf{A} = \frac{\partial \mathbf{A}}{\partial \mathbf{w}} = \sum_{r=1}^{3}\sum_{s=1}^{3} \frac{\partial A_r}{\partial w_s}\mathbf{E}_r \otimes \mathbf{E}_s. \tag{3.7}$$

In addition, the following relation exists between the variation of $\mathbf{A}$ and the variation of $\mathbf{w}$: $\delta\mathbf{A} = \nabla_{\mathbf{w}}\mathbf{A}\delta\mathbf{w}$.

3.3 Variations of the Tangent Vectors

For the variation of the tangent vectors, we find, with the help of Taylor series expansions of $\left\|\mathbf{e}^{k-1}+\delta\mathbf{e}^{k-1}\right\|^{-1}$ and $\left\|\mathbf{e}^{k}+\delta\mathbf{e}^{k}\right\|^{-1}$ about $\delta\mathbf{e}^{k}=0$ and $\delta\mathbf{e}^{k-1}=0$, that

$$\begin{aligned} \delta\mathbf{t}^{k-1} &= \frac{\delta\mathbf{e}^{k-1}}{\left\|\mathbf{e}^{k-1}\right\|} - \left(\frac{\delta\mathbf{e}^{k-1}\cdot\mathbf{t}^{k-1}}{\left\|\mathbf{e}^{k-1}\right\|}\right)\mathbf{t}^{k-1} \\ &= \left(\mathbf{I}-\mathbf{t}^{k-1}\otimes\mathbf{t}^{k-1}\right)\frac{\delta\mathbf{e}^{k-1}}{\left\|\mathbf{e}^{k-1}\right\|}. \end{aligned} \tag{3.8}$$

The corresponding representations for $\delta\mathbf{t}^{k}$, $\delta\mathbf{t}^{k+1}$, $\delta\Delta\mathbf{t}_k$, and $\delta\mathbf{t}_{\mathcal{V}_k}$ are easily inferred. In the sequel, we will make extensive use of the fact that the variation of a unit vector is orthogonal to the vector. That is, if $\mathbf{t}\cdot\mathbf{t}=1$, then $\delta\mathbf{t}\cdot\mathbf{t}=0$.

3.4 Variation of the Turning Angle Between Two Edge Vectors

Consider the angle φ_k formed by two vectors $\mathbf{e}^{k-1}$ and $\mathbf{e}^k$. For this angle, we have the relations

$$\cos(\varphi_k) = \frac{\mathbf{e}^{k-1}\cdot\mathbf{e}^k}{\left\|\mathbf{e}^{k-1}\right\|\left\|\mathbf{e}^k\right\|} = \mathbf{t}^{k-1}\cdot\mathbf{t}^k, \tag{3.9}$$

and

$$\begin{aligned}\sin(\varphi_k) &= \frac{\mathbf{e}^{k-1}\times\mathbf{e}^k}{\left\|\mathbf{e}^{k-1}\times\mathbf{e}^k\right\|}\cdot\left(\frac{\mathbf{e}^{k-1}\times\mathbf{e}^k}{\left\|\mathbf{e}^{k-1}\right\|\left\|\mathbf{e}^k\right\|}\right)\\ &= \frac{\left\|\mathbf{e}^{k-1}\times\mathbf{e}^k\right\|}{\left\|\mathbf{e}^{k-1}\right\|\left\|\mathbf{e}^k\right\|}\\ &= \left\|\mathbf{t}^{k-1}\times\mathbf{t}^k\right\|.\end{aligned} \tag{3.10}$$

We also note that

$$\left\|\mathbf{e}^{k-1}\times\mathbf{e}^k\right\|^2 = \left\|\mathbf{e}^{k-1}\right\|^2\left\|\mathbf{e}^k\right\|^2 - \left(\mathbf{e}^{k-1}\cdot\mathbf{e}^k\right)^2. \tag{3.11}$$

Differentiating $\cos(\varphi_k)$ with respect to $\mathbf{e}^{k-1}$ we find that

$$-\sin(\varphi_k)\frac{\partial\varphi_k}{\partial\mathbf{e}^{k-1}} = \frac{\mathbf{e}^k}{\left\|\mathbf{e}^{k-1}\right\|\left\|\mathbf{e}^k\right\|} - \frac{\mathbf{e}^{k-1}}{\left\|\mathbf{e}^{k-1}\right\|^2}\left(\frac{\mathbf{e}^{k-1}\cdot\mathbf{e}^k}{\left\|\mathbf{e}^{k-1}\right\|\left\|\mathbf{e}^k\right\|}\right). \tag{3.12}$$

Substituting the expression $\sin(\varphi_k) = \left\|\mathbf{t}^{k-1}\times\mathbf{t}^k\right\|$, we conclude that

$$\begin{aligned}\frac{\partial\varphi_k}{\partial\mathbf{e}^{k-1}} &= -\frac{\mathbf{e}^k}{\left\|\mathbf{e}^{k-1}\times\mathbf{e}^k\right\|} + \frac{\mathbf{e}^{k-1}}{\left\|\mathbf{e}^{k-1}\right\|^2}\left(\frac{\mathbf{e}^{k-1}\cdot\mathbf{e}^k}{\left\|\mathbf{e}^{k-1}\times\mathbf{e}^k\right\|}\right)\\ &= \frac{\left(\mathbf{e}^{k-1}\cdot\mathbf{e}^k\right)\mathbf{e}^{k-1} - \left\|\mathbf{e}^{k-1}\right\|^2\mathbf{e}^k}{\left\|\mathbf{e}^{k-1}\right\|^2\left\|\mathbf{e}^{k-1}\times\mathbf{e}^k\right\|}\\ &= \frac{\mathbf{e}^{k-1}\times\left(\mathbf{e}^{k-1}\times\mathbf{e}^k\right)}{\left\|\mathbf{e}^{k-1}\right\|^2\left\|\mathbf{e}^{k-1}\times\mathbf{e}^k\right\|}.\end{aligned} \tag{3.13}$$

That is,

$$\frac{\partial \varphi_k}{\partial \mathbf{e}^{k-1}} = \frac{\mathbf{t}^{k-1}}{\left\|\mathbf{e}^{k-1}\right\|} \times \left(\frac{\mathbf{e}^{k-1} \times \mathbf{e}^{k}}{\left\|\mathbf{e}^{k-1} \times \mathbf{e}^{k}\right\|} \right). \tag{3.14}$$

Similarly,

$$\frac{\partial \varphi_k}{\partial \mathbf{e}^{k}} = -\frac{\mathbf{t}^{k}}{\left\|\mathbf{e}^{k}\right\|} \times \left(\frac{\mathbf{e}^{k-1} \times \mathbf{e}^{k}}{\left\|\mathbf{e}^{k-1} \times \mathbf{e}^{k}\right\|} \right). \tag{3.15}$$

As kindly communicated to us by Etienne Vouga [64], it is straightforward to use the results (3.14) and (3.15) to compute the derivatives $\frac{\partial \vartheta}{\partial \mathbf{a}^1}$ and $\frac{\partial \vartheta}{\partial \mathbf{a}^2}$ for the angle ϑ formed by two vectors $\mathbf{a}^1$ and $\mathbf{a}^2$: $\left\|\mathbf{a}^1\right\| \left\|\mathbf{a}^2\right\| \cos(\vartheta) = \mathbf{a}^1 \cdot \mathbf{a}^2$.

Because the turning angle φ_k is defined by the edge vectors $\mathbf{e}^{k-1}$ and $\mathbf{e}^{k}$, we can combine the representations (3.14) and (3.15) to conclude that

$$\begin{aligned} \delta \varphi_k &= \left(\frac{\mathbf{t}^{k-1}}{\left\|\mathbf{e}^{k-1}\right\|} \times \left(\frac{\mathbf{e}^{k-1} \times \mathbf{e}^{k}}{\left\|\mathbf{e}^{k-1} \times \mathbf{e}^{k}\right\|} \right) \right) \cdot \delta \mathbf{e}^{k-1} - \left(\frac{\mathbf{t}^{k}}{\left\|\mathbf{e}^{k}\right\|} \times \left(\frac{\mathbf{e}^{k-1} \times \mathbf{e}^{k}}{\left\|\mathbf{e}^{k-1} \times \mathbf{e}^{k}\right\|} \right) \right) \cdot \delta \mathbf{e}^{k} \\ &= \left(\frac{\mathbf{e}^{k-1} \times \mathbf{e}^{k}}{\left\|\mathbf{e}^{k-1} \times \mathbf{e}^{k}\right\|} \right) \cdot \left(\frac{\mathbf{t}^{k}}{\left\|\mathbf{e}^{k}\right\|} \times \delta \mathbf{e}^{k} - \frac{\mathbf{t}^{k-1}}{\left\|\mathbf{e}^{k-1}\right\|} \times \delta \mathbf{e}^{k-1} \right). \end{aligned} \tag{3.16}$$

This representation will be used in Chapter 4 to compute the variation of the interior angles of a spherical quadrilateral and a spherical triangle.

3.5 Variation of the Vector $(\kappa \mathbf{b})_k$

Using the representation (2.11) for $(\kappa \mathbf{b})_k$ that features the edge vectors and representations of the form (3.8) for the tangent vector, a representation for the variation of $(\kappa \mathbf{b})_k$ due to a variation of the edge vectors $\mathbf{e}^{k-1}$ and $\mathbf{e}^{k}$ can be found:

$$\begin{aligned} \delta (\kappa \mathbf{b})_k = {} & \frac{2\delta \mathbf{e}^{k-1} \times \mathbf{e}^{k}}{\left\|\mathbf{e}^{k-1}\right\| \left\|\mathbf{e}^{k}\right\| + \mathbf{e}^{k-1} \cdot \mathbf{e}^{k}} + \frac{2\mathbf{e}^{k-1} \times \delta \mathbf{e}^{k}}{\left\|\mathbf{e}^{k-1}\right\| \left\|\mathbf{e}^{k}\right\| + \mathbf{e}^{k-1} \cdot \mathbf{e}^{k}} \\ & \underbrace{- \frac{\left(\mathbf{e}^{k} + \left\|\mathbf{e}^{k}\right\| \mathbf{t}^{k-1}\right) \cdot \delta \mathbf{e}^{k-1}}{\left(\left\|\mathbf{e}^{k-1}\right\| \left\|\mathbf{e}^{k}\right\| + \mathbf{e}^{k-1} \cdot \mathbf{e}^{k}\right)} (\kappa \mathbf{b})_k}_{} \underbrace{- \frac{\left(\mathbf{e}^{k-1} + \left\|\mathbf{e}^{k-1}\right\| \mathbf{t}^{k}\right) \cdot \delta \mathbf{e}^{k}}{\left(\left\|\mathbf{e}^{k-1}\right\| \left\|\mathbf{e}^{k}\right\| + \mathbf{e}^{k-1} \cdot \mathbf{e}^{k}\right)} (\kappa \mathbf{b})_k}_{}. \end{aligned} \tag{3.17}$$

Manipulating this expression further by dividing by the magnitude of the edge vectors results in the following expressions:

$$\begin{aligned}\frac{1}{2}\delta\left(\kappa\mathbf{b}\right)_k &= \frac{\frac{\delta\mathbf{e}^{k-1}}{\left\|\mathbf{e}^{k-1}\right\|}\times\mathbf{t}^k}{1+\mathbf{t}^{k-1}\cdot\mathbf{t}^k}+\frac{\mathbf{t}^{k-1}\times\frac{\delta\mathbf{e}^k}{\left\|\mathbf{e}^k\right\|}}{1+\mathbf{t}^{k-1}\cdot\mathbf{t}^k}\\ &\quad-\left(\frac{\left(\kappa\mathbf{b}\right)_k}{1+\mathbf{t}^{k-1}\cdot\mathbf{t}^k}\right)\mathbf{t}_{\mathcal{V}_k}\cdot\left(\frac{\delta\mathbf{e}^{k-1}}{\left\|\mathbf{e}^{k-1}\right\|}+\frac{\delta\mathbf{e}^k}{\left\|\mathbf{e}^k\right\|}\right).\end{aligned} \tag{3.18}$$

Substituting for the variations of the vertices, we find that

$$\begin{aligned}\frac{1}{2}\delta\left(\kappa\mathbf{b}\right)_k &= \frac{\frac{\delta\mathbf{x}_k-\delta\mathbf{x}_{k-1}}{\left\|\mathbf{e}^{k-1}\right\|}\times\mathbf{t}^k}{1+\mathbf{t}^{k-1}\cdot\mathbf{t}^k}+\frac{\mathbf{t}^{k-1}\times\frac{\delta\mathbf{x}_{k+1}-\delta\mathbf{x}_k}{\left\|\mathbf{e}^k\right\|}}{1+\mathbf{t}^{k-1}\cdot\mathbf{t}^k}\\ &\quad-\left(\frac{\left(\kappa\mathbf{b}\right)_k}{1+\mathbf{t}^{k-1}\cdot\mathbf{t}^k}\right)f\end{aligned} \tag{3.19}$$

where

$$f = \frac{\left(\mathbf{t}^k+\mathbf{t}^{k-1}\right)}{2}\cdot\left(\frac{\delta\mathbf{x}_k-\delta\mathbf{x}_{k-1}}{\left\|\mathbf{e}^{k-1}\right\|}+\frac{\delta\mathbf{x}_{k+1}-\delta\mathbf{x}_k}{\left\|\mathbf{e}^k\right\|}\right). \tag{3.20}$$

With the help of Eqn. (3.7), the representation (3.19) for the variation of the curvature vector can be used to determine the tensors

$$\begin{aligned}\mathbf{G}_{k-1} &= \nabla_{k-1}\left(\kappa\mathbf{b}\right)_k = \frac{\partial\left(\kappa\mathbf{b}\right)_k}{\partial\mathbf{x}_{k-1}},\\ \mathbf{G}_k &= \nabla_k\left(\kappa\mathbf{b}\right)_k = \frac{\partial\left(\kappa\mathbf{b}\right)_k}{\partial\mathbf{x}_k},\\ \mathbf{G}_{k+1} &= \nabla_{k+1}\left(\kappa\mathbf{b}\right)_k = \frac{\partial\left(\kappa\mathbf{b}\right)_k}{\partial\mathbf{x}_{k+1}},\end{aligned} \tag{3.21}$$

which appear in Bergou et al. [4, Section 7]. For example,

$$\mathbf{G}_{k-1} = \frac{2\mathrm{skewt}\left(\mathbf{e}^k\right)}{\left\|\mathbf{e}^{k-1}\right\|\left\|\mathbf{e}^k\right\|+\mathbf{e}^{k-1}\cdot\mathbf{e}^k}+\frac{\left(\kappa\mathbf{b}\right)_k\otimes\left(\underbrace{\mathbf{e}^k+\left\|\mathbf{e}^k\right\|\mathbf{t}^{k-1}}\right)}{\left\|\mathbf{e}^{k-1}\right\|\left\|\mathbf{e}^k\right\|+\mathbf{e}^{k-1}\cdot\mathbf{e}^k}. \tag{3.22}$$

The underbraced term $(\mathbf{e}^k+\left\|\mathbf{e}^k\right\|\mathbf{t}^{k-1})$ in this expression differs from that presented in Bergou et al. [4, Section 7]. The difference can be traced to the underbraced terms in Eqn.

(3.17). Related remarks pertain to $\mathbf{G}_k$ and $\mathbf{G}_{k+1}$. It is also easy to observe from Eqn. (3.19) that

$$\nabla_k (\kappa \mathbf{b})_k = -\nabla_{k+1} (\kappa \mathbf{b})_k - \nabla_{k-1} (\kappa \mathbf{b})_k . \tag{3.23}$$

That is, $\mathbf{G}_{k-1} + \mathbf{G}_k + \mathbf{G}_{k+1} = 0$.

The derivatives of $(\kappa \mathbf{b})_k$ with respect to the edge vectors will be needed to compute gradients of force vector $\mathbf{F}_{t_i}$ in Section 5.5. From (3.19), we find that

$$\frac{\partial (\kappa \mathbf{b})_k}{\partial \mathbf{e}^{k-1}} = -\mathbf{G}_{k-1}, \qquad \frac{\partial (\kappa \mathbf{b})_k}{\partial \mathbf{e}^{k}} = \mathbf{G}_k. \tag{3.24}$$

From the definition of the vector $(\kappa \mathbf{b})_k$, it is straightforward to conclude the remaining gradients of this vector, such as

$$\frac{\partial (\kappa \mathbf{b})_k}{\partial \mathbf{e}^{k-3}}, \qquad \frac{\partial (\kappa \mathbf{b})_k}{\partial \mathbf{e}^{k-2}}, \qquad \frac{\partial (\kappa \mathbf{b})_k}{\partial \mathbf{e}^{k+1}}, \qquad \frac{\partial (\kappa \mathbf{b})_k}{\partial \mathbf{e}^{k+2}}, \tag{3.25}$$

etc., are all identically 0.

3.6 Variation of the Material Vectors $\mathbf{m}_1^k$ and $\mathbf{m}_2^k$

The variations of the vertices rigidly rotates the material vectors, the reference frame vectors, and the Bishop frame vectors. On each edge, the angles subtended by these vectors are unaltered. For instance, the angle ϑ^k between $\mathbf{u}^k$ and $\mathbf{m}_1^k$ and the angle γ^k between $\mathbf{a}_1^k$ and $\mathbf{m}_1^k$ are unchanged: $\delta \gamma^k = 0$ and $\delta \vartheta^k = 0$, among others.

To compute the variation of the material vectors due to variations of the edges, we recall Eqn. (2.90):

$$\begin{aligned}
\dot{\mathbf{m}}_1^k (t) &= \bar{\boldsymbol{\omega}}^k (t) \times \mathbf{m}_1^k (t) \\
&= \dot{\gamma}^k (t) \, \mathbf{m}_2^k (t) - \left(\mathbf{m}_1^k (t) \cdot \dot{\mathbf{t}}^k (t) \right) \mathbf{t}^k (t), \\
\dot{\mathbf{m}}_2^k (t) &= \bar{\boldsymbol{\omega}}^k (t) \times \mathbf{m}_2^k (t) \\
&= -\dot{\gamma}^k (t) \, \mathbf{m}_1^k (t) - \left(\mathbf{m}_2^k (t) \cdot \dot{\mathbf{t}}^k (t) \right) \mathbf{t}^k (t).
\end{aligned} \tag{3.26}$$

Noting that the variations of the edges does not alter the angle γ^k, enables us to conclude that

$$\begin{aligned}
\delta \mathbf{m}_1^k &= -\left(\mathbf{m}_1^k \cdot \delta \mathbf{t}^k \right) \mathbf{t}^k \\
&= \left(-\mathbf{t}^k \otimes \mathbf{m}_1^k \right) \delta \mathbf{t}^k, \\
\delta \mathbf{m}_2^k &= -\left(\mathbf{m}_2^k \cdot \delta \mathbf{t}^k \right) \mathbf{t}^k \\
&= \left(-\mathbf{t}^k \otimes \mathbf{m}_2^k \right) \delta \mathbf{t}^k.
\end{aligned} \tag{3.27}$$

It is important to note that $\delta \mathbf{m}_1^k$ and $\delta \mathbf{m}_2^k$ both lie in the direction of the tangent $\mathbf{t}^k$ and as a result are orthogonal to $(\kappa \mathbf{b})_{k-1}$, $(\kappa \mathbf{b})_k$, and $(\kappa \mathbf{b})_{k+1}$.

3.7 Variations and Gradients of the Curvatures κ_{k_1} and κ_{k_2}

The curvatures associated with the material frame at the kth vertex were defined in Eqn. (6.3):

$$\begin{aligned}\kappa_{k_1} &= \frac{1}{2}\left(\mathbf{m}_2^{k-1}+\mathbf{m}_2^{k}\right)\cdot(\kappa\mathbf{b})_k,\\ \kappa_{k_2} &= -\frac{1}{2}\left(\mathbf{m}_1^{k-1}+\mathbf{m}_1^{k}\right)\cdot(\kappa\mathbf{b})_k.\end{aligned} \tag{3.28}$$

As mentioned previously, the curvatures κ_{k_1} and κ_{k_2} were introduced in Bergou et al. [3] and are known as vertex-based material curvatures. They are used as the bending strains of the discrete elastic rod.

The variations of the curvatures κ_{k_1} and κ_{k_2} due to the variation of the vertices are

$$\begin{aligned}\delta\kappa_{k_1} &= \frac{1}{2}\left(\mathbf{m}_2^{k-1}+\mathbf{m}_2^{k}\right)\cdot\delta(\kappa\mathbf{b})_k+\frac{1}{2}\left(\delta\mathbf{m}_2^{k-1}+\delta\mathbf{m}_2^{k}\right)\cdot(\kappa\mathbf{b})_k,\\ \delta\kappa_{k_2} &= -\frac{1}{2}\left(\mathbf{m}_1^{k-1}+\mathbf{m}_1^{k}\right)\cdot\delta(\kappa\mathbf{b})_k-\frac{1}{2}\left(\delta\mathbf{m}_1^{k-1}+\delta\mathbf{m}_1^{k}\right)\cdot(\kappa\mathbf{b})_k.\end{aligned} \tag{3.29}$$

From the representations (3.27), we observe that $\delta\mathbf{m}_1^k$ is parallel to $\mathbf{t}^k$ and $\delta\mathbf{m}_1^{k-1}$ is parallel to $\mathbf{t}^{k-1}$. Consequently, both of these variations are orthogonal to $\mathbf{b}_k$. Identical remarks apply to $\delta\mathbf{m}_2^k$ and $\delta\mathbf{m}_2^{k-1}$. It follows that we can simplify the expressions for the variations to

$$\begin{aligned}\delta\kappa_{k_1} &= \frac{1}{2}\left(\mathbf{m}_2^{k-1}+\mathbf{m}_2^{k}\right)\cdot\delta(\kappa\mathbf{b})_k,\\ \delta\kappa_{k_2} &= -\frac{1}{2}\left(\mathbf{m}_1^{k-1}+\mathbf{m}_1^{k}\right)\cdot\delta(\kappa\mathbf{b})_k.\end{aligned} \tag{3.30}$$

These final expressions are identical to those in the literature (cf. Bergou et al. [3]).[1]

To compute the gradient of a scalar v with respect to a vector $\mathbf{u}$, we make use of the identities

$$\dot{v}=\frac{\partial v}{\partial\mathbf{u}}\cdot\dot{\mathbf{u}},\qquad \delta v=\frac{\partial v}{\partial\mathbf{u}}\cdot\delta\mathbf{u}. \tag{3.31}$$

Thus, to compute $\frac{\partial\kappa_{k_1}}{\partial\mathbf{e}^{k-1}}$ and $\frac{\partial\kappa_{k_1}}{\partial\mathbf{e}^{k}}$, we appeal to the expression $(3.29)_1$ for $\delta\kappa_{k_1}$ and then invoke the representation (3.18) for $\delta(\kappa\mathbf{b})_k$ with $\delta\mathbf{e}^k$ and $\delta\mathbf{e}^{k-1}$ set to zero, respectively.

[1] It is tempting to assume (in error) that the material vectors are unaltered by the change in the vertices. However, as the variations in $\mathbf{m}_1^{k-1}$, $\mathbf{m}_2^{k-1}$, $\mathbf{m}_1^k$, and $\mathbf{m}_2^k$ induced by variations in the vertices are orthogonal to $(\kappa\mathbf{b})_k$, the variations $\delta\mathbf{m}_1^{k-1}$, $\delta\mathbf{m}_2^{k-1}$, $\delta\mathbf{m}_1^k$, and $\delta\mathbf{m}_2^k$ are absent in the final expressions for $\delta\kappa_{k_1}$ and $\delta\kappa_{k_2}$.

The resulting intermediate expressions for $\frac{\partial \kappa_{k_1}}{\partial \mathbf{e}^{k-1}}$ and $\frac{\partial \kappa_{k_1}}{\partial \mathbf{e}^{k}}$ are exceptionally lengthy:

$$\begin{aligned}\frac{\partial \kappa_{k_1}}{\partial \mathbf{e}^{k-1}} \cdot \delta \mathbf{e}^{k-1} &= \frac{1}{2}\left(\mathbf{m}_2^{k-1}+\mathbf{m}_2^{k}\right)\cdot\left(\frac{2\frac{\delta \mathbf{e}^{k-1}}{\left\|\mathbf{e}^{k-1}\right\|}\times \mathbf{t}^k}{1+\mathbf{t}^{k-1}\cdot\mathbf{t}^k}\right.\\ &\quad \left.-\frac{(\kappa \mathbf{e}_b)_k}{1+\mathbf{t}^{k-1}\cdot\mathbf{t}^k}\left(\mathbf{t}^k+\mathbf{t}^{k-1}\right)\cdot\left(\frac{\delta \mathbf{e}^{k-1}}{\left\|\mathbf{e}^{k-1}\right\|}\right)\right)\\ &= -\left(\frac{1}{2}\left(\mathbf{m}_2^{k-1}+\mathbf{m}_2^{k}\right)\times\left(\frac{2\mathbf{t}^k}{1+\mathbf{t}^{k-1}\cdot\mathbf{t}^k}\right)+\kappa_{k_1}\tilde{\mathbf{t}}\right)\cdot\frac{\delta \mathbf{e}^{k-1}}{\left\|\mathbf{e}^{k-1}\right\|},\end{aligned} \tag{3.32}$$

and

$$\begin{aligned}\frac{\partial \kappa_{k_1}}{\partial \mathbf{e}^{k}} \cdot \delta \mathbf{e}^{k} &= \frac{1}{2}\left(\mathbf{m}_2^{k-1}+\mathbf{m}_2^{k}\right)\cdot\left(\frac{2\mathbf{t}^{k-1}\times\frac{\delta \mathbf{e}^{k}}{\left\|\mathbf{e}^{k}\right\|}}{1+\mathbf{t}^{k-1}\cdot\mathbf{t}^k}\right.\\ &\quad \left.-\frac{(\kappa \mathbf{b})_k}{1+\mathbf{t}^{k-1}\cdot\mathbf{t}^k}\left(\mathbf{t}^k+\mathbf{t}^{k-1}\right)\cdot\left(\frac{\delta \mathbf{e}^{k}}{\left\|\mathbf{e}^{k}\right\|}\right)\right)\\ &= \left(\frac{1}{2}\left(\mathbf{m}_2^{k-1}+\mathbf{m}_2^{k}\right)\times\left(\frac{2\mathbf{t}^{k-1}}{1+\mathbf{t}^{k-1}\cdot\mathbf{t}^k}\right)-\kappa_{k_1}\tilde{\mathbf{t}}\right)\cdot\frac{\delta \mathbf{e}^{k}}{\left\|\mathbf{e}^{k}\right\|}.\end{aligned} \tag{3.33}$$

To simplify these expressions we have used the definition (2.14) of the vector

$$\tilde{\mathbf{t}} = \frac{\mathbf{t}^{k-1}+\mathbf{t}^k}{1+\mathbf{t}^{k-1}\cdot\mathbf{t}^k}. \tag{3.34}$$

In conclusion, we find the following representations for the gradients of κ_{k_1}:

$$\begin{aligned}\frac{\partial \kappa_{k_1}}{\partial \mathbf{e}^{k-1}} &= \frac{1}{\left\|\mathbf{e}^{k-1}\right\|}\left(-\kappa_{k_1}\tilde{\mathbf{t}}+\mathbf{t}^k\times\left(\frac{\mathbf{m}_2^{k-1}+\mathbf{m}_2^{k}}{1+\mathbf{t}^{k-1}\cdot\mathbf{t}^k}\right)\right),\\ \frac{\partial \kappa_{k_1}}{\partial \mathbf{e}^{k}} &= \frac{1}{\left\|\mathbf{e}^{k}\right\|}\left(-\kappa_{k_1}\tilde{\mathbf{t}}-\mathbf{t}^{k-1}\times\left(\frac{\mathbf{m}_2^{k-1}+\mathbf{m}_2^{k}}{1+\mathbf{t}^{k-1}\cdot\mathbf{t}^k}\right)\right).\end{aligned} \tag{3.35}$$

These results agree with the expressions presented in Bergou et al. [3, Appendix A]. The corresponding results for κ_{k_2} are

$$\begin{aligned}
\frac{\partial \kappa_{k_2}}{\partial \mathbf{e}^{k-1}} &= \frac{1}{\left\|\mathbf{e}^{k-1}\right\|}\left(-\kappa_{k_2}\tilde{\mathbf{t}} - \mathbf{t}^k \times \left(\frac{\mathbf{m}_1^{k-1} + \mathbf{m}_1^k}{1 + \mathbf{t}^{k-1}\cdot\mathbf{t}^k}\right)\right), \\
\frac{\partial \kappa_{k_2}}{\partial \mathbf{e}^{k}} &= \frac{1}{\left\|\mathbf{e}^{k}\right\|}\left(-\kappa_{k_2}\tilde{\mathbf{t}} + \mathbf{t}^{k-1} \times \left(\frac{\mathbf{m}_1^{k-1} + \mathbf{m}_1^k}{1 + \mathbf{t}^{k-1}\cdot\mathbf{t}^k}\right)\right).
\end{aligned} \tag{3.36}$$

We shall shortly use these expressions to compute Hessians.

3.8 Gradients and Time Derivative of the Reference Twist m^k_{ref}

As shall be discussed in Chapter 4 (cf. Eqn. (4.44)), the variation of the reference twist is the component of the discrete curvature vector along the variation in the averaged tangent vector:

$$\frac{dm^k_{\text{ref}}}{d\varepsilon} = (\kappa \mathbf{b})_k \cdot \frac{d\mathbf{t}_{\mathcal{V}_k}}{d\varepsilon}, \tag{3.37}$$

where ε is a scalar used to parameterize the change in the vector $\mathbf{t}_{\mathcal{V}_k}$. It is interesting to note an immediate implication of this result: If the vertices are only displaced in the plane normal to $\mathbf{b}_k$, there will be no change to the reference twist.

Invoking expressions such as Eqn. (3.8) to compute $\delta \mathbf{t}_{\mathcal{V}_k} = \frac{d\mathbf{t}_{\mathcal{V}_k}}{d\varepsilon}\delta\varepsilon$, we find that

$$\delta m^k_{\text{ref}} = \frac{\mathbf{t}^{k-1} \times \mathbf{t}^k}{1 + \mathbf{t}^{k-1}\cdot\mathbf{t}^k} \cdot \left(\frac{\delta \mathbf{e}^{k-1}}{\left\|\mathbf{e}^{k-1}\right\|} + \frac{\delta \mathbf{e}^k}{\left\|\mathbf{e}^k\right\|}\right), \tag{3.38}$$

where $\delta m^k_{\text{ref}} = \frac{dm^k_{\text{ref}}}{d\varepsilon}\delta\varepsilon$. Whence,

$$\begin{aligned}
\frac{\partial m^k_{\text{ref}}}{\partial \mathbf{e}^{k-1}} &= \left(\frac{1}{2\left\|\mathbf{e}^{k-1}\right\|}\right)(\kappa\mathbf{b})_k\,,\\
\frac{\partial m^k_{\text{ref}}}{\partial \mathbf{e}^{k}} &= \left(\frac{1}{2\left\|\mathbf{e}^{k}\right\|}\right)(\kappa\mathbf{b})_k\,,\\
\frac{\partial m^k_{\text{ref}}}{\partial \mathbf{x}_{k-1}} &= -\left(\frac{1}{2\left\|\mathbf{e}^{k-1}\right\|}\right)(\kappa\mathbf{b})_k\,,\\
\frac{\partial m^k_{\text{ref}}}{\partial \mathbf{x}_{k+1}} &= \left(\frac{1}{2\left\|\mathbf{e}^{k}\right\|}\right)(\kappa\mathbf{b})_k\,,\\
\frac{\partial m^k_{\text{ref}}}{\partial \mathbf{x}_{k}} &= -\left(\frac{1}{2\left\|\mathbf{e}^{k}\right\|}-\frac{1}{2\left\|\mathbf{e}^{k-1}\right\|}\right)(\kappa\mathbf{b})_k\,.
\end{aligned} \tag{3.39}$$

These representations for the gradients of m^k_{ref} agree with expressions for the variation of an angle m in Bergou et al. [3, Appendix A], and modulo a sign difference (which we believe to be a typographical error) for the variation of an angle ψ_k in Bergou et al. [4, Section 6, Eqn. (9)] and a related expression in Kaldor et al. [26, Appendix A] for the derivatives of an angle $\hat{\theta}^k$. Referring to Eqn. (2.81), the quantity m in [3] corresponds to $m_k = \gamma^k - \gamma^{k-1} + m^k_{\text{ref}}$. The angle $\hat{\theta}^k$ in Kaldor et al. [26, Appendix A] corresponds to the angle m^k_{ref}.

For future purposes, we will also need to compute $\dot{m}^k_{\text{ref}}$. Appealing to Eqn. (3.38), after replacing the variation with the time derivative, we quickly find that

$$\dot{m}^k_{\text{ref}} = \frac{\mathbf{t}^{k-1}\times\mathbf{t}^k}{1+\mathbf{t}^{k-1}\cdot\mathbf{t}^k}\cdot\left(\frac{\dot{\mathbf{e}}^{k-1}}{\left\|\mathbf{e}^{k-1}\right\|}+\frac{\dot{\mathbf{e}}^{k}}{\left\|\mathbf{e}^{k}\right\|}\right). \tag{3.40}$$

Substituting for the curvature vector and the time derivatives of the edge vectors, it can be shown that the time derivative has the following representation:

$$\begin{aligned}
\dot{m}^k_{\text{ref}} \;=\; & -\frac{1}{2\left\|\mathbf{e}^{k-1}\right\|}(\kappa\mathbf{b})_k\cdot\dot{\mathbf{x}}_{k-1}. + \frac{1}{2\left\|\mathbf{e}^{k}\right\|}(\kappa\mathbf{b})_k\cdot\dot{\mathbf{x}}_{k+1}\\
& + \left(\frac{1}{2\left\|\mathbf{e}^{k-1}\right\|}-\frac{1}{2\left\|\mathbf{e}^{k}\right\|}\right)(\kappa\mathbf{b})_k\cdot\dot{\mathbf{x}}_k.
\end{aligned} \tag{3.41}$$

This representation will be used in Section 5.4 when constitutive relations for forces and moments are established.

3.9 Preliminary Results for Computing Hessians

We now turn to computing the Hessians of the twist m_k and the curvatures κ_{k_1} and κ_{k_2}. The reader is referred to Section 3.2 for details on the notation used in defining these second order tensors. As a preliminary calculation, we note that

$$\begin{aligned}
\frac{\partial}{\partial \mathbf{e}^i}\left(\frac{1}{\left\|\mathbf{e}^k\right\|}\right) &= -\frac{\mathbf{e}^i}{\left\|\mathbf{e}^i\right\|^3}\delta_i^k,\\
\frac{\partial}{\partial \mathbf{e}^i}\left(\mathbf{t}^k = \frac{\mathbf{e}^k}{\left\|\mathbf{e}^k\right\|}\right) &= \frac{1}{\left\|\mathbf{e}^k\right\|}\left(\mathbf{I} - \frac{\mathbf{e}^k}{\left\|\mathbf{e}^k\right\|}\otimes\frac{\mathbf{e}^k}{\left\|\mathbf{e}^k\right\|}\right)\delta_i^k,\\
\frac{\partial}{\partial \mathbf{e}^i}\left(\frac{\mathbf{e}^k}{\left\|\mathbf{e}^k\right\|}\times\mathbf{a}\right) &= -\frac{1}{\left\|\mathbf{e}^k\right\|}\left(\left(\frac{\mathbf{e}^k}{\left\|\mathbf{e}^k\right\|}\times\mathbf{a}\right)\otimes\frac{\mathbf{e}^k}{\left\|\mathbf{e}^k\right\|} + \operatorname{skewt}(\mathbf{a})\right)\delta_i^k\\
&= -\frac{1}{\left\|\mathbf{e}^k\right\|}\left(\left(\mathbf{t}^k\times\mathbf{a}\right)\otimes\mathbf{t}^k + \operatorname{skewt}(\mathbf{a})\right)\delta_i^k,\\
\frac{\partial}{\partial \mathbf{e}^i}\left(\left(\kappa\mathbf{b}\right)_k\times\mathbf{a}\right) &= \left(\frac{\partial\left(\kappa\mathbf{b}\right)_k}{\partial \mathbf{e}^i}\right)^T\mathbf{a}.
\end{aligned} \tag{3.42}$$

The vector $\mathbf{a}$ in Eqn. $(3.42)_{3,4}$ is assumed to be constant, δ_i^k is the Kronecker delta, and the gradient of $\left(\kappa\mathbf{b}\right)_k$ can be inferred from Eqn. (3.18). The identities (3.42) are appealed to extensively in the sequel.

It is convenient to define a scalar χ:

$$\chi = 1 + \mathbf{t}^{k-1}\cdot\mathbf{t}^k. \tag{3.43}$$

Whence,

$$\begin{aligned}
\frac{\partial\chi}{\partial \mathbf{e}^{k-1}} &= \frac{1}{\left\|\mathbf{e}^{k-1}\right\|}\left(\mathbf{I} - \mathbf{t}^{k-1}\otimes\mathbf{t}^{k-1}\right)\mathbf{t}^k,\\
\frac{\partial\chi}{\partial \mathbf{e}^{k}} &= \frac{1}{\left\|\mathbf{e}^{k}\right\|}\left(\mathbf{I} - \mathbf{t}^{k}\otimes\mathbf{t}^{k}\right)\mathbf{t}^{k-1},
\end{aligned} \tag{3.44}$$

and

$$\begin{aligned}
\frac{\partial\tilde{\mathbf{t}}}{\partial \mathbf{e}^{k-1}} &= \frac{1}{\chi\left\|\mathbf{e}^{k-1}\right\|}\left(\left(\mathbf{I} - \mathbf{t}^{k-1}\otimes\mathbf{t}^{k-1}\right) - \tilde{\mathbf{t}}\otimes\left(\left(\mathbf{I} - \mathbf{t}^{k-1}\otimes\mathbf{t}^{k-1}\right)\mathbf{t}^k\right)\right),\\
\frac{\partial\tilde{\mathbf{t}}}{\partial \mathbf{e}^{k}} &= \frac{1}{\chi\left\|\mathbf{e}^{k}\right\|}\left(\left(\mathbf{I} - \mathbf{t}^{k}\otimes\mathbf{t}^{k}\right) - \tilde{\mathbf{t}}\otimes\left(\left(\mathbf{I} - \mathbf{t}^{k}\otimes\mathbf{t}^{k}\right)\mathbf{t}^{k-1}\right)\right),
\end{aligned} \tag{3.45}$$

where it might be helpful for some readers to recall that $\chi\tilde{\mathbf{t}} = \mathbf{t}^{k-1} + \mathbf{t}^k$.

3.10 Hessians of the Reference Twist m^k_{ref}

The first Hessian we compute pertains to m^k_{ref}. To proceed, we recall from Eqn. (3.39) that

$$\frac{\partial m^k_{\text{ref}}}{\partial \mathbf{e}^{k-1}} = \left(\frac{1}{2\left\|\mathbf{e}^{k-1}\right\|}\right)(\kappa\mathbf{b})_k, \qquad \frac{\partial m^k_{\text{ref}}}{\partial \mathbf{e}^{k}} = \left(\frac{1}{2\left\|\mathbf{e}^{k}\right\|}\right)(\kappa\mathbf{b})_k. \tag{3.46}$$

Using Eqn. $(3.42)_1$, we find that

$$\frac{\partial^2 m^k_{\text{ref}}}{\partial \mathbf{e}^k \partial \mathbf{e}^k} = -\text{sym}\left(\frac{1}{2\left\|\mathbf{e}^k\right\|^3}(\kappa\mathbf{b})_k \otimes \mathbf{e}^k - \frac{1}{2\left\|\mathbf{e}^k\right\|}\frac{\partial (\kappa\mathbf{b})_k}{\partial \mathbf{e}^k}\right). \tag{3.47}$$

Referring to Eqn. (3.18), we previously computed the variation of $(\kappa\mathbf{b})_k$ and this expression can be used to infer a representation for $\frac{\partial(\kappa\mathbf{b})_k}{\partial \mathbf{e}^k}$:

$$\frac{\partial (\kappa\mathbf{b})_k}{\partial \mathbf{e}^k} = -\frac{2}{\left\|\mathbf{e}^k\right\|}\left(\frac{(\kappa\mathbf{b})_k}{1+\mathbf{t}^{k-1}\cdot\mathbf{t}^k}\right)\otimes\mathbf{t}_{\mathcal{V}_k} + \frac{2\,\text{skewt}\left(\mathbf{t}^{k-1}\right)}{\left\|\mathbf{e}^k\right\|\left(1+\mathbf{t}^k\cdot\mathbf{t}^{k-1}\right)}. \tag{3.48}$$

Substituting this expression in Eqn. (3.47) and noting that the symmetric part of a skew-symmetric tensor is 0, we conclude that a portion of the Hessian has the following representations:

$$\begin{aligned}\frac{\partial^2 m^k_{\text{ref}}}{\partial \mathbf{e}^k \partial \mathbf{e}^k} &= -\frac{1}{\left\|\mathbf{e}^k\right\|^2}\text{sym}\left(\frac{1}{2}(\kappa\mathbf{b})_k\otimes\mathbf{t}^k + \left(\frac{(\kappa\mathbf{b})_k}{1+\mathbf{t}^{k-1}\cdot\mathbf{t}^k}\right)\otimes\mathbf{t}_{\mathcal{V}_k}\right)\\ &= -\frac{1}{2\left\|\mathbf{e}^k\right\|^2}\text{sym}\left((\kappa\mathbf{b})_k\otimes\mathbf{t}^k + (\kappa\mathbf{b})_k\otimes\tilde{\mathbf{t}}\right).\end{aligned} \tag{3.49}$$

In writing the second representation, we used the definition (2.14) of the vector $\tilde{\mathbf{t}}$. A similar line of argument yields the representations

$$\begin{aligned}\frac{\partial^2 m^k_{\text{ref}}}{\partial \mathbf{e}^{k-1} \partial \mathbf{e}^{k-1}} &= -\frac{1}{\left\|\mathbf{e}^{k-1}\right\|^2}\text{sym}\left(\frac{1}{2}(\kappa\mathbf{b})_k\otimes\mathbf{t}^{k-1} + \left(\frac{(\kappa\mathbf{b})_k}{1+\mathbf{t}^{k-1}\cdot\mathbf{t}^k}\right)\otimes\mathbf{t}_{\mathcal{V}_k}\right)\\ &= -\frac{1}{2\left\|\mathbf{e}^{k-1}\right\|^2}\text{sym}\left((\kappa\mathbf{b})_k\otimes\mathbf{t}^{k-1} + (\kappa\mathbf{b})_k\otimes\tilde{\mathbf{t}}\right).\end{aligned} \tag{3.50}$$

The third part of the Hessian is the easiest to compute:

$$\begin{aligned}\left(\frac{\partial^2 m^k_{\text{ref}}}{\partial \mathbf{e}^{k-1}\partial \mathbf{e}^k}\right)^T &= \frac{\partial^2 m^k_{\text{ref}}}{\partial \mathbf{e}^k \partial \mathbf{e}^{k-1}} \\ &= \frac{1}{2\left\|\mathbf{e}^{k-1}\right\|}\frac{\partial\left(\kappa\mathbf{b}\right)_k}{\partial \mathbf{e}^k} \\ &= \frac{\text{skewt}\left(\mathbf{t}^{k-1}\right)}{\left\|\mathbf{e}^{k-1}\right\|\left\|\mathbf{e}^k\right\|\left(1+\mathbf{t}^k\cdot\mathbf{t}^{k-1}\right)} - \frac{1}{\left\|\mathbf{e}^{k-1}\right\|\left\|\mathbf{e}^k\right\|}\left(\frac{\left(\kappa\mathbf{b}\right)_k}{1+\mathbf{t}^{k-1}\cdot\mathbf{t}^k}\right)\otimes\mathbf{t}_{\nu_k}.\end{aligned} \tag{3.51}$$

Observe that we appealed to Eqn. (3.48) to establish the final form of the representation. For completeness, we note that the representations (3.49), (3.50), and (3.51) are identical to the expressions for the Hessian of m recorded in Bergou et al. [3, Appendix A].

3.11 Hessians of the Curvatures κ_{k_1} and κ_{k_2}

The computation of the Hessians for the curvatures κ_{k_1} and κ_{k_2} are considerably lengthier than the corresponding calculations for the twist. We restrict ourselves to a brief summary of the computations and invite the reader to compare our expressions (cf. Eqns. (3.55), (3.57), and (3.58)) to those recorded in Bergou et al. [3, Appendix A].

Starting from Eqn. $(3.35)_1$:

$$\begin{aligned}\frac{\partial\kappa_{k_1}}{\partial\mathbf{e}^{k-1}} &= \frac{1}{\left\|\mathbf{e}^{k-1}\right\|}\left(-\kappa_{k_1}\tilde{\mathbf{t}}+\frac{1}{\chi}\mathbf{t}^k\times\left(\mathbf{m}_2^{k-1}+\mathbf{m}_2^k\right)\right) \\ &= \frac{1}{\left\|\mathbf{e}^{k-1}\right\|}\left(-\kappa_{k_1}\tilde{\mathbf{t}}+\mathbf{t}^k\times\tilde{\mathbf{m}}_2\right),\end{aligned} \tag{3.52}$$

where

$$\tilde{\mathbf{m}}_2 = \frac{1}{\chi}\left(\mathbf{m}_2^{k-1}+\mathbf{m}_2^k\right). \tag{3.53}$$

Hence,

$$\frac{\partial \kappa_{k_1}}{\partial \mathbf{e}^{k-1}\partial \mathbf{e}^{k-1}} = -\frac{1}{\left\|\mathbf{e}^{k-1}\right\|}\mathrm{sym}\left(\tilde{\mathbf{t}}\otimes\underbrace{\frac{\partial \kappa_{k_1}}{\partial \mathbf{e}^{k-1}}}_{(3.52)} + \underbrace{\frac{\partial \kappa_{k_1}}{\partial \mathbf{e}^{k-1}}}_{(3.52)}\otimes\mathbf{t}^k + \kappa_{k_1}\underbrace{\frac{\partial \tilde{\mathbf{t}}}{\partial \mathbf{e}^{k-1}}}_{(3.45)}\right)$$
$$-\frac{1}{\left\|\mathbf{e}^{k-1}\right\|}\mathrm{sym}\left(\frac{1}{\chi^2}\left(\mathbf{t}^k\times\left(\mathbf{m}_2^{k-1}+\mathbf{m}_2^k\right)\right)\otimes\underbrace{\frac{\partial \chi}{\partial \mathbf{e}^{k-1}}}_{(3.44)}\right)$$
$$-\frac{1}{\left\|\mathbf{e}^{k-1}\right\|}\mathrm{sym}\left(\frac{1}{\chi}\underbrace{\left(\frac{\partial \mathbf{t}^k}{\partial \mathbf{e}^{k-1}}\right)^T}_{=0}\left(\mathbf{m}_2^{k-1}+\mathbf{m}_2^k\right)\right). \tag{3.54}$$

The equations numbers below the underbrace indicate the substitutions that we can use to evaluate an expression. After combining terms in the above expression, we find that

$$\frac{\partial \kappa_{k_1}}{\partial \mathbf{e}^{k-1}\partial \mathbf{e}^{k-1}} = -\frac{1}{\left\|\mathbf{e}^{k-1}\right\|}\mathrm{sym}\left(\left(\tilde{\mathbf{t}}+\mathbf{t}^k\right)\otimes\underbrace{\frac{\partial \kappa_{k_1}}{\partial \mathbf{e}^{k-1}}}_{(3.52)} + \kappa_{k_1}\underbrace{\frac{\partial \tilde{\mathbf{t}}}{\partial \mathbf{e}^{k-1}}}_{(3.45)}\right)$$
$$-\frac{1}{\left\|\mathbf{e}^{k-1}\right\|}\mathrm{sym}\left(\frac{1}{\chi}\left(\mathbf{t}^k\times\tilde{\mathbf{m}}_2\right)\otimes\underbrace{\frac{\partial \chi}{\partial \mathbf{e}^{k-1}}}_{(3.44)}\right). \tag{3.55}$$

To find the second set of terms for the Hessian, we start from Eqn. $(3.35)_2$:

$$\frac{\partial \kappa_{k_1}}{\partial \mathbf{e}^{k}} = -\frac{1}{\left\|\mathbf{e}^{k}\right\|}\left(\kappa_{k_1}\tilde{\mathbf{t}}+\mathbf{t}^{k-1}\times\tilde{\mathbf{m}}_2\right). \tag{3.56}$$

Paralleling the previous set of calculations, we find the following representation:

$$\frac{\partial \kappa_{k_1}}{\partial \mathbf{e}^{k}\partial \mathbf{e}^{k}} = -\frac{1}{\left\|\mathbf{e}^{k}\right\|}\mathrm{sym}\left(\left(\tilde{\mathbf{t}}+\mathbf{t}^{k-1}\right)\otimes\underbrace{\frac{\partial \kappa_{k_1}}{\partial \mathbf{e}^{k}}}_{(3.56)} + \kappa_{k_1}\underbrace{\frac{\partial \tilde{\mathbf{t}}}{\partial \mathbf{e}^{k}}}_{(3.45)}\right)$$
$$-\frac{1}{\left\|\mathbf{e}^{k}\right\|}\mathrm{sym}\left(\frac{1}{\chi}\left(\mathbf{t}^{k-1}\times\tilde{\mathbf{m}}_2\right)\otimes\underbrace{\frac{\partial \chi}{\partial \mathbf{e}^{k}}}_{(3.44)}\right). \tag{3.57}$$

To compute the final components of the Hessian, we again start from the expression (3.52) for $\frac{\partial \kappa_{k_1}}{\partial \mathbf{e}^{k-1}}$ and take the derivative of this expression with respect to $\mathbf{e}^k$. With some minor rearranging, we find that

$$\frac{\partial \kappa_{k_1}}{\partial \mathbf{e}^k \partial \mathbf{e}^{k-1}} = -\frac{1}{\left\|\mathbf{e}^{k-1}\right\|}\left(\tilde{\mathbf{t}} \otimes \underbrace{\frac{\partial \kappa_{k_1}}{\partial \mathbf{e}^k}}_{(3.56)} + \kappa_{k_1} \underbrace{\frac{\partial \tilde{\mathbf{t}}}{\partial \mathbf{e}^k}}_{(3.45)}\right)$$
$$-\frac{1}{\left\|\mathbf{e}^{k-1}\right\|}\left(\frac{1}{\chi}\left(\mathbf{t}^k \times \tilde{\mathbf{m}}_2\right) \otimes \underbrace{\frac{\partial \chi}{\partial \mathbf{e}^k}}_{(3.44)} + \underbrace{\left(\frac{\partial \mathbf{t}^k}{\partial \mathbf{e}^k}\right)^T}_{(3.42)} \tilde{\mathbf{m}}_2\right). \tag{3.58}$$

The corresponding expressions for the Hessian of κ_{k_2} are obtained from Eqns. (3.55), (3.57), and (3.58) by setting $\kappa_{k_1} \to \kappa_{k_2}$ and $\tilde{\mathbf{m}}_2 \to \tilde{\mathbf{m}}_1$.

Chapter 4

Spherical Excess and Reference Twist

4.1 Introduction

The method by which a component of the rotation of the cross-section is computed in discrete elastic rods is exceptional and exploits a phenomenon in differential geometry known as a holonomy. In particular, a classic result from spherical geometry is used to show that the change in the reference twist can be related to a solid angle or, as it is also known in this context, spherical excess:

$$f^k(\varepsilon) = \Delta m^k_{\text{ref}}(\varepsilon) = m^k_{\text{ref}}(\varepsilon) - m^k_{\text{ref}}(0). \tag{4.1}$$

In addition, the following expression for the variation of the reference twist is employed in [3, 26]:

$$\frac{dm^k_{\text{ref}}}{d\varepsilon} = (\kappa \mathbf{b})_k \cdot \frac{d\mathbf{t}_{\mathcal{V}_k}}{d\varepsilon}. \tag{4.2}$$

The purpose of the present chapter is to provide details on the calculations needed to establish these representations for $\Delta m^k_{\text{ref}}(\varepsilon)$ and its derivative.

By way of background, the method used to establish the aforementioned representations has its genesis in the following remarkable result which can be found in Kelvin and Tait's Treatise on Natural Philosophy [27, 59, Section 123]. Imagine a line element in a rigid body which we define by a unit vector $\mathbf{e} = \mathbf{e}(t)$ that is fixed to the rigid body. Suppose after a time interval $t_1 - t_0$, $\mathbf{e}(t_1) = \mathbf{e}(t_0)$. Then, the rotation $\Delta\nu$ of the body about $\mathbf{e}(t_0)$ during the time interval can be determined modulo 2π by computing the solid angle A enclosed by the path traced out by $\mathbf{e}(t)$ on the unit sphere and the integral of a component of the angular velocity vector $\boldsymbol{\omega}$ of the rigid body:

$$\Delta\nu = \int_{t_0}^{t_1} \boldsymbol{\omega} \cdot \mathbf{e}(\tau)\, d\tau + A \quad \text{modulo } 2\pi. \tag{4.3}$$

The proof of this result employs the Gauss-Bonnet theorem to relate a line integral to A.[1] The solid angle (or spherical excess) A is known as a holonomy.

In the theory of rods, the unit vector of interest is the unit tangent vector $\mathbf{e}_t$ and the curve it traces out on the unit sphere is known as the tangent indicatrix or tantrix c_t (cf. Figure 4.1). Suppose after an interval $s_1 - s_0$ of the arclength parameter s, $\mathbf{e}_t(s_1) = \mathbf{e}_t(s_0)$, then Eqn. (4.3) can be used to determine the relative rotation of the cross-section of the rod about $\mathbf{e}_t$ in the interval $s_1 - s_0$. We also note that Fuller, in a celebrated paper [14], combines Eqn. (4.3) with Călugăreanu's theorem relating the linking number L_k, twist T_w, and writhe W_r of a ribbon to show that the writhe of a closed non-self-intersecting curve satisfies the identity

$$2\pi + 2\pi W_r = A \quad \text{modulo } 2\pi. \tag{4.4}$$

For the ribbon used in Fuller's argument, $\Delta\nu = 0$ modulo 2π.

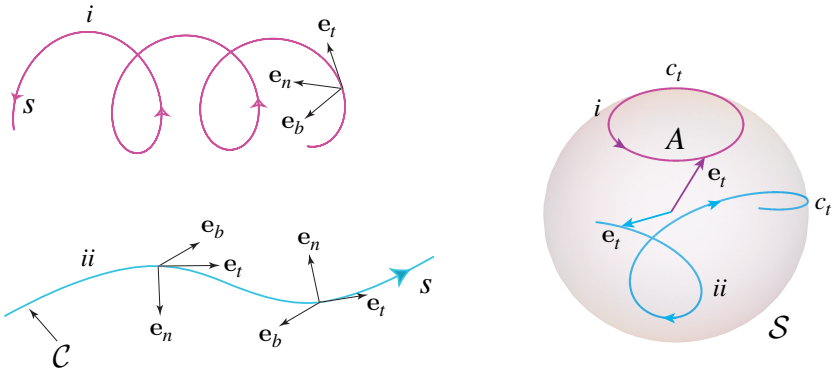

Fig. 4.1 *A pair of space curves $\mathcal{C}$ and their tangent indicatrices on the unit sphere $\mathcal{S}$. The solid angle A enclosed by the tangent indicatrix c_t (or tantrix) of the unit tangent vector $\mathbf{e}_t$ on $\mathcal{S}$ is intimately related to the rotation of the cross-section of a rod which has a centerline $\mathcal{C}$. The arrow indicates the direction of increasing arclength parameter s.*

In the discrete elastic rod formulation, the reference twist m^k_{ref} along the kth edge and its variation are determined by measuring the solid angle traced by the tangent vector $\mathbf{t}^k$ on the unit sphere. The computations exploit results from spherical geometry and the calculations are related to Eqns. (4.3) and (4.4). Several readers may find it more helpful to simply start with the example discussed in Section 4.6 where the computation of a solid angle is used to determine the reference twist, before exploring the earlier sections of this chapter. We also take this opportunity to recommend the texts of Henderson [20] and Pressley [50] for additional background on the classic differential geometry used in this chapter.

[1] As discussed in [38, 41, 44, 66], Kelvin and Tait's result has been independently rediscovered several times since 1867. The most notable instance lies in a wonderful paper by Goodman and Robinson [16] where it is used to compute drift in navigation estimates.

4.2 Background from Spherical Geometry

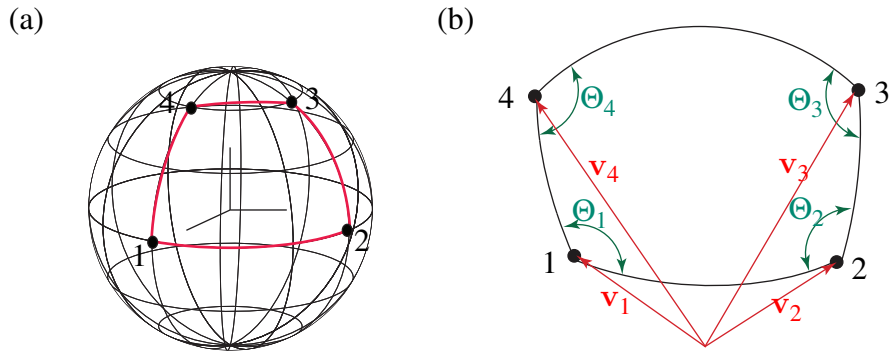

Fig. 4.2 *(a) The four vertices of a spherical quadrilateral on a sphere of unit radius. The sides of the quadrilateral are great circles connecting the vertices. (b) Schematic of the unit vectors* $\mathbf{v}_1,\ldots,\mathbf{v}_4$ *defining the respective vertices* $1,\ldots,4$ *and labelling of the interior angles* $\Theta_1,\ldots,\Theta_4$.

Consider the closed path on the unit sphere shown in Figure 4.2(a). The quadrilateral is formed by four points on the unit sphere connected by arcs of great circles and is known as a spherical quadrilateral. From classic results in spherical trigonometry (cf. [58, 60]), it is known that the Gaussian curvature of the unit sphere $K = 1$ and that the solid angle (or spherical excess) E formed by the quadrilateral on the unit sphere is

$$E = \Theta_1 + \Theta_2 + \Theta_3 + \Theta_4 - 2\pi. \tag{4.5}$$

The angles $\Theta_1,\ldots,\Theta_4$ are known as interior angles. Referring to Figure 4.2(b), it is convenient for future purposes to use the unit vectors $\mathbf{v}_1,\ldots,\mathbf{v}_4$ to define the interior angles. To do so, we note that the great circle connecting 1 to 2, say, lies on a plane perpendicular to $\mathbf{v}_1 \times \mathbf{v}_2$. Whence, we can define unit vectors that are normal to the sides of the quadrilateral as follows:

$$\mathbf{n}_1 = \frac{\mathbf{v}_1 \times \mathbf{v}_2}{\|\mathbf{v}_1 \times \mathbf{v}_2\|}, \qquad \mathbf{n}_2 = -\frac{\mathbf{v}_1 \times \mathbf{v}_2}{\|\mathbf{v}_1 \times \mathbf{v}_2\|},$$

$$\mathbf{n}_3 = \frac{\mathbf{v}_2 \times \mathbf{v}_3}{\|\mathbf{v}_2 \times \mathbf{v}_3\|}, \quad \ldots, \quad \mathbf{n}_8 = -\frac{\mathbf{v}_4 \times \mathbf{v}_1}{\|\mathbf{v}_4 \times \mathbf{v}_1\|}. \tag{4.6}$$

In addition, referring to Figure 4.3, the unit tangent vectors to the sides of the spherical quadrilateral at the vertices are

$$\mathbf{c}_1 = \frac{(\mathbf{v}_1 \times \mathbf{v}_2) \times \mathbf{v}_1}{\|(\mathbf{v}_1 \times \mathbf{v}_2) \times \mathbf{v}_1\|}, \qquad \mathbf{c}_2 = -\frac{(\mathbf{v}_1 \times \mathbf{v}_2) \times \mathbf{v}_2}{\|(\mathbf{v}_1 \times \mathbf{v}_2) \times \mathbf{v}_2\|},$$

$$\mathbf{c}_3 = \frac{(\mathbf{v}_2 \times \mathbf{v}_3) \times \mathbf{v}_2}{\|(\mathbf{v}_2 \times \mathbf{v}_3) \times \mathbf{v}_2\|}, \quad \ldots, \quad \mathbf{c}_8 = -\frac{(\mathbf{v}_4 \times \mathbf{v}_1) \times \mathbf{v}_1}{\|(\mathbf{v}_4 \times \mathbf{v}_1) \times \mathbf{v}_1\|}. \tag{4.7}$$

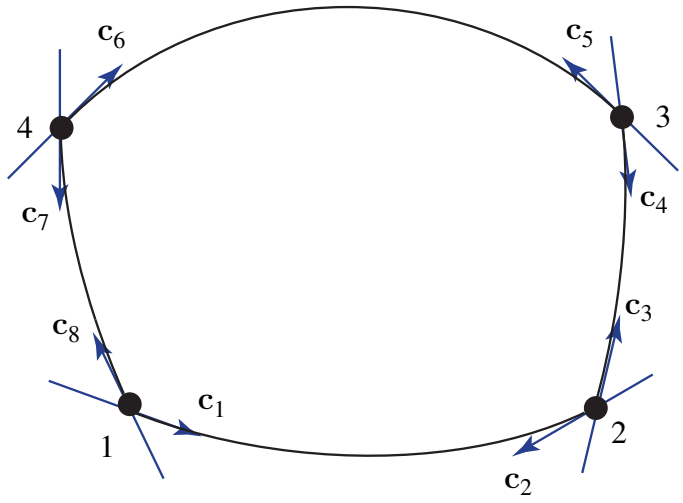

Fig. 4.3 *Schematic of the unit tangent vectors* $\mathbf{c}_1,\ldots,\mathbf{c}_8$ *that are tangent to the arcs forming a spherical quadrilateral on the unit sphere.*

The expressions for these unit tangent vectors can be simplified using identities of the form

$$(\mathbf{v}_1 \times \mathbf{v}_2) \times \mathbf{v}_1 = \mathbf{v}_2 - (\mathbf{v}_1 \cdot \mathbf{v}_2)\,\mathbf{v}_1. \tag{4.8}$$

The angle Θ_1 can be defined using $\mathbf{c}_1$ and $\mathbf{c}_8$:

$$\cos(\Theta_1) = \mathbf{c}_1 \cdot \mathbf{c}_8. \tag{4.9}$$

However, because

$$((\mathbf{v}_1 \times \mathbf{v}_2) \times \mathbf{v}_1) \cdot ((\mathbf{v}_1 \times \mathbf{v}_4) \times \mathbf{v}_1) = (\mathbf{v}_1 \times \mathbf{v}_2) \cdot (\mathbf{v}_1 \times \mathbf{v}_4) \tag{4.10}$$

and

$$\|(\mathbf{v}_1 \times \mathbf{v}_2) \times \mathbf{v}_1\|^2 = 1 - (\mathbf{v}_1 \cdot \mathbf{v}_2)^2 = \|\mathbf{v}_1 \times \mathbf{v}_2\|^2, \tag{4.11}$$

we can also use the normal vectors $\mathbf{n}_1$ and $\mathbf{n}_8$ to define the angle Θ_1:

$$\begin{aligned}\cos(\Theta_1) &= \mathbf{c}_1 \cdot \mathbf{c}_8 = \mathbf{n}_1 \cdot \mathbf{n}_8 \\ &= \left(\frac{\mathbf{v}_1 \times \mathbf{v}_2}{\|\mathbf{v}_1 \times \mathbf{v}_2\|}\right) \cdot \left(\frac{\mathbf{v}_1 \times \mathbf{v}_4}{\|\mathbf{v}_1 \times \mathbf{v}_4\|}\right).\end{aligned} \tag{4.12}$$

This observation greatly facilitates the forthcoming computations. For future reference, we note that it is straightforward to establish the following expressions:

$$\begin{aligned}\cos(\Theta_2) &= \left(\frac{\mathbf{v}_2 \times \mathbf{v}_3}{\|\mathbf{v}_2 \times \mathbf{v}_3\|}\right) \cdot \left(\frac{\mathbf{v}_2 \times \mathbf{v}_1}{\|\mathbf{v}_2 \times \mathbf{v}_1\|}\right), \\ \cos(\Theta_3) &= \left(\frac{\mathbf{v}_3 \times \mathbf{v}_4}{\|\mathbf{v}_3 \times \mathbf{v}_4\|}\right) \cdot \left(\frac{\mathbf{v}_3 \times \mathbf{v}_2}{\|\mathbf{v}_3 \times \mathbf{v}_2\|}\right), \\ \cos(\Theta_4) &= \left(\frac{\mathbf{v}_4 \times \mathbf{v}_1}{\|\mathbf{v}_4 \times \mathbf{v}_1\|}\right) \cdot \left(\frac{\mathbf{v}_4 \times \mathbf{v}_3}{\|\mathbf{v}_4 \times \mathbf{v}_3\|}\right).\end{aligned} \tag{4.13}$$

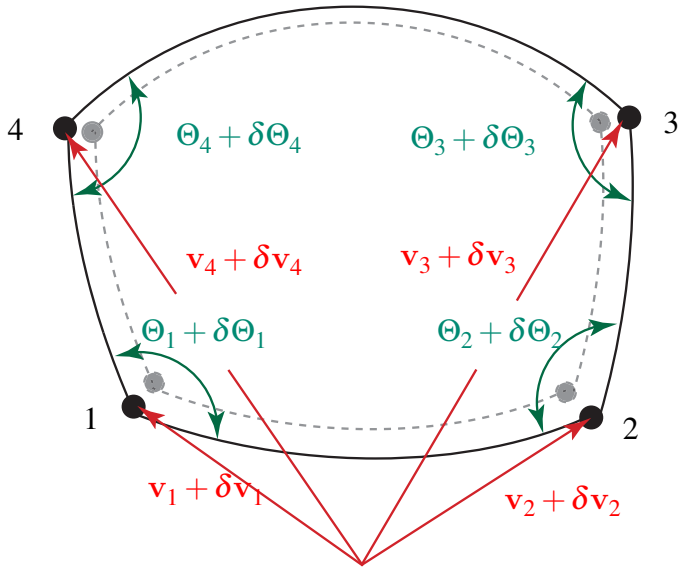

Fig. 4.4 *The perturbed spherical quadrilateral formed by displacing the vertices.*

4.2.1 An Expression for the Variation in the Spherical Excess

As shown in Figure 4.4, we now consider the case where each of the vertices are displaced by an incremental amount:

$$\mathbf{v}_1 \to \mathbf{v}_1+\delta\mathbf{v}_1, \quad \mathbf{v}_2 \to \mathbf{v}_2+\delta\mathbf{v}_2, \quad \mathbf{v}_3 \to \mathbf{v}_3+\delta\mathbf{v}_3, \quad \mathbf{v}_4 \to \mathbf{v}_4+\delta\mathbf{v}_4. \tag{4.14}$$

To compute the resulting change δE in E, we consider the respective changes $\delta\Theta_1,\ldots,\delta\Theta_4$ in the interior angles. We start with the change in the angle Θ_1 as the changes in the other three angles can be established easily once an expression for $\delta\Theta_1$ has been found.

The interior angle Θ_1 is formed by the tangent vectors $\mathbf{c}_1$ and $\mathbf{c}_8$ and is equal to the angle formed by $\mathbf{n}_1$ and $\mathbf{n}_8$. The latter pair of unit vectors are parallel to $\mathbf{v}_1\times\mathbf{v}_2$ and $\mathbf{v}_1\times\mathbf{v}_4$. Thus, an expression for the variation of Θ_1 can be computed starting from the expression (4.12) for $\cos(\Theta_1)$:

$$\delta\Theta_1 \;=\; \frac{\partial\Theta_1}{\partial(\mathbf{v}_1\times\mathbf{v}_2)}\cdot\delta(\mathbf{v}_1\times\mathbf{v}_2)+\frac{\partial\Theta_1}{\partial(\mathbf{v}_1\times\mathbf{v}_4)}\cdot\delta(\mathbf{v}_1\times\mathbf{v}_4). \tag{4.15}$$

With the help of Eqns. (3.14) and (3.15), we find that

$$\begin{aligned}\delta\Theta_1 \;=\; &-\left(\frac{(\mathbf{v}_1\times\mathbf{v}_2)\times(\mathbf{v}_1\times\mathbf{v}_4)}{\|(\mathbf{v}_1\times\mathbf{v}_2)\times(\mathbf{v}_1\times\mathbf{v}_4)\|}\right)\cdot\left(\left(\frac{\mathbf{v}_1\times\mathbf{v}_2}{\|\mathbf{v}_1\times\mathbf{v}_2\|^2}\right)\times(\delta\mathbf{v}_1\times\mathbf{v}_2+\mathbf{v}_1\times\delta\mathbf{v}_2)\right)\\ &+\left(\frac{(\mathbf{v}_1\times\mathbf{v}_2)\times(\mathbf{v}_1\times\mathbf{v}_4)}{\|(\mathbf{v}_1\times\mathbf{v}_2)\times(\mathbf{v}_1\times\mathbf{v}_4)\|}\right)\cdot\left(\left(\frac{\mathbf{v}_1\times\mathbf{v}_4}{\|\mathbf{v}_1\times\mathbf{v}_4\|^2}\right)\times(\delta\mathbf{v}_1\times\mathbf{v}_4+\mathbf{v}_1\times\delta\mathbf{v}_4)\right).\end{aligned} \tag{4.16}$$

Noting that $\mathbf{v}_1$ is a unit vector,

$$(\mathbf{v}_1 \times \mathbf{v}_2) \times (\mathbf{v}_1 \times \mathbf{v}_4) = ((\mathbf{v}_1 \times \mathbf{v}_2) \cdot \mathbf{v}_4)\, \mathbf{v}_1, \tag{4.17}$$

and that the triad $\{\mathbf{v}_1, \mathbf{v}_2, \mathbf{v}_4\}$ is right-handed, we can conclude that

$$\left(\frac{(\mathbf{v}_1 \times \mathbf{v}_2) \times (\mathbf{v}_1 \times \mathbf{v}_4)}{\|(\mathbf{v}_1 \times \mathbf{v}_2) \times (\mathbf{v}_1 \times \mathbf{v}_4)\|} \right) = \mathbf{v}_1. \tag{4.18}$$

This conclusion dramatically simplifies the expression for $\delta\Theta_1$:

$$\begin{aligned} \delta\Theta_1 &= -\mathbf{v}_1 \cdot \left(\left(\frac{\mathbf{v}_1 \times \mathbf{v}_2}{\|\mathbf{v}_1 \times \mathbf{v}_2\|^2} \right) \times (\delta\mathbf{v}_1 \times \mathbf{v}_2 + \mathbf{v}_1 \times \delta\mathbf{v}_2) \right) \\ &\quad + \mathbf{v}_1 \cdot \left(\left(\frac{\mathbf{v}_1 \times \mathbf{v}_4}{\|\mathbf{v}_1 \times \mathbf{v}_4\|^2} \right) \times (\delta\mathbf{v}_1 \times \mathbf{v}_4 + \mathbf{v}_1 \times \delta\mathbf{v}_4) \right). \end{aligned} \tag{4.19}$$

Repeatedly invoking triple product identities and noting that $\delta\mathbf{v} \cdot \mathbf{v} = 0$ for any unit vector $\mathbf{v}$, we arrive at the expression

$$\begin{aligned} \delta\Theta_1 &= -\left(\frac{\mathbf{v}_1 \times \mathbf{v}_2}{\|\mathbf{v}_1 \times \mathbf{v}_2\|^2} \right) \cdot (\delta\mathbf{v}_2 - (\mathbf{v}_1 \cdot \mathbf{v}_2)\, \delta\mathbf{v}_1) \\ &\quad + \left(\frac{\mathbf{v}_1 \times \mathbf{v}_4}{\|\mathbf{v}_1 \times \mathbf{v}_4\|^2} \right) \cdot (\delta\mathbf{v}_4 - (\mathbf{v}_1 \cdot \mathbf{v}_4)\, \delta\mathbf{v}_1). \end{aligned} \tag{4.20}$$

The corresponding expressions for the other three angles are

$$\begin{aligned} \delta\Theta_2 &= \left(\frac{\mathbf{v}_2 \times \mathbf{v}_3}{\|\mathbf{v}_2 \times \mathbf{v}_3\|^2} \right) \cdot ((\mathbf{v}_2 \cdot \mathbf{v}_3)\, \delta\mathbf{v}_2 - \delta\mathbf{v}_3) \\ &\quad - \left(\frac{\mathbf{v}_2 \times \mathbf{v}_1}{\|\mathbf{v}_2 \times \mathbf{v}_1\|^2} \right) \cdot ((\mathbf{v}_2 \cdot \mathbf{v}_1)\, \delta\mathbf{v}_2 - \delta\mathbf{v}_1), \end{aligned}$$

$$\begin{aligned} \delta\Theta_3 &= \left(\frac{\mathbf{v}_3 \times \mathbf{v}_4}{\|\mathbf{v}_3 \times \mathbf{v}_4\|^2} \right) \cdot ((\mathbf{v}_3 \cdot \mathbf{v}_4)\, \delta\mathbf{v}_3 - \delta\mathbf{v}_4) \\ &\quad - \left(\frac{\mathbf{v}_3 \times \mathbf{v}_2}{\|\mathbf{v}_3 \times \mathbf{v}_2\|^2} \right) \cdot ((\mathbf{v}_3 \cdot \mathbf{v}_2)\, \delta\mathbf{v}_3 - \delta\mathbf{v}_2), \end{aligned}$$

$$\begin{aligned} \delta\Theta_4 &= \left(\frac{\mathbf{v}_4 \times \mathbf{v}_1}{\|\mathbf{v}_4 \times \mathbf{v}_1\|^2} \right) \cdot ((\mathbf{v}_4 \cdot \mathbf{v}_1)\, \delta\mathbf{v}_4 - \delta\mathbf{v}_1) \\ &\quad - \left(\frac{\mathbf{v}_4 \times \mathbf{v}_3}{\|\mathbf{v}_4 \times \mathbf{v}_3\|^2} \right) \cdot ((\mathbf{v}_4 \cdot \mathbf{v}_3)\, \delta\mathbf{v}_4 - \delta\mathbf{v}_3). \end{aligned} \tag{4.21}$$

Adding these expressions together and using identities such as $\|\mathbf{v}_3 \times \mathbf{v}_4\|^2 = 1 - (\mathbf{v}_3 \cdot \mathbf{v}_4)^2$, we find that

$$\begin{aligned}\delta E &= \delta\Theta_1 + \delta\Theta_2 + \delta\Theta_3 + \delta\Theta_4 \\ &= -\left(\frac{\mathbf{v}_1 \times \mathbf{v}_2}{1+(\mathbf{v}_1 \cdot \mathbf{v}_2)}\right) \cdot (\delta\mathbf{v}_1 + \delta\mathbf{v}_2) - \left(\frac{\mathbf{v}_2 \times \mathbf{v}_3}{1+(\mathbf{v}_2 \cdot \mathbf{v}_3)}\right) \cdot (\delta\mathbf{v}_2 + \delta\mathbf{v}_3) \\ &\quad -\left(\frac{\mathbf{v}_3 \times \mathbf{v}_4}{1+(\mathbf{v}_3 \cdot \mathbf{v}_4)}\right) \cdot (\delta\mathbf{v}_3 + \delta\mathbf{v}_4) - \left(\frac{\mathbf{v}_4 \times \mathbf{v}_1}{1+(\mathbf{v}_4 \cdot \mathbf{v}_1)}\right) \cdot (\delta\mathbf{v}_4 + \delta\mathbf{v}_1)\,.\end{aligned} \tag{4.22}$$

This expression for the variation of the spherical excess is the basis for the central result of this chapter (cf. Eqn. (4.44)).

4.3 Spherical Excess and an Angle of Rotation for a Compound Rotation

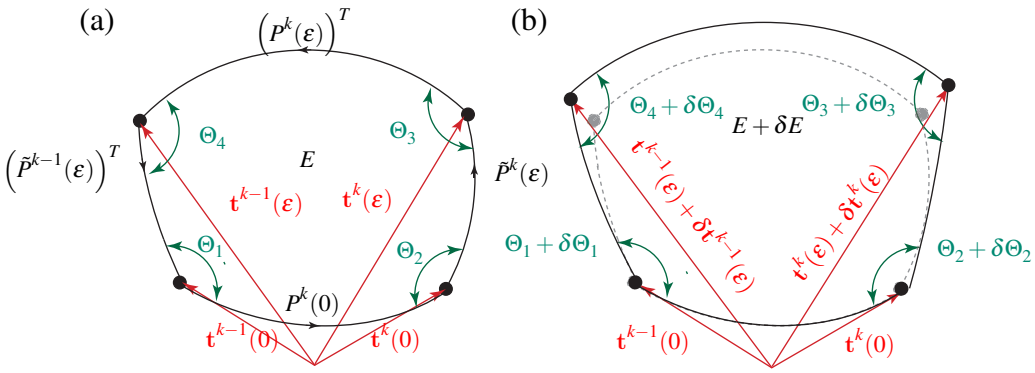

Fig. 4.5 *(a) The four vertices of a quadrilateral on a sphere of unit radius. The vertices are defined by the unit vectors* $\mathbf{t}^{k-1}(0)$, $\mathbf{t}^k(0)$, $\mathbf{t}^{k-1}(\varepsilon)$, *and* $\mathbf{t}^k(\varepsilon)$ *and the sides of the quadrilateral are great circles connecting the vertices. (b) The perturbed quadrilateral which is obtained by displacing the vertices:* $\mathbf{x}_{k-1}(\varepsilon) \to \mathbf{x}_{k-1}(\varepsilon) + \delta\mathbf{x}_{k-1}(\varepsilon)$, $\mathbf{x}_k(\varepsilon) \to \mathbf{x}_k(\varepsilon) + \delta\mathbf{x}_k(\varepsilon)$, *and* $\mathbf{x}_{k+1}(\varepsilon) \to \mathbf{x}_{k+1}(\varepsilon) + \delta\mathbf{x}_{k+1}(\varepsilon)$.

4.3.1 A Composition of Parallel Transports

To examine one aspect of how the twist is computed in discrete elastic rods, we consider a set of configurations of the discrete elastic rod that are parameterized by a single parameter ε:

$$\mathbf{x}_0(\varepsilon), \ldots, \mathbf{x}_{n-1}(\varepsilon), \tag{4.23}$$

with concomitant expressions for the tangent vectors and edge vectors. The parameter ε will be used to track a variation of the discrete curve. Next, we consider a pair of connected edges, $\mathbf{e}^{k-1}(0) = \mathbf{e}^{k-1}(\varepsilon = 0)$ and $\mathbf{e}^{k}(0) = \mathbf{e}^{k}(\varepsilon = 0)$, and imagine their associated tangent vectors mapped to the unit sphere (cf. Figure 4.5(a)). We recall from Chapter 2 that the pair of tangent vectors are related by the rotation $P^{\mathbf{t}^k(\varepsilon=0)}_{\mathbf{t}^{k-1}(\varepsilon=0)}$:

$$P^k(0) \equiv P^{\mathbf{t}^k(0)}_{\mathbf{t}^{k-1}(0)} = \mathbf{R}\left(\varphi_k(0), \mathbf{b}_k(0)\right), \tag{4.24}$$

where the discretized binormal vector at $\mathbf{x}_k(0)$ and the turning angle are defined by

$$\mathbf{b}_k(0) = \frac{\mathbf{t}^{k-1}(0) \times \mathbf{t}^k(0)}{\left\| \mathbf{t}^{k-1}(0) \times \mathbf{t}^k(0) \right\|}, \qquad \cos\left(\varphi_k(0)\right) = \mathbf{t}^k(0) \cdot \mathbf{t}^{k-1}(0). \tag{4.25}$$

The axis of rotation is orthogonal to $\mathbf{t}^{k-1}(0) = \mathbf{t}^{k-1}(\varepsilon = 0)$ and $\mathbf{t}^{k}(0) = \mathbf{t}^{k}(\varepsilon = 0)$ and thus the path connecting the trace of $\mathbf{t}^{k-1}(0)$ to $\mathbf{t}^{k}(0)$ can be considered an arc of a great circle (i.e., a geodesic on the sphere).

If we now imagine the same edges as displaced, then it is easy to see that the ends of the tangent vectors $\mathbf{t}^{k-1}(\varepsilon)$ and $\mathbf{t}^{k}(\varepsilon)$ will occupy new points on the unit sphere, where ε is non-zero. We recall that the tangent vectors $\mathbf{t}^{k-1}(\varepsilon)$ and $\mathbf{t}^{k}(\varepsilon)$ are related by a rotation:

$$P^k(\varepsilon) \equiv P^{\mathbf{t}^k(\varepsilon)}_{\mathbf{t}^{k-1}(\varepsilon)} = \mathbf{R}\left(\varphi_k(\varepsilon), \mathbf{b}_k(\varepsilon)\right), \tag{4.26}$$

where the discretized binormal vector at $\mathbf{x}_k(\varepsilon)$ and the turning angle are defined by

$$\mathbf{b}_k(\varepsilon) = \frac{\mathbf{t}^{k-1}(\varepsilon) \times \mathbf{t}^k(\varepsilon)}{\left\| \mathbf{t}^{k-1}(\varepsilon) \times \mathbf{t}^k(\varepsilon) \right\|}, \qquad \cos\left(\varphi_k(\varepsilon)\right) = \mathbf{t}^k(\varepsilon) \cdot \mathbf{t}^{k-1}(\varepsilon). \tag{4.27}$$

Again, the path joining $\mathbf{t}^{k-1}(\varepsilon)$ and $\mathbf{t}^{k}(\varepsilon)$ on the unit sphere is a great circle.

We recall from Chapter 2 that the rotations $P^k(0)$ and $P^k(\varepsilon)$ were associated with space-parallel transport and were used to define the Bishop triads on edges. The next pair of rotations we employ are examples of the time-parallel transport operators that were used to define the reference frames in Chapter 2. The first of these rotations, which we denote by $\tilde{P}^{k-1}(\varepsilon)$ transforms $\mathbf{t}^{k-1}(0)$ to $\mathbf{t}^{k-1}(\varepsilon)$ and the second rotation, which we denote by $\tilde{P}^{k}(\varepsilon)$ transforms $\mathbf{t}^{k}(0)$ to $\mathbf{t}^{k}(\varepsilon)$ (cf. Figure 2.8 on Page 12). The latter rotation is defined by

$$\tilde{P}^k(\varepsilon) \equiv P^{\mathbf{t}^k(\varepsilon)}_{\mathbf{t}^{k}(0)} = \mathbf{R}\left(\alpha^k(\varepsilon), \mathbf{h}^k(\varepsilon)\right), \tag{4.28}$$

where the axis and angle of rotation are

$$\mathbf{h}^k(\varepsilon) = \frac{\mathbf{t}^{k}(0) \times \mathbf{t}^k(\varepsilon)}{\left\| \mathbf{t}^{k}(\varepsilon) \times \mathbf{t}^k(0) \right\|}, \qquad \cos\left(\alpha^k(\varepsilon)\right) = \mathbf{t}^k(0) \cdot \mathbf{t}^k(\varepsilon). \tag{4.29}$$

The corresponding representation for $\tilde{P}^{k-1}(\varepsilon)$ is readily inferred from Eqn. (4.28). Again, the presumed paths connecting the respective tangent vectors on the sphere are great circles (cf. Figure 4.5(a)).

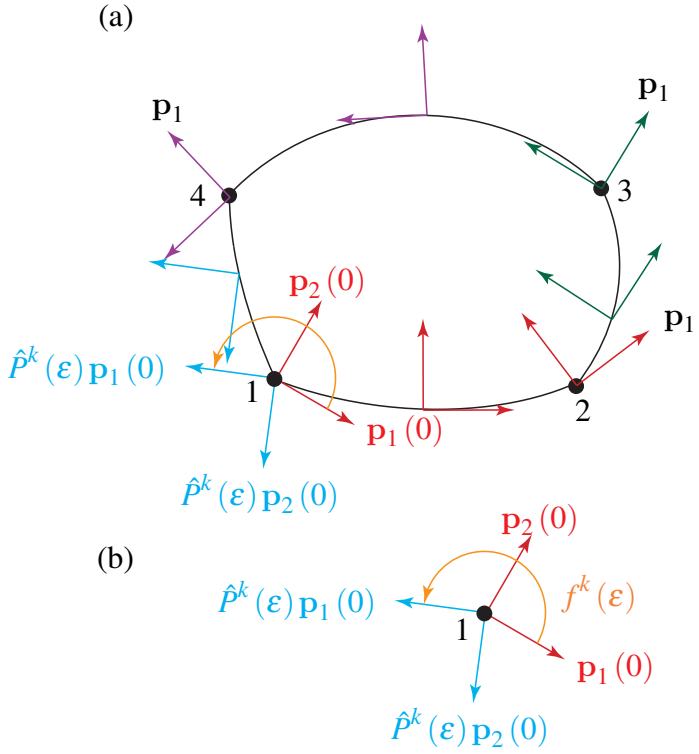

Fig. 4.6 *(a) Schematic of the parallel propagation of a pair of vectors* $\mathbf{p}_1$ *and* $\mathbf{p}_2$ *around the sides of the quadrilateral. (b) The relative rotation of the pair* $\mathbf{p}_1 - \mathbf{p}_2$ *about* $\mathbf{t}^{k-1}$ *induced by the transport is the angle* $f^k(\varepsilon)$.

Now consider the product

$$\hat{P}^k(\varepsilon) \;=\; \left(\tilde{P}^{k-1}(\varepsilon)\right)^T \left(P^k(\varepsilon)\right)^T \tilde{P}^k(\varepsilon) P^k(0). \tag{4.30}$$

To understand this product, note that

$$\begin{aligned} &\mathbf{t}^k(0) = P^k(0)\mathbf{t}^{k-1}(0), \qquad \mathbf{t}^k(\varepsilon) = \tilde{P}^k(\varepsilon)\mathbf{t}^k(0), \\ &\mathbf{t}^{k-1}(\varepsilon) = \left(P^k(\varepsilon)\right)^T \mathbf{t}^k(\varepsilon), \qquad \mathbf{t}^{k-1}(0) = \left(\tilde{P}^{k-1}(\varepsilon)\right)^T \mathbf{t}^{k-1}(\varepsilon). \end{aligned} \tag{4.31}$$

Thus, the product of the four rotations (parallel transports) is a rotation about $\mathbf{t}^{k-1}(0)$ through an angle $f^k(\varepsilon)$:

$$\left(\tilde{P}^{k-1}(\varepsilon)\right)^T \left(P^k(\varepsilon)\right)^T \tilde{P}^k(\varepsilon) P^k(0) = \mathbf{R}\left(f^k(\varepsilon), \mathbf{t}^{k-1}(0)\right). \tag{4.32}$$

While $\mathbf{t}^{k-1}$ is transported back to its original location, the angle $f^k(\varepsilon)$ may not be zero.

4.3.2 Computing the Angle $f^k(\varepsilon)$

There are two approaches that we can use to explain the computation of the angle $f^k(\varepsilon)$. Both are intimately related to the concept of the holonomy of a connection induced by parallel transport of a vector around a closed path. The first approach uses the kinetic analogy and compares the rotation of the Bishop triad to a corotational frame on a rigid body. Here we imagine a rigid body that is free to rotate about a fixed point. We choose a set of material points in the rigid body and use them to define a unit vector $\mathbf{r}$. We then align the rigid body at time t_0 such that $\mathbf{r}(t_0) = \mathbf{t}^k(0)$. In a thought experiment, we now move the rigid body so that $\mathbf{r}(t)$ traces out the boundary of the quadrilateral shown in Figure 4.5(a) and the motion of the body is such that $\boldsymbol{\omega} \cdot \mathbf{r}(t) = 0$. In other words, the corotational basis that is fixed to the rigid body is equivalent to a Bishop frame. After a time $t_1 - t_0$, $\mathbf{r}(t_1) = \mathbf{r}(t_0) = \mathbf{t}^k(0)$ and the rigid body will have rotated about $\mathbf{r}(t_0)$ through an angle $f^k(\varepsilon)$. Appealing to Eqn. (4.3), the relative rotation of the rigid body in this case is given by the following decomposition:

$$f^k(\varepsilon) = \int_{t_0}^{t_1} \underbrace{\boldsymbol{\omega} \cdot \mathbf{r}(\tau)}_{=0} d\tau + E, \tag{4.33}$$

where E is the solid angle enclosed by the quadrilateral. As curves connecting the ends of the vectors are great circles (i.e., geodesics on the unit sphere), the solid angle enclosed by the quadrilateral is simply given by the sum of the interior angles:

$$f^k(\varepsilon) = E = \Theta_1 + \Theta_2 + \Theta_3 + \Theta_4. \tag{4.34}$$

Thus, f^k can be determined by measuring a solid angle on the sphere.

The second equivalent approach to compute the angle is to consider the parallel transport of a pair of orthonormal vectors $\mathbf{p}_1$ and $\mathbf{p}_2$ during the compound rotation.[2] For convenience, we choose $\mathbf{p}_1(0)$ to be tangent to the arc traced by $\mathbf{t}^{k-1}(0)$ as shown in Figure 4.6. After parallel propagation of the vector $\mathbf{p}_1$ along the quadrilateral of great circles connecting the vertices $1, \ldots, 4$ we find that this vector will have rotated by an amount E upon its return to 1. Thus, we again conclude that $f^k(\varepsilon) = E$.

4.4 The Angle $f^k(\varepsilon)$ and the Reference Twist $m^k_{\mathbf{ref}}(\varepsilon) - m^k_{\mathbf{ref}}(0)$

We now have the pieces in place to relate the spherical excess to an increment in the reference twist. This result is discussed in Bergou et al. [3] and Kaldor et al. [26] and we intend our forthcoming discussion to complement their expositions.

[2] Additional examples of parallel transport of vectors along a curve on a surface can be found in the textbooks on elementary differential geometry (see, e.g., [20, 50]).

To proceed, we consider the propagation of the reference frame vector $\mathbf{a}_1^{k-1}$ along the quadrilateral discussed in the previous section. We shall make frequent appeal to the identities (cf. Eqns. (2.20) and (2.23))

$$\begin{aligned}
&\mathbf{a}_1^k(t+\Delta t) = \bar{P}^k(t,\Delta t)\,\mathbf{a}_1^k(t),\\
&\mathbf{a}_1^{k+1}(t) = \cos\left(m_{\text{ref}}^{k+1}(t)\right) P_{\mathbf{t}^k}^{\mathbf{t}^{k+1}}(t)\mathbf{a}_1^k(t) + \sin\left(m_{\text{ref}}^{k+1}(t)\right) P_{\mathbf{t}^k}^{\mathbf{t}^{k+1}}(t)\mathbf{a}^k T
\end{aligned} \tag{4.35}$$

Initially, $\mathbf{a}_1^{k-1} = \mathbf{a}_1^{k-1}(0)$. Thus, as the vector is transported from the vertex at 1 to the vertex at 2:

$$P^k(0)\mathbf{a}_1^{k-1}(0) = \cos\left(m_{\text{ref}}^k(0)\right)\mathbf{a}_1^k(0) - \sin\left(m_{\text{ref}}^k(0)\right)\mathbf{a}_2^k(0). \tag{4.36}$$

The transport in this case is not a parallel transport in time of $\mathbf{a}_1^{k-1}(0)$. Along the vertex from 2 to 3, the propagation of $P^k(0)\mathbf{a}_1^{k-1}(0)$ is parallel in time and so we readily conclude that

$$\tilde{P}^k(\varepsilon)P^k(0)\mathbf{a}_1^{k-1}(0) = \cos\left(m_{\text{ref}}^k(0)\right)\mathbf{a}_1^k(\varepsilon) - \sin\left(m_{\text{ref}}^k(0)\right)\mathbf{a}_2^k(\varepsilon). \tag{4.37}$$

The operation on the vector $\tilde{P}^k(\varepsilon)P^k(0)\mathbf{a}_1^{k-1}(0)$ from vertex 3 to 4 is parallel in space and so we need to invert Eqn. (2.23) to get the appropriate transformation. After some manipulations we find that

$$\left(P^k(\varepsilon)\right)^T \tilde{P}^k(\varepsilon)P^k(0)\mathbf{a}_1^{k-1}(0) = \cos\left(\Delta m_{\text{ref}}^k(\varepsilon)\right)\mathbf{a}_1^{k-1}(\varepsilon) + \sin\left(\Delta m_{\text{ref}}^k(\varepsilon)\right)\mathbf{a}_2^{k-1}(\varepsilon), \tag{4.38}$$

where

$$\Delta m_{\text{ref}}^k(\varepsilon) = m_{\text{ref}}^k(\varepsilon) - m_{\text{ref}}^k(0). \tag{4.39}$$

The final transformation features a parallel transport in time from 4 to 1:

$$\begin{aligned}
\left(\tilde{P}^{k-1}(\varepsilon)\right)^T \left(P^k(\varepsilon)\right)^T \tilde{P}^k(\varepsilon)P^k(0)\mathbf{a}_1^{k-1}(0) \;=\; &\cos\left(\Delta m_{\text{ref}}^k(\varepsilon)\right)\mathbf{a}_1^{k-1}(0)\\
&+\sin\left(\Delta m_{\text{ref}}^k(\varepsilon)\right)\mathbf{a}_2^{k-1}(0).
\end{aligned} \tag{4.40}$$

This result leads us to the conclusion that $\mathbf{a}_1^{k-1}$ has been rotated by an angle $\Delta m_{\text{ref}}^k(\varepsilon)$. From our earlier results in Section 4.3.2, we can immediately conclude that

$$f^k(\varepsilon) = \Delta m_{\text{ref}}^k(\varepsilon) = m_{\text{ref}}^k(\varepsilon) - m_{\text{ref}}^k(0). \tag{4.41}$$

This result is of great use in establishing an expression for the variation of $m_{\text{ref}}^k(t)$ when the vertices are varied.

4.5 Variations of the Twist m_k and Reference Twist $\delta m^k_{\mathbf{ref}}$

If the vertices $\mathbf{x}_{k-1}(\varepsilon)$, $\mathbf{x}_k(\varepsilon)$, and $\mathbf{x}_{k+1}(\varepsilon)$ are perturbed, then $\mathbf{t}^{k-1}(\varepsilon)$ and $\mathbf{t}^k(\varepsilon)$ will be displaced as shown in Figure 4.5(b). The associated variation in the spherical excess E is

$$\delta E = \delta\Theta_1 + \delta\Theta_2 + \delta\Theta_3 + \delta\Theta_4. \tag{4.42}$$

To express this variation in terms of the variations to the tangent vectors, we use a result due to Etienne Vouga [64]. Applying Eqn. (4.22) to the situation at hand:

$$\begin{aligned}
\delta E &= \delta\Theta_1 + \delta\Theta_2 + \delta\Theta_3 + \delta\Theta_4 \\
&= -\left(\frac{\mathbf{t}^k(\varepsilon)\times\mathbf{t}^{k-1}(\varepsilon)}{1+\mathbf{t}^k(\varepsilon)\cdot\mathbf{t}^{k-1}(\varepsilon)}\right)\cdot\left(\delta\mathbf{t}^k(\varepsilon)+\delta\mathbf{t}^{k-1}(\varepsilon)\right) \\
&\quad \underbrace{-\left(\frac{\mathbf{t}^k(0)\times\mathbf{t}^k(\varepsilon)}{1+\mathbf{t}^k(0)\cdot\mathbf{t}^k(\varepsilon)}\right)\cdot\delta\mathbf{t}^k(\varepsilon)} \underbrace{-\left(\frac{\mathbf{t}^{k-1}(\varepsilon)\times\mathbf{t}^{k-1}(0)}{1+\mathbf{t}^{k-1}(\varepsilon)\cdot\mathbf{t}^{k-1}(0)}\right)\cdot\delta\mathbf{t}^{k-1}(\varepsilon)}.
\end{aligned} \tag{4.43}$$

Taking the limit as $\varepsilon\to 0$, the underbraced terms vanish and we can conclude that

$$\begin{aligned}
\frac{dm^k_{\mathrm{ref}}}{d\varepsilon} &= \left(\frac{\mathbf{t}^{k-1}(0)\times\mathbf{t}^k(0)}{1+\mathbf{t}^k(0)\cdot\mathbf{t}^{k-1}(0)}\right)\cdot\left(\frac{d\mathbf{t}^k}{d\varepsilon}(0)+\frac{d\mathbf{t}^{k-1}}{d\varepsilon}(0)\right) \\
&= (\kappa\mathbf{b})_k\cdot\frac{d\mathbf{t}_{\mathcal{V}_k}}{d\varepsilon}.
\end{aligned} \tag{4.44}$$

In the final expression we have removed the explicit dependency on ε.

To compute the variation of the discrete integrated twist m_k, we recall from Eqn. (2.81) that

$$m_k = \gamma^k - \gamma^{k-1} + m^k_{\mathrm{ref}}. \tag{4.45}$$

However, a variation of the vertices is equivalent to rigidly rotating the material vectors, the reference vectors, and the Bishop frame vectors. Thus, the angles between these vectors are preserved:

$$\delta\gamma^k = 0, \qquad \delta\gamma^{k-1} = 0. \tag{4.46}$$

Consequently,

$$\delta m_k = \delta m^k_{\mathrm{ref}}. \tag{4.47}$$

Thus, the expression for the variation of m_k is identical to the expression for the variation of m^k_{ref}. The resulting expression is used in Bergou et al. [3] and differs by a sign from the expression used in Kaldor et al. [26].[3]

[3] We have been unable to resolve this sign difference, but based on the example discussed in Section 4.6, we believe the sign difference is a typographical error.

4.6 A Rod with Three Vertices

To explore the formulae for m^k_{ref} and δm^k_{ref}, we return to the example of a rod with three vertices that was discussed in Section 2.5.4. For the reader's convenience, the configurations of the rod are reproduced in Figure 4.7. We recall, from Eqn. (2.48), expressions for the tangent vectors:

$$\mathbf{t}^0(\varepsilon) = \mathbf{E}_1, \qquad \mathbf{t}^1(\varepsilon) = \frac{1}{\sqrt{2+\varepsilon^2}}(\mathbf{E}_1 + \mathbf{E}_2 + \varepsilon \mathbf{E}_3). \tag{4.48}$$

Our goal is to establish an expression for the solid angle formed by the three vectors $\mathbf{t}^0$, $\mathbf{t}^1(\varepsilon = 0)$, and $\mathbf{t}^1(\varepsilon)$ as a function of ε. In addition, we wish to examine the rate of change of this angle with ε. These results will then be compared to our earlier derivations of the reference twist m^1_{ref} for this simple rod in Section 2.5.4. In particular, we are able to demonstrate how Eqns. (4.41) and (4.44) relating spherical excess and its variation to m^k_{ref} and δm^k_{ref} yield results that are consistent with computations of these quantities involving the parallel transport operators in Section 2.5.4.

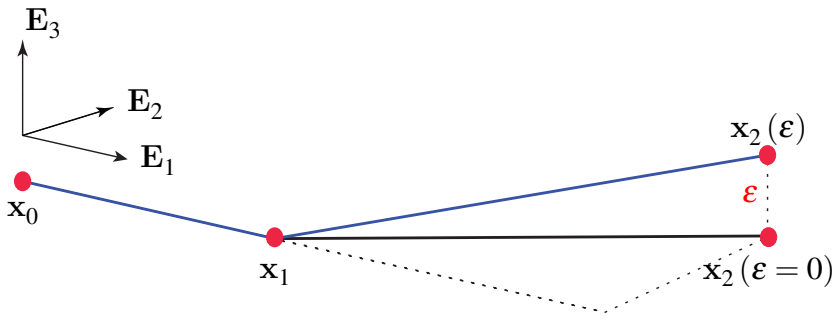

Fig. 4.7 *The configurations of a rod which has three vertices. When $\varepsilon = 0$, all of the vertices lie on a horizontal plane. As ε is increased from 0, the third vertex rises above this plane and a reference twist is induced in the second edge.*

4.6.1 Spherical Excess and Reference Twist

The excess E for the spherical triangle formed by $\mathbf{t}^0(0)$, $\mathbf{t}^1(0)$, and $\mathbf{t}^1(\varepsilon)$ is

$$E = \Theta_1 + \Theta_2 + \Theta_3 - \pi. \tag{4.49}$$

As can be seen from Figure 4.8, the interior angles Θ_1, Θ_2, and Θ_3 in this equation can be defined using the tangent vectors:

$$\begin{aligned}
\cos(\Theta_1) &= \frac{\mathbf{t}^0(0)\times\mathbf{t}^1(0)}{\left\|\mathbf{t}^0(0)\times\mathbf{t}^1(0)\right\|}\cdot\frac{\mathbf{t}^0(0)\times\mathbf{t}^1(\varepsilon)}{\left\|\mathbf{t}^0(0)\times\mathbf{t}^1(\varepsilon)\right\|},\\
\cos(\Theta_2) &= \frac{\mathbf{t}^1(0)\times\mathbf{t}^0(0)}{\left\|\mathbf{t}^1(0)\times\mathbf{t}^0(0)\right\|}\cdot\frac{\mathbf{t}^1(0)\times\mathbf{t}^1(\varepsilon)}{\left\|\mathbf{t}^1(0)\times\mathbf{t}^1(\varepsilon)\right\|},\\
\cos(\Theta_3) &= \frac{\mathbf{t}^1(\varepsilon)\times\mathbf{t}^0(0)}{\left\|\mathbf{t}^1(\varepsilon)\times\mathbf{t}^0(0)\right\|}\cdot\frac{\mathbf{t}^1(\varepsilon)\times\mathbf{t}^1(0)}{\left\|\mathbf{t}^1(\varepsilon)\times\mathbf{t}^1(0)\right\|}.
\end{aligned} \tag{4.50}$$

The procedure used to compute these expressions is identical to that used earlier with the spherical quadrilateral (see Page 48).

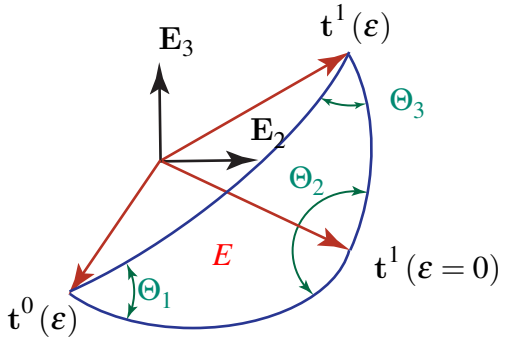

Fig. 4.8 *Spherical triangle formed by the three tangent vectors* $\mathbf{t}^0(\varepsilon)=\mathbf{E}_1$, $\mathbf{t}^1(0)=\frac{1}{\sqrt{2}}(\mathbf{E}_1+\mathbf{E}_2)$, *and* $\mathbf{t}^1(\varepsilon)=\frac{1}{\sqrt{2+\varepsilon^2}}(\mathbf{E}_1+\mathbf{E}_2+\varepsilon\mathbf{E}_3)$. *As* ε *increases from* 0 *to* 1, *the spherical excess* E *increases from* 0 *to* $\frac{\pi}{12}$.

Substituting for the tangent vectors and computing the inner products, we find that

$$\cos(\Theta_1)=\frac{1}{\sqrt{1+\varepsilon^2}},\qquad \Theta_2=\frac{\pi}{2},\qquad \cos(\Theta_3)=\frac{|\varepsilon|}{\sqrt{2}\sqrt{1+\varepsilon^2}}. \tag{4.51}$$

Consequently,

$$E=\cos^{-1}\left(\frac{1}{\sqrt{1+\varepsilon^2}}\right)+\cos^{-1}\left(\frac{|\varepsilon|}{\sqrt{2}\sqrt{1+\varepsilon^2}}\right)-\frac{\pi}{2}. \tag{4.52}$$

Comparing this result to the expression $\tilde{m}_{\text{ref}}$ for m^1_{ref} that we found in Section 2.5.4 on Page 19, we find that $E=m^1_{\text{ref}}$ when $\varepsilon>0$, as anticipated. For example, when $\varepsilon=1$, then $E=\frac{\pi}{12}$. The function (4.52) for $E(\varepsilon)$ is shown in Figure 4.9(a). Clearly, when $\varepsilon<0$, then we can only state that $\left|m^1_{\text{ref}}\right|=E$.

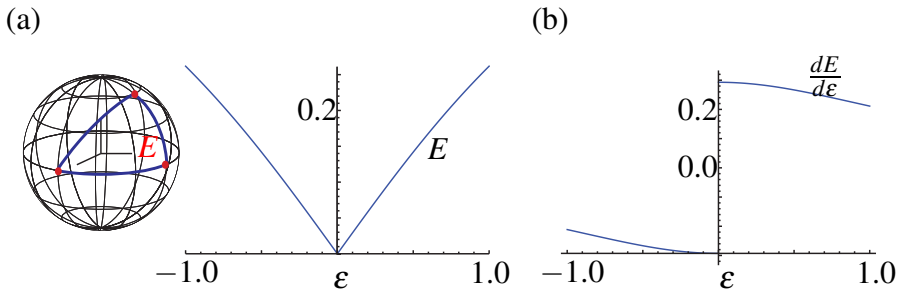

Fig. 4.9 *(a) The spherical excess E as a function of ε computed using Eqn. (4.52) for the spherical triangle shown in Figure 4.7. (b) The corresponding value of $\frac{dE}{d\varepsilon}$ computed using Eqn. (4.56).*

4.6.2 Variation of the Spherical Excess

To establish an expression for the variation of the excess E, we repeat the constructions leading to (4.22). This time the construction is applied to the spherical triangle where only one of the vertices is varied: $\delta \mathbf{t}^0(0) = 0$ and $\delta \mathbf{t}^1(0) = 0$. With a modest amount of work, we find that

$$\delta E = \left(\frac{\mathbf{t}^1(\varepsilon) \times \mathbf{t}^1(0)}{1 + \mathbf{t}^1(0) \cdot \mathbf{t}^1(\varepsilon)} \right) \cdot \delta \mathbf{t}^1(\varepsilon) + \left(\frac{\mathbf{t}^0(0) \times \mathbf{t}^1(\varepsilon)}{1 + \mathbf{t}^0(0) \cdot \mathbf{t}^1(\varepsilon)} \right) \cdot \delta \mathbf{t}^1(\varepsilon). \tag{4.53}$$

Whence,

$$\frac{dE}{d\varepsilon} = \left(\frac{\mathbf{t}^1(\varepsilon) \times \mathbf{t}^1(0)}{1 + \mathbf{t}^1(0) \cdot \mathbf{t}^1(\varepsilon)} \right) \cdot \frac{d\mathbf{t}^1}{d\varepsilon} + \left(\frac{\mathbf{t}^0(0) \times \mathbf{t}^1(\varepsilon)}{1 + \mathbf{t}^0(0) \cdot \mathbf{t}^1(\varepsilon)} \right) \cdot \frac{d\mathbf{t}^1}{d\varepsilon}. \tag{4.54}$$

For the application of interest:

$$\frac{d\mathbf{t}^1}{d\varepsilon} = \frac{1}{\sqrt{2+\varepsilon^2}} \mathbf{E}_3 - \left(\frac{\varepsilon}{2+\varepsilon^2} \right) \mathbf{t}^1(\varepsilon). \tag{4.55}$$

Substituting the expressions for the tangent vectors and $\frac{d\mathbf{t}^1}{d\varepsilon}$ into Eqn. (4.54) enables us to conclude that

$$\frac{dE}{d\varepsilon} = \frac{-\operatorname{sgn}(\varepsilon)|\varepsilon| + \varepsilon\sqrt{2+\varepsilon^2}}{\left(1+\varepsilon^2\right)\sqrt{\varepsilon^2\left(2+\varepsilon^2\right)}}. \tag{4.56}$$

As can be observed from Figure 4.9 (b), when $\varepsilon > 0$ this expression is precisely in agreement with $\frac{d\tilde{m}_{\text{ref}}}{d\varepsilon}$ for the function $\tilde{m}_{\text{ref}}$ that we found previously in Section 2.5.4.

Chapter 5

Equations of Motion and Energetic Considerations

5.1 Introduction

In the discrete elastic rod formulation, a state vector q is formulated using the components of the position vectors of the n vertices and the rotations of the material frames relative to the reference frames on each of the $n-1$ edges:

$$\begin{aligned}\mathsf{q} = \Big[&\mathbf{x}_0 \cdot \mathbf{E}_1, \mathbf{x}_0 \cdot \mathbf{E}_2, \mathbf{x}_0 \cdot \mathbf{E}_3, \gamma^0, \ldots, \mathbf{x}_{(n-2)} \cdot \mathbf{E}_1, \mathbf{x}_{(n-2)} \cdot \mathbf{E}_2, \\ &\mathbf{x}_{(n-2)} \cdot \mathbf{E}_3, \gamma^{n-2}, \mathbf{x}_{(n-1)} \cdot \mathbf{E}_1, \mathbf{x}_{(n-1)} \cdot \mathbf{E}_2, \mathbf{x}_{(n-1)} \cdot \mathbf{E}_3\Big]^T. \end{aligned} \tag{5.1}$$

Complementing this vector, a pair of generalized force vectors are also formulated:

$$\begin{aligned}\mathsf{F}_{\text{ext}} &= \mathsf{F}_{\text{ext}}\left(t_k, \mathsf{q}\left(t_k\right), \dot{\mathsf{q}}\left(t_k\right)\right) = \left[\mathsf{F}_{\text{ext}}^0, \ldots, \mathsf{F}_{\text{ext}}^{(4n-1)}\right]^T, \\ \mathsf{F}_{\text{int}} &= \mathsf{F}_{\text{int}}\left(\mathsf{q}\left(t_k\right), \dot{\mathsf{q}}\left(t_k\right)\right) = \left[\mathsf{F}_{\text{int}}^0, \ldots, \mathsf{F}_{\text{int}}^{(4n-1)}\right]^T. \end{aligned} \tag{5.2}$$

As discussed in Bergou et al. [3], the motion of the rod is determined by using Newton's method to solve the following equations for $\mathsf{q}\left(t_{k+1}\right)$ and $\dot{\mathsf{q}}\left(t_{k+1}\right)$:

$$\begin{aligned}&\left(t_{k+1} - t_k\right)\dot{\mathsf{q}}\left(t_{k+1}\right) = \mathsf{q}\left(t_{k+1}\right) - \mathsf{q}\left(t_k\right), \\ &\mathsf{M}\left(\dot{\mathsf{q}}\left(t_{k+1}\right) - \dot{\mathsf{q}}\left(t_k\right)\right) = \left(t_{k+1} - t_k\right)\left(\mathsf{F}_{\text{ext}}\left(t_k, \mathsf{q}\left(t_k\right), \dot{\mathsf{q}}\left(t_k\right)\right) + \mathsf{F}_{\text{int}}\left(\mathsf{q}\left(t_{k+1}\right), \dot{\mathsf{q}}\left(t_{k+1}\right)\right)\right). \end{aligned} \tag{5.3}$$

In these equations, M is a mass matrix and we shall explore shortly how the components of this matrix are prescribed. An additional purpose of this chapter is to explore prescriptions for the components of F_{int} in terms of the gradients of elastic energies and viscous damping forces and the components F_{ext} in terms of assigned forces and moments.

Newton's method requires the gradient of the internal forces (or Hessians of the elastic energies). Having banded Hessians reduces the computational expense. This is one of the reasons why the reference frame and time-parallel transport was employed in [3, 26] as opposed to space-parallel transport of the Bishop frame in the earlier formulation [4].

5.2 Kinetic Energies, Momenta, and Inertias

Prescriptions for kinetic energies and inertias for the discrete rod follow standard procedures that are adopted from classic rod theories. In particular, volume and surface integrals are used to determine weighted inertias and mass parameters. The most comprehensive work in the literature on these types of approximations is arguably Green et al. [17] and their work significantly influenced our exposition.[1]

The velocity vector of the kth vertex is simply denoted by $\dot{\mathbf{x}}_k$. Expressions for $\dot{\mathbf{m}}_1^k$ and $\dot{\mathbf{m}}_2^k$ were established earlier (cf. Eqn (2.90)):

$$\begin{aligned}
\dot{\mathbf{m}}_1^k(t) &= \bar{\boldsymbol{\omega}}^k(t) \times \mathbf{m}_1^k(t) \\
&= \dot{\gamma}^k(t)\,\mathbf{m}_2^k(t) - \left(\mathbf{m}_1^k(t) \cdot \dot{\mathbf{t}}^k(t)\right)\mathbf{t}^k(t), \\
\dot{\mathbf{m}}_2^k(t) &= \bar{\boldsymbol{\omega}}^k(t) \times \mathbf{m}_2^k(t) \\
&= -\dot{\gamma}^k(t)\,\mathbf{m}_1^k(t) - \left(\mathbf{m}_2^k(t) \cdot \dot{\mathbf{t}}^k(t)\right)\mathbf{t}^k(t).
\end{aligned} \tag{5.4}$$

As mentioned previously, the velocity of the material vectors have two components: one due to the twist $\dot{\gamma}^k$ and the other due to the motion of the edge vector $\mathbf{e}^k$ (i.e., bending).

5.2.1 Masses and Inertias

In the sequel, we assume that the discrete curve approximates the centerline of the three-dimensional body that the rod is modeling. The body is divided into a series of segments with each segment modeled using an edge of the discrete elastic curve. We assume that the fixed reference configuration of each segment of the body can be parameterized by a Cartesian coordinate system $x_1 - x_2 - x_3$ with x_3 parameterizing the centerline and x_1 and x_2 parameterizing the cross-section (cf. Figure 5.1). For simplicity, we assume that x_1 and x_2 are principal axes of the cross-section and the material vectors $\mathbf{m}_1^k$ and $\mathbf{m}_2^k$ in the fixed reference configuration are parallel to these axes and are labelled with an overbar in Figure 5.1.

The mass M_i associated with the ith vertex is the average mass of the edges meeting at this vertex:

$$M_i = \frac{1}{2}\left(M^i + M^{i-1}\right). \tag{5.5}$$

[1] A discussion of the developments in Green et al. [17] along with illustrative examples, can be found in [47, Chapter 5]. We also refer the reader to the review article by Naghdi [42] and Rubin's textbook [51].

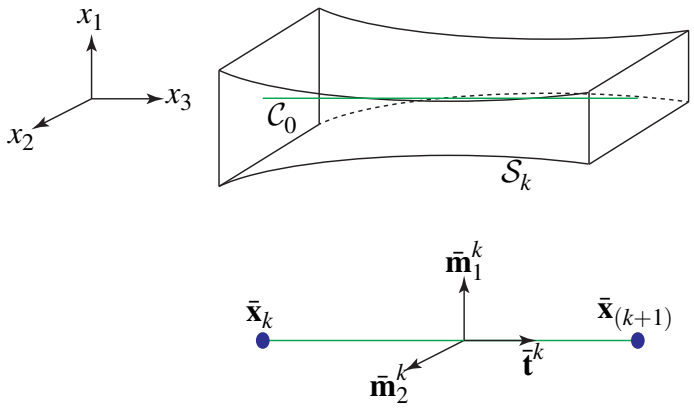

Fig. 5.1 *Reference configuration for a segment $\mathcal{S}_k$ of a three-dimensional body that the kth edge of a discrete elastic rod is modeling. The line $\mathcal{C}_0$ that will be approximated by the edge is shown. On this line, which is often chosen to be the centerline of the segment $\mathcal{S}_k$, the Cartesian coordinates x_1 and x_2 are both 0. The reference state of the kth edge is also shown and the reference values of the kinematic quantities associated with the discrete elastic rod are distinguished by an overbar.*

For a homogeneous rod with a uniform cross-section in its reference configuration (or reference state),

$$M^i = \rho_0 A^i \left\| \bar{\mathbf{e}}^i \right\|, \tag{5.6}$$

where ρ_0 is the mass density per unit volume in the reference configuration, A^i is the cross-sectional area in the reference configuration, and $\left\| \bar{\mathbf{e}}^i \right\|$ denotes the length of the ith edge in the reference configuration. If the rod is not homogeneous or of a uniform cross-section, then M^i must be computed using a more primitive prescription:

$$M^i = \int\int\int \rho_0 dx_1 dx_2 dx_3, \tag{5.7}$$

where the integration is performed over the segment of the three-dimensional body that the ith edge is modeling.

The mass moments of inertia associated with the ith edge are defined with the help of volume integrals:

$$\begin{aligned}
\rho_0^i &= \int\int\int \rho_0 dx_1 dx_2 dx_3, \\
\rho_0^i I_1^i &= \int\int\int x_1^2 \rho_0 dx_1 dx_2 dx_3, \qquad \rho_0^i I_2^i = \int\int\int x_2^2 \rho_0 dx_1 dx_2 dx_3, \\
\rho_0^i I^i &= \rho_0^i I_1^i + \rho_0^i I_2^i.
\end{aligned} \tag{5.8}$$

Thus, for a segment of length ℓ of a homogeneous rod with a rectangular cross-section of height h (in the x_2 direction) and width w (in the x_1 direction):

$$\rho_0^i I_1^i = \rho_0 \ell \frac{wh^3}{12} = \frac{M^i h^2}{12}, \qquad \rho_0^i I_2^i = \rho_0 \ell \frac{hw^3}{12} = \frac{M^i w^2}{12}. \tag{5.9}$$

Observe that we have used the definition of the mass M^i of the ith edge to simplify these expressions.

The mass matrix M can now be prescribed:

$$\mathsf{M} = \begin{bmatrix} M_0 & 0 & 0 & 0 & \cdots\cdots & 0 & 0 & 0 & 0 \\ 0 & M_0 & 0 & 0 & \cdots\cdots & 0 & 0 & 0 & 0 \\ 0 & 0 & M_0 & 0 & \cdots\cdots & 0 & 0 & 0 & 0 \\ 0 & 0 & 0 & \rho_0^0 I^0 & \cdots\cdots & 0 & 0 & 0 & 0 \\ & \ddots & & & \ddots & & & \ddots & \\ & \ddots & & & \ddots & & & \ddots & \\ & \ddots & & & \ddots & & & \ddots & \\ & \ddots & & & \ddots & & & \ddots & \\ 0 & 0 & 0 & 0 & \cdots\cdots & \rho_0^{(n-2)} I^{(n-2)} & 0 & 0 & 0 \\ 0 & 0 & 0 & 0 & \cdots\cdots & 0 & M_{(n-1)} & 0 & 0 \\ 0 & 0 & 0 & 0 & \cdots\cdots & 0 & 0 & M_{(n-1)} & 0 \\ 0 & 0 & 0 & 0 & \cdots\cdots & 0 & 0 & 0 & M_{(n-1)} \end{bmatrix}. \tag{5.10}$$

The reader is invited to relate the components of this matrix to the components of the vector q (cf. Eqn. (6.33)). It is also important to note that the masses in this matrix are associated with a vertex while the inertias are associated with an edge.

5.2.2 Linear Momentum, Angular Momentum, and Kinetic Energy

The masses and inertias we have defined are central to the definitions of momenta and kinetic energy. The linear momentum $\mathbf{G}$ of the discrete elastic rod is the sum of the linear momenta of the vertices:

$$\mathbf{G} = \sum_{k=0}^{n-1} M_k \dot{\mathbf{x}}_k. \tag{5.11}$$

The rod in this case has n vertices and $n-1$ edges. This expression for the linear momentum can also be expressed in terms of the velocity vector of the center of mass of each edge:

$$\mathbf{G} = \sum_{k=0}^{n-2} \frac{M^k}{2} \left(\dot{\mathbf{x}}_k + \dot{\mathbf{x}}_{k+1} \right). \tag{5.12}$$

Similarly, the angular momentum of the rod relative to a fixed point O is

$$\mathbf{H}_O = \sum_{k=0}^{n-1} (\mathbf{x}_k \times M_k \dot{\mathbf{x}}_k) + \sum_{k=0}^{n-2} \left(\mathbf{m}_1^k \times \rho_0^k I_2^k \dot{\mathbf{m}}_1^k + \mathbf{m}_2^k \times \rho_0^k I_1^k \dot{\mathbf{m}}_2^k \right). \tag{5.13}$$

Finally, we note that the following expression denotes a kinetic energy T^* of the rod:

$$T^* = \frac{1}{2} \sum_{k=0}^{n-1} (\dot{\mathbf{x}}_k \cdot M_k \dot{\mathbf{x}}_k) + \frac{1}{2} \sum_{k=0}^{n-2} \left(\dot{\mathbf{m}}_1^k \cdot \rho_0^k I_2^k \dot{\mathbf{m}}_1^k + \dot{\mathbf{m}}_2^k \cdot \rho_0^k I_1^k \dot{\mathbf{m}}_2^k \right). \tag{5.14}$$

In this expression for T^*,

$$\dot{\mathbf{m}}_1^k \cdot \rho_0^k I_2^k \dot{\mathbf{m}}_1^k = \rho_0^k I_2^k \left(\dot{\gamma}^k \right)^2 + \rho_0^k I_2^k \left(\mathbf{m}_1^k \cdot \left(\frac{\dot{\mathbf{x}}_{k+1}(t) - \dot{\mathbf{x}}_k(t)}{\| \mathbf{x}_{k+1}(t) - \mathbf{x}_k(t) \|} \right) \right). \tag{5.15}$$

Here, we used the representation (2.40) for $\dot{\mathbf{t}}^k$. The kinetic energy T that plays a role in the sequel is defined by a portion of T^*:

$$T = \frac{1}{2} \dot{\mathsf{q}}^T \mathsf{M} \dot{\mathsf{q}} = \frac{1}{2} \sum_{k=0}^{n-1} (\dot{\mathbf{x}}_k \cdot M_k \dot{\mathbf{x}}_k) + \frac{1}{2} \sum_{k=0}^{n-2} \rho_0^k I_2^k \left(\dot{\gamma}^k \right)^2. \tag{5.16}$$

For future reference, we note that $\dot{T} = \dot{\mathsf{q}} \cdot \mathsf{M} \ddot{\mathsf{q}}$.

5.3 Elastic Energies

Expressions for the gradients and Hessians of kinematical quantities were computed in Chapter 3. We now use these representations in order to compute the internal forces associated with the potential energy function for the discrete elastic rod. As the rod is allowed to twist, stretch and bend, the potential energy function will feature bending strains, twisting strains, and extensional strains. In its simplest form, the elastic potential energy E_e can be decomposed into the sum of three energies, stretching , twisting, and bending:

$$E_e = E_s + E_t + E_b. \tag{5.17}$$

Consistent with [3], we assume that each edge has an elliptical cross-section with major and minor radii a^i and b^j, respectively, so that the cross-sectional area $A^j = \pi a^j b^j$. At the vertices, we define $a_i = \left(a^{i-1} + a^i \right)/2$ and $b_i = \left(b^{i-1} + b^i \right)/2$, so that the cross-sectional area at the vertices are $A_i = \pi a_i b_i$.

The decomposition of E_e assumes that there is no inherent coupling between bending, twisting, and stretching of the rod. More complex energies E_e are possible. Indeed, if the discrete elastic rod formulation were to be used to model DNA strands or wire rope, then

these more complex energies would be needed to model twist-stretch and twist-bending coupling that is observed in these systems.[2]

The respective extensional E_s, twisting E_t, and bending E_b elastic energy functions are assumed to be quadratic functions of the strains:

$$\begin{aligned}
E_s &= \frac{1}{2}\sum_{j=0}^{n-2} EA^j \left(\frac{\left\|\mathbf{e}^j\right\|}{\left\|\bar{\mathbf{e}}^j\right\|} - 1 \right)^2 \left\|\bar{\mathbf{e}}^j\right\|, \\
E_t &= \frac{1}{2}\sum_{i=1}^{n-2} \frac{GA_i(a_i^2+b_i^2)}{4} \frac{(m_i-\bar{m}_i)^2}{\bar{\ell}_i}, \\
E_b &= \frac{1}{2}\sum_{i=0}^{n-2} \frac{EA_i a_i^2}{4\bar{\ell}_i}(\kappa_{i_1}-\bar{\kappa}_{i_1})^2 + \frac{EA_i b_i^2}{4\bar{\ell}_i}(\kappa_{i_2}-\bar{\kappa}_{i_2})^2.
\end{aligned} \tag{5.18}$$

In these expressions, the overbars ornamenting ℓ_k, $\mathbf{e}^j$, m_i, κ_{i_1}, and κ_{i_2} denote the values of these quantities in a fixed reference configuration, and E and G denote the Young's modulus and the shear modulus, respectively. Observe that the expression for E_t was simplified slightly because

$$m_0 = 0, \qquad \bar{m}_0 = 0. \tag{5.19}$$

The discrete twist m_i has several representations (cf. Eqn. (2.81)):

$$\begin{aligned}
m_i &= \vartheta^i - \vartheta^{i-1} \\
&= \gamma^j - \gamma^{j-1} + m^i_{\text{ref}}.
\end{aligned} \tag{5.20}$$

We recall that the referential twist m^i_{ref} is needed in order to accommodate the parallel transport of the reference vectors $\mathbf{a}^i_1$ and $\mathbf{a}^i_2$. When interpreting Eqn. (6.18), it is important to note that the stretching is a quantity associated with the edges while the twisting and bending are associated with the vertices.

The expression for stretching energy E_s is similar to that found in other discrete elastic rod formulations such as Lang et al. [30], Loock et al. [36], and Lv et al. [37]. However, the bending and twisting energies found in Eqn. (6.18) differ from these works in the manner in which the bending and torsional strains are defined. We take this opportunity to note that the perspectives of Lang et al. and Lv et al.'s of a discrete elastic rod as a collection of masses connected by springs may be useful for many readers.

[2] For further details on constitutive relations, material symmetry, and coupled deformation in elastic rods, we refer the reader to [1, 19, 33, 45, 47] and references therein.

5.4 Forces, Moments, and Gradients of Elastic Energies

In addition to the twisting moment $M_{t_{3_k}}\mathbf{t}^k$ acting on the kth edge, a force $\mathbf{F}_{e_i}$ acting on the ith vertex can be prescribed by solving an energy balance:

$$\dot{E}_e = -\sum_{k=0}^{n-2} M_{t_{3_k}}\dot{\gamma}^k - \sum_{i=0}^{n-1}\mathbf{F}_{e_i}\cdot\dot{\mathbf{x}}_i. \tag{5.21}$$

This energy balance pertains to the mechanical power of the forces acting on the vertices and the moments acting on the edges. What is perhaps not obvious is that the term $M_{t_{3_k}}\dot{\gamma}^k$ in this expression is a simplification of the expression for the mechanical power of the moment $M_{t_{3_k}}\mathbf{t}^k$ acting on the discrete elastic rod:

$$M_{t_{3_k}}\mathbf{t}^k\cdot\bar{\boldsymbol{\omega}}^k = M_{t_{3_k}}\mathbf{t}^k\cdot\left(\dot{\gamma}^k\mathbf{t}^k + \mathbf{t}^k\times\dot{\mathbf{t}}^k\right), \tag{5.22}$$

where the angular velocity vector $\bar{\boldsymbol{\omega}}^k$ is defined by Eqn. (2.87). For the choice of E_e we have selected, it is possible to decompose the force vector at the ith vertex:

$$\mathbf{F}_{e_i} = \mathbf{F}_{s_i} + \mathbf{F}_{t_i} + \mathbf{F}_{b_i}. \tag{5.23}$$

Here, the force $\mathbf{F}_{s_i}$ is associated with stretching, the force $\mathbf{F}_{t_i}$ is associated with twisting or torsion, and the force $\mathbf{F}_{b_i}$ is associated with bending or flexure. These forces and the aforementioned moments can be prescribed by assuming that they satisfy the following energy balance for all motions of the rod:

$$\dot{E}_s + \dot{E}_t + \dot{E}_b = -\sum_{k=0}^{n-2} M_{t_{3_k}}\dot{\gamma}^k - \sum_{i=0}^{n-1}\left(\mathbf{F}_{s_i} + \mathbf{F}_{t_i} + \mathbf{F}_{b_i}\right)\cdot\dot{\mathbf{x}}_i. \tag{5.24}$$

That is, the mechanical power of the forces $\mathbf{F}_{e_i}$ balances the negative of the time-rate of change of the elastic energy. The energies E_s, E_t, and E_b are functions of $\mathbf{e}^k$ and m_i. After the time derivatives of the energies have been taken, we substitute for $\dot{\mathbf{e}}^k$ and $\dot{m}_k$ in terms of $\dot{\gamma}^j$ and $\dot{\mathbf{x}}_i$:

$$\begin{aligned}
&\dot{\mathbf{e}}^0 = \dot{\mathbf{x}}_1 - \dot{\mathbf{x}}_0, \quad \ldots, \quad \dot{\mathbf{e}}^k = \dot{\mathbf{x}}_{k+1} - \dot{\mathbf{x}}_k, \quad \ldots, \quad \dot{\mathbf{e}}^{n-2} = \dot{\mathbf{x}}_{n-1} - \dot{\mathbf{x}}_{n-2},\\
&\dot{m}_0 = \dot{\gamma}^0, \quad \ldots, \quad \dot{m}_k = \dot{\gamma}^k - \dot{\gamma}^{k-1} + \dot{m}^k_{\text{ref}}, \quad \ldots, \quad \dot{m}_{n-2} = \dot{\gamma}^{n-2} - \dot{\gamma}^{n-1} + \dot{m}^{n-2}_{\text{ref}}.
\end{aligned} \tag{5.25}$$

The expression for $\dot{m}^k_{\text{ref}}$ in terms of the velocity vectors of the vertices is given in Eqn. (3.41).

After some rearranging, we find that Eqn. (6.22) can be expressed as

$$\sum_{k=0}^{n-2}\Gamma^k\dot{\gamma}^k + \sum_{i=0}^{n-1}\mathbf{X}_i\cdot\dot{\mathbf{x}}_i = 0. \tag{5.26}$$

In this equation,

$$
\begin{aligned}
\mathbf{X}_0 &= -\frac{\partial E_e}{\partial \mathbf{e}^0} + \mathbf{F}_{s_0} + \mathbf{F}_{t_0} + \mathbf{F}_{b_0}, \\
\Gamma^0 &= \frac{\partial E_e}{\partial m_0} - \frac{\partial E_e}{\partial m_1} + M_{t_{3_0}}, \\
\mathbf{X}_k &= -\frac{\partial E_e}{\partial \mathbf{e}^k} + \frac{\partial E_e}{\partial \mathbf{e}^{k-1}} + \mathbf{F}_{s_k} + \mathbf{F}_{t_k} + \mathbf{F}_{b_k}, \\
\Gamma^k &= \frac{\partial E_e}{\partial m_k} - \frac{\partial E_e}{\partial m_{k+1}} + M_{t_{3_k}}, \\
\mathbf{X}_{n-1} &= \frac{\partial E_e}{\partial \mathbf{e}^{n-2}} + \mathbf{F}_{s_{n-1}} + \mathbf{F}_{t_{n-1}} + \mathbf{F}_{b_{n-1}}, \\
\Gamma^{n-2} &= \frac{\partial E_e}{\partial m_{n-2}} + M_{t_{3_{n-2}}},
\end{aligned}
\tag{5.27}
$$

where $E_e = E_b + E_s + E_t$. As Γ^k and $\mathbf{X}_i$ are independent of the rates $\dot{\mathbf{x}}_i$ and $\dot{\gamma}^k$, and Eqn. (6.23) is assumed to hold for all motions of the rod, we conclude that $\Gamma^k = 0$ and $\mathbf{X}_i = 0$.[3] In this manner, we find lengthy expressions for $M_{t_{3_k}}$, $\mathbf{F}_{t_i}$, $\mathbf{F}_{s_i}$, and $\mathbf{F}_{b_i}$ in terms of the derivatives of the energies that are energetically consistent. The expressions are recorded in Section 5.5.

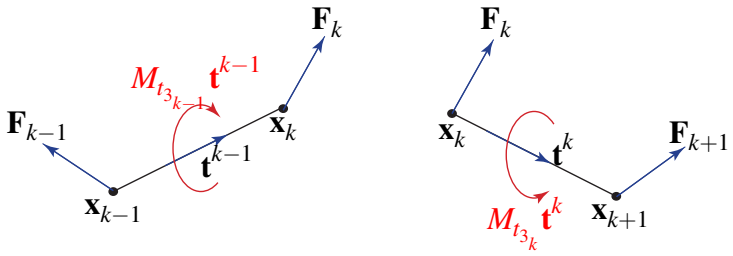

Fig. 5.2 *Three vertices of a discrete elastic rod and the internal forces and the twisting moment associated with the vertices and edges. The forces are produced by elastic deformation and viscous damping, $\mathbf{F}_k = \mathbf{F}_{d_k} + \mathbf{F}_{e_k}$, are discussed in Sections 5.5 and* **??**.

5.5 Hessians of the Elastic Energies

The gradients and Hessians of the elastic energies are needed in order to solve the discrete time equations for the configuration of the rod. The discrete equations are found by imposing the Euler-Lagrange necessary condition for the extremization of a functional.

[3] A procedure of this type is used in continuum mechanics to prescribe constitutive relations for the Cauchy stress tensor for a hyperelastic material. For further details on this matter, see the text books by Chadwick [8] or Gurtin [18].

Consistent with Eqns. (6.22) and (6.23), the negative of the gradient of a potential energy can be identified with an internal force (or moment) in the rod (cf. Figure 5.2). As Newton's method is used to solve the set of implicit equations (cf. Eqn. (6.37)) provided by the Euler-Lagrange necessary condition, expressions for the Hessians of the energies are also needed in order to compute Jacobians. We remind the reader that background on the notation for Hessians and gradients were presented in Section 3.2.

From Eqn. (6.23), we find an expression for the internal force $\mathbf{F}_{s_j}$ due to stretching acting on the vertex $\mathbf{x}_j$ in terms of the stretching energy E_s:

$$\begin{aligned}
\mathbf{F}_{s_0} &= \frac{\partial E_s}{\partial \mathbf{e}^0} = EA^0 \left(\frac{\left\| \mathbf{e}^0 \right\|}{\left\| \bar{\mathbf{e}}^0 \right\|} - 1 \right) \mathbf{t}^0, \\
\mathbf{F}_{s_j} &= -\frac{\partial E_s}{\partial \mathbf{e}^{j-1}} + \frac{\partial E_s}{\partial \mathbf{e}^j} = -EA^{j-1} \left(\frac{\left\| \mathbf{e}^{j-1} \right\|}{\left\| \bar{\mathbf{e}}^{j-1} \right\|} - 1 \right) \mathbf{t}^{j-1} + EA^j \left(\frac{\left\| \mathbf{e}^j \right\|}{\left\| \bar{\mathbf{e}}^j \right\|} - 1 \right) \mathbf{t}^j, \\
\mathbf{F}_{s_{n-1}} &= -\frac{\partial E_s}{\partial \mathbf{e}^{n-2}} = -EA^{n-2} \left(\frac{\left\| \mathbf{e}^{n-2} \right\|}{\left\| \bar{\mathbf{e}}^{n-2} \right\|} - 1 \right) \mathbf{t}^{n-2}.
\end{aligned} \tag{5.28}$$

As anticipated, the components of the forces $\mathbf{F}_{s_k}$ are parallel to tangent vectors to the edges that meet at the kth vertex. The associated Hessian can be computed from the following expression:

$$\frac{\partial E_s}{\partial \mathbf{e}^k \partial \mathbf{e}^j} = \left(EA^j \left(\frac{1}{\left\| \bar{\mathbf{e}}^j \right\|} - \frac{1}{\left\| \mathbf{e}^j \right\|} \right) (\mathbf{I} - \mathbf{t}^j \otimes \mathbf{t}^j) + \frac{EA^j}{\left\| \bar{\mathbf{e}}^j \right\|} \mathbf{t}^j \otimes \mathbf{t}^j \right) \delta_k^j, \tag{5.29}$$

where δ_k^j is the Kronecker delta: $\delta_k^j = 1$ if $j = k$ and is otherwise 0. Further simplification of the Hessian leads to the following representation:

$$\begin{aligned}
\frac{\partial^2 E_s}{\partial m_k \partial m_i} &= 0, \\
\frac{\partial E_s}{\partial \mathbf{e}^k \partial \mathbf{e}^j} &= \left(EA^j \left(\frac{1}{\left\| \bar{\mathbf{e}}^j \right\|} - \frac{1}{\left\| \mathbf{e}^j \right\|} \right) \mathbf{I} + \frac{EA^j}{\left\| \mathbf{e}^j \right\|} \mathbf{t}^j \otimes \mathbf{t}^j \right) \delta_k^j.
\end{aligned} \tag{5.30}$$

The Hessian formed by the components of $\frac{\partial E_s}{\partial \mathbf{e}^k \partial \mathbf{e}^j}$ will be sparse with elements banded along the diagonal. For the elastic energies specified here, there is no coupling between twisting and stretching, and hence $\frac{\partial^2 E_s}{\partial m_k \partial m_i} = 0$.

Again appealing to Eqn. (6.23), the internal force $\mathbf{F}_{t_i}$ due to twisting (or torsion) acting on the vertex $\mathbf{x}_i$ and the twisting moment $M_{t_{3_k}} \mathbf{t}^k$ acting on the kth edge are computed using

the twisting energy E_t:

$$\begin{aligned}
\mathbf{F}_{t_0} &= \frac{\partial E_t}{\partial \mathbf{e}^0} \\
&= \frac{\partial E_t}{\partial m_1}\left(\frac{1}{2\left\|\mathbf{e}^0\right\|}(\kappa\mathbf{b})_1\right), \\
M_{t_{3_0}} &= -\frac{\partial E_t}{\partial m_0} + \frac{\partial E_t}{\partial m_1}, \\
\mathbf{F}_{t_i} &= -\frac{\partial E_t}{\partial \mathbf{e}^{i-1}} + \frac{\partial E_t}{\partial \mathbf{e}^i} \\
&= \frac{\partial E_t}{\partial m_i}\left(\frac{1}{2\left\|\mathbf{e}^i\right\|} - \frac{1}{2\left\|\mathbf{e}^{i-1}\right\|}\right)(\kappa\mathbf{b})_i \\
&\quad - \frac{\partial E_t}{\partial m_{i-1}}\left(\frac{1}{2\left\|\mathbf{e}^{i-1}\right\|}\right)(\kappa\mathbf{b})_{i-1} + \frac{\partial E_t}{\partial m_{i+1}}\left(\frac{1}{2\left\|\mathbf{e}^i\right\|}\right)(\kappa\mathbf{b})_{i+1}, \\
M_{t_{3_k}} &= -\frac{\partial E_t}{\partial m_k} + \frac{\partial E_t}{\partial m_{k+1}}, \\
\mathbf{F}_{t_{n-1}} &= -\frac{\partial E_t}{\partial \mathbf{e}^{n-2}} \\
&= \frac{\partial E_t}{\partial m_{n-2}}\left(\frac{1}{2\left\|\mathbf{e}^{n-2}\right\|} - \frac{1}{2\left\|\mathbf{e}^{n-3}\right\|}\right)(\kappa\mathbf{b})_{n-2} \\
&\quad - \frac{\partial E_t}{\partial m_{n-3}}\left(\frac{1}{2\left\|\mathbf{e}^{n-3}\right\|}\right)(\kappa\mathbf{b})_{n-3}, \\
M_{t_{3_{n-2}}} &= -\frac{\partial E_t}{\partial m_{n-2}},
\end{aligned} \tag{5.31}$$

where

$$\frac{\partial E_t}{\partial m_k} = \frac{GA_k\left(a_k^2 + b_k^2\right)}{4\bar{\ell}_k}(m_k - \bar{m}_k), \tag{5.32}$$

and

$$\begin{aligned}
\frac{\partial E_t}{\partial \mathbf{e}^i} &= \frac{GA_i\left(a_i^2 + b_i^2\right)}{4\bar{\ell}_i}(m_i - \bar{m}_i)\frac{\partial m_i}{\partial \mathbf{e}^i} \\
&\quad + \frac{GA_{i+1}\left(a_{i+1}^2 + b_{i+1}^2\right)}{4\bar{\ell}_{i+1}}(m_{i+1} - \bar{m}_{i+1})\frac{\partial m_{i+1}}{\partial \mathbf{e}^i}.
\end{aligned} \tag{5.33}$$

The force terms in Eqn. (5.31) can be directly attributed to the fact that the referential twist m^k_{ref} is a function of the position vectors of the vertices. We have provided two representations for $\mathbf{F}_{t_i}$. The first is easiest to use when computing the Hessian of E_t and the second allows one to see that the twisting force is directly related to the discrete integrated curvature vectors and produce couples in the edges of the discretized rod.

In the interest of brevity, we refrain from writing the full expressions for the components of the Hessian associated with the torsion of the rod. However, we hope to provide sufficient detail so that the interested reader can establish the lengthy expressions for themselves. To begin computing the Hessian associated with $\mathbf{F}_{t_i}$ and $M_{t_{3_k}}$, we first appeal to the identities

$$\frac{\partial}{\partial \mathbf{e}^k}\left(\frac{1}{\left\|\mathbf{e}^j\right\|}\right) = -\frac{\delta^j_k}{\left\|\mathbf{e}^k\right\|^3}\mathbf{e}^k, \qquad \frac{\partial\left(\kappa\mathbf{b}\right)_k}{\partial m_j} = 0, \tag{5.34}$$

and the expressions for the derivatives $\frac{\partial(\kappa\mathbf{b})_k}{\partial \mathbf{e}^j}$ that can be found in Eqn. (3.24) in Section 3.5. In addition, several components of the Hessian can be computed from[4]

$$\begin{aligned}
\frac{\partial^2 E_t}{\partial m_i \partial m_k} &= \frac{GA_k\left(a_k^2+b_k^2\right)}{4\bar{\ell}_k}\delta^i_k, \\
\frac{\partial^2 E_t}{\partial \mathbf{e}^k \partial \mathbf{e}^i} &= \frac{GA_i\left(a_i^2+b_i^2\right)}{4\bar{\ell}_i}\left(\frac{\partial m_i}{\partial \mathbf{e}^i}\otimes\frac{\partial m_i}{\partial \mathbf{e}^k} + (m_i-\bar{m}_i)\frac{\partial^2 m_i}{\partial \mathbf{e}^k\partial \mathbf{e}^i}\right) \\
&\quad + \frac{GA_{i+1}\left(a_{i+1}^2+b_{i+1}^2\right)}{4\bar{\ell}_{i+1}}\left(\frac{\partial m_{i+1}}{\partial \mathbf{e}^i}\otimes\frac{\partial m_{i+1}}{\partial \mathbf{e}^k} + (m_{i+1}-\bar{m}_{i+1})\frac{\partial^2 m_{i+1}}{\partial \mathbf{e}^k\partial \mathbf{e}^i}\right).
\end{aligned} \tag{5.35}$$

When computing the derivatives of m_k, it is important to note that the angles γ^k are unaltered by changes to the edge vectors $\mathbf{e}^0,\ldots\mathbf{e}^{n-2}$. Consequently,

$$\frac{\partial m_i}{\partial \mathbf{e}^k} = \frac{\partial m^i_{\text{ref}}}{\partial \mathbf{e}^k}, \qquad \frac{\partial^2 m_i}{\partial \mathbf{e}^j\partial \mathbf{e}^k} = \frac{\partial^2 m^i_{\text{ref}}}{\partial \mathbf{e}^j\partial \mathbf{e}^k}. \tag{5.36}$$

Expressions for the derivatives of m^i_{ref} can be found in Sections 3.8 and 3.10.

[4] Given a vector-valued function $\mathbf{a}(\mathbf{b})$ where $\mathbf{b}$ is a vector, we recall from Section 3.2 that $\frac{\partial \mathbf{a}}{\partial \mathbf{b}} = \sum_{r=1}^3\sum_{s=1}^3 \frac{\partial a_r}{\partial b_s}\mathbf{E}_r\otimes\mathbf{E}_s$ where $\mathbf{a}=\sum_{r=1}^3 a_r\mathbf{E}_r$ and $\mathbf{b}=\sum_{s=1}^3 b_s\mathbf{E}_s$.

The following expression for the internal force due to bending $\mathbf{F}_{b_i}$ acting at the vertex $\mathbf{x}_i$ is computed using the bending energy E_b by appealing to Eqn. (6.23):

$$\begin{aligned}
\mathbf{F}_{b_0} &= \frac{\partial E_b}{\partial \mathbf{e}^0}, \\
\mathbf{F}_{b_i} &= -\frac{\partial E_b}{\partial \mathbf{e}^{i-1}} + \frac{\partial E_b}{\partial \mathbf{e}^i}, \\
\mathbf{F}_{b_{n-1}} &= -\frac{\partial E_b}{\partial \mathbf{e}^{n-2}},
\end{aligned} \tag{5.37}$$

where

$$\begin{aligned}
\frac{\partial E_b}{\partial \mathbf{e}^i} = \frac{EA_i}{4\bar{\ell}_i} \Bigg[& a_i^2 \left(\kappa_{i_1} - \bar{\kappa}_{i_1} \right) \frac{\partial \kappa_{i_1}}{\partial \mathbf{e}^i} + b_i^2 \left(\kappa_{i_2} - \bar{\kappa}_{i_2} \right) \frac{\partial \kappa_{i_2}}{\partial \mathbf{e}^i} \\
& + a_{i+1}^2 \left(\kappa_{(i+1)_1} - \bar{\kappa}_{(i+1)_1} \right) \frac{\partial \kappa_{(i+1)_1}}{\partial \mathbf{e}^i} + b_{i+1}^2 \left(\kappa_{(i+1)_2} - \bar{\kappa}_{(i+1)_2} \right) \frac{\partial \kappa_{(i+1)_2}}{\partial \mathbf{e}^i} \Bigg].
\end{aligned} \tag{5.38}$$

The associated Hessian has the following representation:

$$\begin{aligned}
\frac{\partial^2 E_b}{\partial m_k \partial m_i} &= 0, \\
\frac{\partial^2 E_b}{\partial \mathbf{e}^k \partial \mathbf{e}^i} = \frac{EA_i}{4\bar{\ell}_i} \Bigg[& a_i^2 \left(\kappa_{i_1} - \bar{\kappa}_{i_1} \right) \frac{\partial^2 \kappa_{i_1}}{\partial \mathbf{e}^k \partial \mathbf{e}^i} + a_i^2 \frac{\partial \kappa_{i_1}}{\partial \mathbf{e}^i} \otimes \frac{\partial \kappa_{i_1}}{\partial \mathbf{e}^k} \\
& + b_i^2 \left(\kappa_{i_2} - \bar{\kappa}_{i_2} \right) \frac{\partial^2 \kappa_{i_2}}{\partial \mathbf{e}^k \partial \mathbf{e}^i} + b_i^2 \frac{\partial \kappa_{i_2}}{\partial \mathbf{e}^i} \otimes \frac{\partial \kappa_{i_2}}{\partial \mathbf{e}^k} \\
& + a_{i+1}^2 \left(\kappa_{(i+1)_1} - \bar{\kappa}_{(i+1)_1} \right) \frac{\partial^2 \kappa_{(i+1)_1}}{\partial \mathbf{e}^k \partial \mathbf{e}^i} + a_{i+1}^2 \frac{\partial \kappa_{(i+1)_1}}{\partial \mathbf{e}^i} \otimes \frac{\partial \kappa_{(i+1)_1}}{\partial \mathbf{e}^k} \\
& + b_{i+1}^2 \left(\kappa_{(i+1)_2} - \bar{\kappa}_{(i+1)_2} \right) \frac{\partial^2 \kappa_{(i+1)_2}}{\partial \mathbf{e}^k \partial \mathbf{e}^i} + b_{i+1}^2 \frac{\partial \kappa_{(i+1)_2}}{\partial \mathbf{e}^i} \otimes \frac{\partial \kappa_{(i+1)_2}}{\partial \mathbf{e}^k} \Bigg].
\end{aligned} \tag{5.39}$$

In the interests of brevity, we have refrained from substituting for the derivatives of κ_{k_1}, κ_{k_2}, and m_k. The relevant substitutions can be found in Sections 3.10 and 3.11.

5.6 Composing the Generalized Force Vector F_{int}

The discrete formulation has a generalized force vector F_{int} of size $4n-1$. If we consider the kth node and the $(k-1)$th and kth edges bounding this vertex, then the components

of the force vector are

$$\begin{bmatrix} \vdots \\ \mathsf{F}_{\text{int}}^{4k-1} \\ \mathsf{F}_{\text{int}}^{4k} \\ \mathsf{F}_{\text{int}}^{4k+1} \\ \mathsf{F}_{\text{int}}^{4k+2} \\ \mathsf{F}_{\text{int}}^{4k+3} \\ \vdots \end{bmatrix} = \begin{bmatrix} \vdots \\ M_{t_{3_{k-1}}} \\ \mathbf{F}_k \cdot \mathbf{E}_1 \\ \mathbf{F}_k \cdot \mathbf{E}_2 \\ \mathbf{F}_k \cdot \mathbf{E}_3 \\ M_{t_{3_k}} \\ \vdots \end{bmatrix}. \tag{5.40}$$

where the resultant elastic and dissipative force acting on the kth node has the decomposition

$$\mathbf{F}_k = \mathbf{F}_{d_k} + \mathbf{F}_{s_k} + \mathbf{F}_{t_k} + \mathbf{F}_{b_k}. \tag{5.41}$$

The moment $M_{t_{3_k}}\mathbf{t}^k$ on the kth edge is associated with the twisting of the rod. Referring to Eqn. (6.26), we observe that, in contrast to classic rod theories, the moment induced by bending the rod must be implemented by a force couple. That is, the force $\frac{\partial E_b}{\partial \mathbf{e}^k}$ acts on the kth vertex, while the force $-\frac{\partial E_b}{\partial \mathbf{e}^k}$ acts on the $(k+1)$th vertex and thereby produces a force couple.

5.7 Composing the Generalized Force Vector F_{ext} from Applied Forces and Applied Moments

The discrete formulation has a generalized force vector F_{ext} of size $4n-1$. This array accommodates applied forces acting on the vertices and applied moments acting on an edge that are parallel to that edge. Applied moments acting on an edge that have components in the plane normal to the tangent vector to the edge must be accommodated using a force couple.

Given a force $\mathbf{P}$ acting on the vertex $\mathbf{x}_k$, a moment $M_a\mathbf{t}^{k-1}$ acting on the $(k-1)$th edge, and a moment $M_b\mathbf{t}^k$ acting on the kth edge, then

$$\begin{bmatrix} \vdots \\ \mathsf{F}_{\text{ext}}^{4k-1} \\ \mathsf{F}_{\text{ext}}^{4k} \\ \mathsf{F}_{\text{ext}}^{4k+1} \\ \mathsf{F}_{\text{ext}}^{4k+2} \\ \mathsf{F}_{\text{ext}}^{4k+3} \\ \vdots \end{bmatrix} = \begin{bmatrix} \vdots \\ M_a \\ \mathbf{P} \cdot \mathbf{E}_1 \\ \mathbf{P} \cdot \mathbf{E}_2 \\ \mathbf{P} \cdot \mathbf{E}_3 \\ M_b \\ \vdots \end{bmatrix}. \tag{5.42}$$

The force couple requires a more detailed discussion which we now present by way of an example.

5.8 Work-Energy Theorem

A work-energy theorem for the discrete elastic rod can be formulated with the help of the earlier expressions for E_e and T and the equations of motion. First, we need to recognize that Eqn. (6.37) are the discretized version of

$$\mathsf{M}\ddot{q} = \mathsf{F}_{\text{ext}} + \mathsf{F}_{\text{int}}. \tag{5.43}$$

Next, we use Eqn. (6.22) and the identity $\dot{T} = \dot{\mathsf{q}} \cdot \mathsf{M}\ddot{\mathsf{q}}$, to establish the desired theorem:

$$\frac{d}{dt}(T + E_e) = \sum_{k=0}^{n-1} \mathbf{F}_{d_k} \cdot \dot{\mathbf{x}}_k + \mathsf{F}_{\text{ext}} \cdot \dot{\mathsf{q}}. \tag{5.44}$$

If some of the external generalized forces F_{ext} in this expression are conservative then a potential energy function U composed of E_e and the potential energy of the applied forces can be composed. A work-energy theorem for the total energy $E_T = T + U$ can then be established from Eqn. (5.44).

Chapter 6

Planar Discrete Elastic Rods

6.1 Introduction

We consider Bergou et al.'s [2, 3, 4] formulation of a discrete elastic rod discussed earlier in previous chapters. Their theory is sufficiently general to model the stretching, torsional, and flexural deformations of an extensible, flexible elastic rod. In this section, we restrict the theory to the planar case. Thus, the rod is free to move in a plane and the torsional deformation of the rod is ignored. The resulting simplifications to Bergou et al.'s formulation are considerable and we refer to the theory as planar discrete elastic rod (PDER) in the sequel.

In a discrete elastic rod formulation, the centerline of the rod is discretized into a series of $n-1$ segments (edges). The position vectors of the nodes that define these edges are denoted by $\mathbf{x}_0, \ldots, \mathbf{x}_{n-1}$ (cf. Figure 6.1). The edge vector $\mathbf{e}^i$ and the associated unit vector $\mathbf{t}^i$ are defined as follows:

$$\mathbf{e}^i = \mathbf{x}_{i+1} - \mathbf{x}_i, \qquad \mathbf{t}^i = \frac{\mathbf{e}^i}{\left\|\mathbf{e}^i\right\|}. \tag{6.1}$$

For the planar discrete elastic rod, it is convenient to identify the material vector (director) $\mathbf{m}_1^k$ with the unit normal vector for each edge and the material vector (director) $\mathbf{m}_2^k = \mathbf{E}_3 = \mathbf{E}_1 \times \mathbf{E}_2$:

$$\mathbf{m}_1^k = \mathbf{n}^k = \mathbf{E}_3 \times \mathbf{t}^k, \qquad \mathbf{m}_2^k = \mathbf{E}_3. \tag{6.2}$$

Thus, $\left\{\mathbf{t}^k, \mathbf{n}^k, \mathbf{E}_3\right\}$ always form an orthonormal triad of vectors.

For the discrete elastic rod, a signed curvature κ_k is defined at the kth vertex:

$$\kappa_k = \frac{2\sin(\varphi_k)}{1+\cos(\varphi_k)} = 2\tan\left(\frac{\varphi_k}{2}\right), \tag{6.3}$$

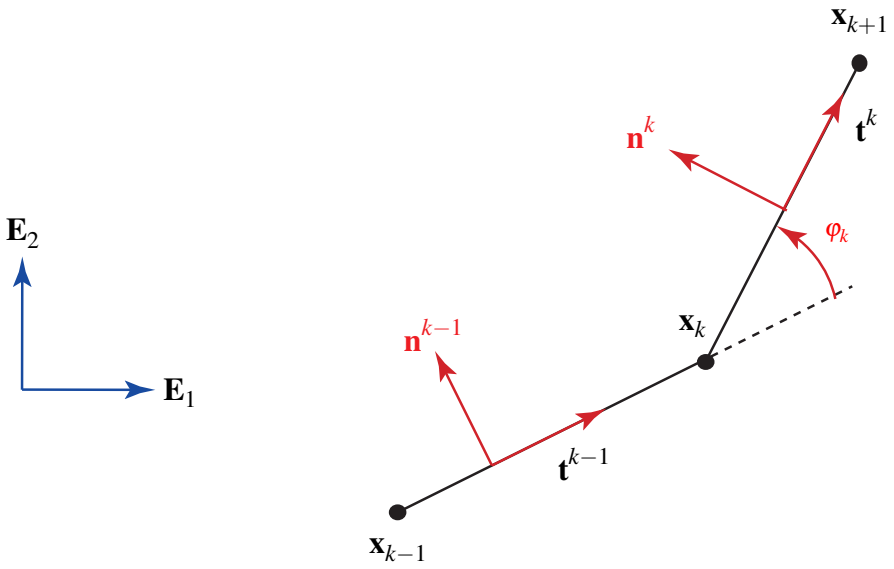

Fig. 6.1 *Three vertices $\mathbf{x}_{k-1}$, $\mathbf{x}_k$, and $\mathbf{x}_{k+1}$ of a planar discrete elastic rod. This figure also illustrates the pairs of unit vectors $\{\mathbf{t}_k, \mathbf{n}_k\}$ associated with the edges. $\mathbf{E}_1$ and $\mathbf{E}_2$ denote the inertial reference frame.*

where φ_k is the turning angle at the kth vertex. In comparison to the curvature of a continuous curve, κ_k is easily measured in soft actuators where optical methods are used to track a set of discrete points. The curvature κ_k is dimensionless and, as shown in Figure 6.2, this function is not defined when the edges are antiparallel. Let δ_i^k be the Kronecker delta: $\delta_i^k = 1$ if $i = k$ and is otherwise 0. We observe that

$$\begin{aligned} \frac{\partial \kappa_k}{\partial \varphi_i} &= \frac{2\delta_i^k}{1+\cos(\varphi_k)} \\ &= \frac{2\delta_i^k}{1+\mathbf{t}^{k-1}\cdot\mathbf{t}^k}. \end{aligned} \tag{6.4}$$

The discrete integrated curvature vector $\kappa_k \mathbf{E}_3$ at the vertex $\mathbf{x}_k$ is used to quantify the bending strain of the rod:

$$\kappa_k \mathbf{E}_3 = \frac{2\mathbf{t}^{k-1}\times\mathbf{t}^k}{1+\mathbf{t}^{k-1}\cdot\mathbf{t}^k}. \tag{6.5}$$

The representation 6.5 can be considered a specialization of the three-dimensional curvature vector to the planar discrete rod. The curvature κ_k can be considered as a simplified planar version of the curvatures κ_{k_1} and κ_{k_2} introduced in Bergou et al. [3]. The latter are known as vertex-based material curvatures.

For future reference, the variation of κ_k as the edges of the discrete rod are varied will be needed.The following are intermediate results from [25, Chapter 6] that can be used to

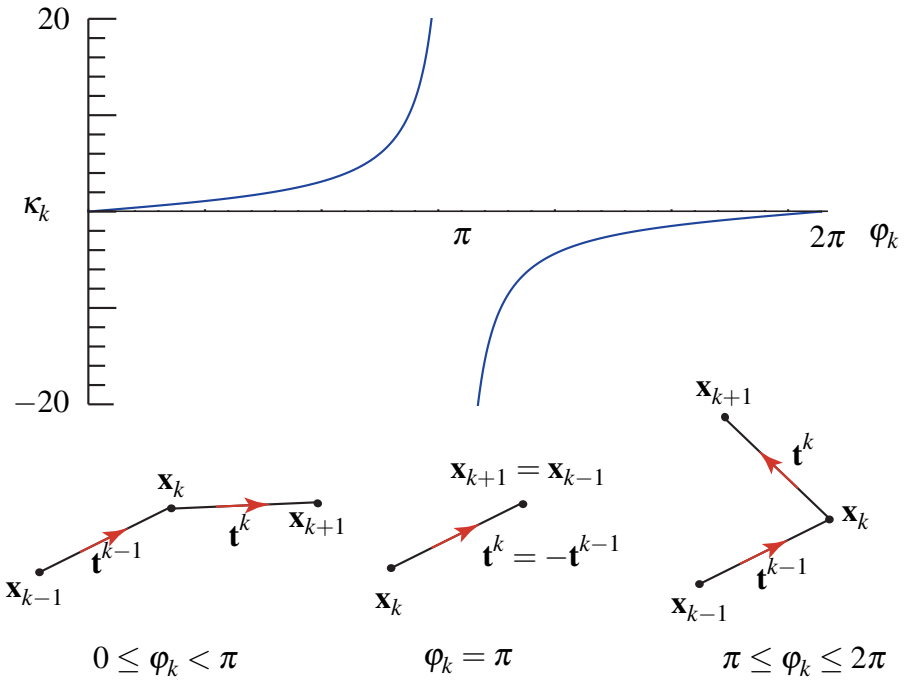

Fig. 6.2 *The discrete curvature κ_k as a function of the turning angle φ_k. When $\varphi_k = \pi$, the edges of the rod are coincident and, as φ_k passes through π, the edges self-intersect. Such behavior is non-physical and is penalized by the forces in the rod, which in proportion to κ_k, become unbounded at $\varphi_k = \pi$.*

compute these variations:

$$\begin{aligned}
\frac{\partial \varphi_k}{\partial \mathbf{e}^{k-2}} &= \mathbf{0}, \\
\frac{\partial \varphi_k}{\partial \mathbf{e}^{k-1}} &= \frac{\mathbf{e}^{k-1}}{\left\|\mathbf{e}^{k-1}\right\|^2} \times \frac{\mathbf{e}^{k-1} \times \mathbf{e}^k}{\left\|\mathbf{e}^{k-1} \times \mathbf{e}^k\right\|}, \\
\frac{\partial \varphi_k}{\partial \mathbf{e}^k} &= \frac{\mathbf{e}^k}{\left\|\mathbf{e}^k\right\|^2} \times \frac{\mathbf{e}^{k-1} \times \mathbf{e}^k}{\left\|\mathbf{e}^{k-1} \times \mathbf{e}^k\right\|}, \\
\frac{\partial \varphi_k}{\partial \mathbf{e}^{k+1}} &= \mathbf{0}.
\end{aligned} \tag{6.6}$$

One can verify that the resulting vectors are orthogonal to $\mathbf{E}_3$ as expected. Indeed, for the planar case of interest we can simplify 6.6 using the identities

$$\mathbf{t}^{k-1} \times \mathbf{t}^k = (\mathbf{n}^{k-1} \cdot \mathbf{t}^k)\mathbf{E}_3 = -(\mathbf{t}^{k-1} \cdot \mathbf{n}^k)\mathbf{E}_3. \tag{6.7}$$

Thus, we have the following simplifications of (6.6):

$$\frac{\partial \varphi_k}{\partial \mathbf{e}^{k-2}} = 0, \quad \frac{\partial \varphi_k}{\partial \mathbf{e}^{k-1}} = -\frac{1}{\left\|\mathbf{e}^{k-1}\right\|}\mathbf{n}^{k-1},$$
$$\frac{\partial \varphi_k}{\partial \mathbf{e}^{k}} = \frac{1}{\left\|\mathbf{e}^{k}\right\|}\mathbf{n}^{k}, \qquad \frac{\partial \varphi_k}{\partial \mathbf{e}^{k+1}} = 0. \tag{6.8}$$

6.2 Prescribing a Mass Matrix

Following Bergou et al. [2, 3, 4], the mass M_i associated with the ith vertex is the average mass of the edges meeting at this vertex:

$$M_0 = \frac{1}{2}M^0,$$
$$M_i = \frac{1}{2}\left(M^i + M^{i-1}\right), \qquad (i = 1,\ldots,n-2),$$
$$M_{n-1} = \frac{1}{2}M^{n-2}. \tag{6.9}$$

For a homogeneous rod with a uniform cross-section in its reference configuration (or reference state),

$$M^i = \rho_0 A^i \left\|\bar{\mathbf{e}}^i\right\|, \qquad (i = 0,\ldots,n-2), \tag{6.10}$$

where ρ_0 is the mass density per unit volume in the reference configuration, A^i is the cross-sectional area in the reference configuration, and $\left\|\bar{\mathbf{e}}^i\right\|$ denotes the length of the ith edge in the reference configuration. If the rod is not homogeneous or of a uniform cross-section, then M^i must be computed using a more primitive prescription:

$$M^i = \int\int\int \rho_0 dx_1 dx_2 dx_3,, \qquad (i = 0,\ldots,n-2), \tag{6.11}$$

where the integration is performed over the segment of the three-dimensional body that the ith edge is modeling.

The mass moments of inertia associated with the ith edge are defined with the help of volume integrals:

$$\rho_0^i I^i = \int\int\int x_2^2 \rho_0 dx_1 dx_2 dx_3, \qquad (i = 0,\ldots,n-2). \tag{6.12}$$

Thus, for a segment of length ℓ of a homogeneous rod with a rectangular cross-section of height h (in the x_2 direction) and width w (in the out-of-plane x_3 direction):

$$\rho_0^i I^i = \rho_0 \ell \frac{hw^3}{12} = \frac{M^i w^2}{12}. \tag{6.13}$$

Observe that we have used the definition of the mass M^i of the ith edge to simplify the expression for $\rho_0^i I^i$.

The mass matrix M can now be prescribed:

$$\mathsf{M} = \begin{bmatrix} M_0 & 0 & \cdots\cdots & 0 & 0 \\ 0 & M_0 & \cdots\cdots & 0 & 0 \\ & \ddots & \ddots & \ddots & \\ & \ddots & \ddots & \ddots & \\ 0 & 0 & \cdots\cdots & M_{n-1} & 0 \\ 0 & 0 & \cdots\cdots & 0 & M_{n-1} \end{bmatrix}. \tag{6.14}$$

This matrix can be used to formulate an expression for the kinetic energy T of the rod:

$$T = \frac{1}{2}\dot{\mathsf{q}}^T \mathsf{M}\dot{\mathsf{q}} = \frac{1}{2}\sum_{k=0}^{n-1}\left(\dot{\mathsf{x}}_k^T M_k \dot{\mathsf{x}}_k\right). \tag{6.15}$$

where

$$\dot{\mathsf{x}}_k = \left[\dot{x}_{k_1}, \dot{x}_{k_2}\right]^T. \tag{6.16}$$

The mass matrix in the expression for T is always positive definite.

6.3 Forces and Energies

For the planar rod theory, we assume that the elastic energy is incorporated into the stretching and bending of the rod: torsion is ignored. The elastic potential energy E_e is a function of the stretching of the edges and the turning angles between the adjacent edges. A simple choice of the function E_e is an additive decomposition of a stretching energy E_s and a bending energy E_b:

$$E_e = E_s + E_b. \tag{6.17}$$

The respective extensional E_s and bending E_b elastic energy functions are assumed to be quadratic functions of the strains:

$$\begin{aligned} E_s &= \frac{1}{2}\sum_{j=0}^{n-2} EA^j \left(\frac{\left\|\mathbf{e}^j\right\|}{\left\|\bar{\mathbf{e}}^j\right\|} - 1\right)^2 \left\|\bar{\mathbf{e}}^j\right\| \\ E_b &= \frac{1}{2}\sum_{i=1}^{n-2} \frac{EI_i}{\bar{\ell}^i}(\kappa_i - \bar{\kappa}_i)^2. \end{aligned} \tag{6.18}$$

In these expressions, the overbars ornamenting ℓ^k, $\mathbf{e}^j$, and κ_i denote the values of these quantities in a fixed reference configuration, and E denotes the Young's modulus. The moment of inertia in the bending energy is based on the average of the mass moments of inertia:

$$I_i = \frac{1}{2}\left(I^i + I^{i-1}\right). \tag{6.19}$$

This averaged quantity is considered a vertex-based measure. In the sequel, the intrinsic curvature $\bar{\kappa}_i$ at the vertex will change depending on the actuation of the SMA actuator that the PDER is modeling. Modeling the actuation using the intrinsic curvature is also a strategy used in models of pneunet actuators (cf. [11]).

The force $\mathbf{F}_{e_i}$ acting on the ith vertex can be prescribed by solving an energy balance that equates the negative of the time rate of change to the elastic energy to the combined mechanical power of the forces $\mathbf{F}_{e_0}, \ldots, \mathbf{F}_{e_{n-1}}$ [25]:

$$\dot{E}_e = -\sum_{i=0}^{n-1} \mathbf{F}_{e_i} \cdot \dot{\mathbf{x}}_i. \tag{6.20}$$

For the choice of E_e we have selected, it is possible to decompose the force vector at the ith vertex as follows:

$$\mathbf{F}_{e_i} = \mathbf{F}_{s_i} + \mathbf{F}_{b_i}. \tag{6.21}$$

Here, the force $\mathbf{F}_{s_i}$ is associated with stretching and the force $\mathbf{F}_{b_i}$ is associated with bending or flexure. These forces can be prescribed by assuming that they satisfy the following energy balance for all motions of the rod i.e.,:

$$\dot{E}_s + \dot{E}_b = -\sum_{i=0}^{n-1} \left(\mathbf{F}_{s_i} + \mathbf{F}_{b_i}\right) \cdot \dot{\mathbf{x}}_i. \tag{6.22}$$

After some rearranging, we find that Eqn. (6.22) can be expressed as

$$\sum_{i=0}^{n-1} \mathbf{X}_i \cdot \dot{\mathbf{x}}_i = 0. \tag{6.23}$$

In this equation,

$$\begin{aligned}
\mathbf{X}_0 &= -\frac{\partial E_e}{\partial \mathbf{e}^0} + \mathbf{F}_{s_0} + \mathbf{F}_{b_0}, \\
\mathbf{X}_k &= -\frac{\partial E_e}{\partial \mathbf{e}^k} + \frac{\partial E_e}{\partial \mathbf{e}^{k-1}} + \mathbf{F}_{s_k} + \mathbf{F}_{b_k}, \\
\mathbf{X}_{n-1} &= \frac{\partial E_e}{\partial \mathbf{e}^{n-2}} + \mathbf{F}_{s_{n-1}} + \mathbf{F}_{b_{n-1}}.
\end{aligned} \tag{6.24}$$

From Eqn. (6.23), we find an expression for the internal force $\mathbf{F}_{s_j}$ due to stretching acting on the vertex $\mathbf{x}_j$ in terms of the stretching energy E_s:

$$\begin{aligned}
\mathbf{F}_{s_0} &= \frac{\partial E_s}{\partial \mathbf{e}^0} = EA^0 \left(\frac{\left\| \mathbf{e}^0 \right\|}{\left\| \bar{\mathbf{e}}^0 \right\|} - 1 \right) \mathbf{t}^0, \\
\mathbf{F}_{s_j} &= -\frac{\partial E_s}{\partial \mathbf{e}^{j-1}} + \frac{\partial E_s}{\partial \mathbf{e}^j} = -EA^{j-1} \left(\frac{\left\| \mathbf{e}^{j-1} \right\|}{\left\| \bar{\mathbf{e}}^{j-1} \right\|} - 1 \right) \mathbf{t}^{j-1} + EA^j \left(\frac{\left\| \mathbf{e}^j \right\|}{\left\| \bar{\mathbf{e}}^j \right\|} - 1 \right) \mathbf{t}^j, \\
\mathbf{F}_{s_{n-1}} &= -\frac{\partial E_s}{\partial \mathbf{e}^{n-2}} = -EA^{n-2} \left(\frac{\left\| \mathbf{e}^{n-2} \right\|}{\left\| \bar{\mathbf{e}}^{n-2} \right\|} - 1 \right) \mathbf{t}^{n-2}.
\end{aligned} \tag{6.25}$$

As anticipated, the components of the forces $\mathbf{F}_{s_k}$ are parallel to tangent vectors to the edges that meet at the kth vertex.

The following expression for the internal force due to bending $\mathbf{F}_{b_i}$ acting at the vertex $\mathbf{x}_i$ is computed using the bending energy E_b by appealing to Eqn. (6.23):

$$\begin{aligned}
\mathbf{F}_{b_0} &= \frac{\partial E_b}{\partial \mathbf{e}^0}, \\
\mathbf{F}_{b_i} &= -\frac{\partial E_b}{\partial \mathbf{e}^{i-1}} + \frac{\partial E_b}{\partial \mathbf{e}^i}, \\
\mathbf{F}_{b_{n-1}} &= -\frac{\partial E_b}{\partial \mathbf{e}^{n-2}},
\end{aligned} \tag{6.26}$$

where

$$\frac{\partial E_b}{\partial \mathbf{e}^k} = \frac{EI_k}{\bar{\ell}_k} \left[(\kappa_k - \bar{\kappa}_k) \frac{\partial \kappa_k}{\partial \mathbf{e}^k} \right] + \frac{EI_{k+1}}{\bar{\ell}_{k+1}} \left[(\kappa_{k+1} - \bar{\kappa}_{k+1}) \frac{\partial \kappa_{k+1}}{\partial \mathbf{e}^k} \right]. \tag{6.27}$$

We note that

$$\begin{aligned}
\frac{\partial \kappa_k}{\partial \mathbf{e}^{k-2}} &= \frac{2}{1+\cos(\varphi_k)} \frac{\partial \varphi_k}{\partial \mathbf{e}^{k-2}} = \mathbf{0}, \\
\mathbf{k}_{k-1} = \frac{\partial \kappa_k}{\partial \mathbf{e}^{k-1}} &= \frac{2}{1+\cos(\varphi_k)} \frac{\partial \varphi_k}{\partial \mathbf{e}^{k-1}}, \\
\mathbf{k}_k = \frac{\partial \kappa_k}{\partial \mathbf{e}^k} &= \frac{2}{1+\cos(\varphi_k)} \frac{\partial \varphi_k}{\partial \mathbf{e}^k}, \\
\frac{\partial \kappa_k}{\partial \mathbf{e}^{k+1}} &= \frac{2}{1+\cos(\varphi_k)} \frac{\partial \varphi_k}{\partial \mathbf{e}^{k+1}} = \mathbf{0}.
\end{aligned} \tag{6.28}$$

Representations for $\frac{\partial \kappa_k}{\partial \mathbf{e}^{k-1}}$ and $\frac{\partial \kappa_k}{\partial \mathbf{e}^{k}}$ can be found using (6.6):

$$\begin{aligned}
\frac{\partial \kappa_k}{\partial \mathbf{e}^{k-1}} &= \frac{2}{1+\mathbf{t}^{i-1}\cdot\mathbf{t}^{i}}\left(\frac{\mathbf{e}^{i-1}}{\left\|\mathbf{e}^{i-1}\right\|^2}\times\frac{\mathbf{e}^{i-1}\times\mathbf{e}^{i}}{\left\|\mathbf{e}^{i-1}\times\mathbf{e}^{i}\right\|}\right)\\
&= \frac{1}{\left\|\mathbf{t}^{i-1}\times\mathbf{t}^{i}\right\|\left\|\mathbf{e}^{i-1}\right\|^2}\left(\mathbf{e}^{i-1}\times\kappa_i\mathbf{E}_3\right)\\
&= -\frac{2}{l^{i-1}(1+\mathbf{t}^{i-1}\cdot\mathbf{t}^{i})}\mathbf{n}^{i-1},\\
\frac{\partial \kappa_k}{\partial \mathbf{e}^{k}} &= -\frac{2}{1+\mathbf{t}^{i-1}\cdot\mathbf{t}^{i}}\left(\frac{\mathbf{e}^{i}}{\left\|\mathbf{e}^{i}\right\|^2}\times\frac{\mathbf{e}^{i-1}\times\mathbf{e}^{i}}{\left\|\mathbf{e}^{i-1}\times\mathbf{e}^{i}\right\|}\right)\\
&= \frac{-1}{\left\|\mathbf{t}^{i-1}\times\mathbf{t}^{i}\right\|\left\|\mathbf{e}^{i}\right\|^2}\left(\mathbf{e}^{i}\times\kappa_i\mathbf{E}_3\right)\\
&= \frac{2}{l^{i-1}(1+\mathbf{t}^{i-1}\cdot\mathbf{t}^{i})}\mathbf{n}^{i-1},
\end{aligned} \tag{6.29}$$

In these expressions, $\mathbf{n}^k = \mathbf{E}_3\times\mathbf{t}^k$ is the unit normal vector to the kth edge.

6.4 Composing the Generalized Force Vectors F_{int} and F_{ext}

The discrete formulation has a generalized internal force vector F_{int} of size $2n-2$. If we consider the kth node and the $(k-1)$th and kth edges bounding this vertex, then the components of the force vector are

$$\begin{bmatrix} \vdots \\ \mathsf{F}_{\text{int}}^{2k+1} \\ \mathsf{F}_{\text{int}}^{2k+2} \\ \vdots \end{bmatrix} = \begin{bmatrix} \vdots \\ \mathbf{F}_k\cdot\mathbf{E}_1 \\ \mathbf{F}_k\cdot\mathbf{E}_2 \\ \vdots \end{bmatrix}. \tag{6.30}$$

where the resultant elastic forces and dissipative force $\mathbf{F}_{d_k}$ acting on the kth node has the decomposition

$$\mathbf{F}_k = \mathbf{F}_{d_k} + \mathbf{F}_{s_k} + \mathbf{F}_{b_k}. \tag{6.31}$$

For future reference, we note that if a force $\mathbf{P}$ acts on the vertex $\mathbf{x}_k$, then this force contributes as follows to the components of the generalized force:

$$\begin{bmatrix} \vdots \\ \mathsf{F}_{\text{ext}}^{2k+1} \\ \mathsf{F}_{\text{ext}}^{2k+2} \\ \vdots \end{bmatrix} = \begin{bmatrix} \vdots \\ \mathbf{P}\cdot\mathbf{E}_1 \\ \mathbf{P}\cdot\mathbf{E}_2 \\ \vdots \end{bmatrix}. \tag{6.32}$$

Examples of the force $\mathbf{P}$ in the sequel will include contact and friction forces acting on a node.

6.5 State Space Formulation and Lagrange's Equations of Motion

In the planar formulation of the discrete elastic rod formulation, a $2n$-dimensional state vector q is formulated using the components of the position vectors of the n vertices:

$$\mathsf{q} = \left[q^1,\ldots,q^{2n}\right] = \left[\mathbf{x}_0\cdot\mathbf{E}_1,\mathbf{x}_0\cdot\mathbf{E}_2,\ldots,\mathbf{x}_{(n-1)}\cdot\mathbf{E}_1,\mathbf{x}_{(n-1)}\cdot\mathbf{E}_2\right]^T. \tag{6.33}$$

Complementing this vector, a pair of $2n$-dimensional generalized force vectors are also formulated:

$$\begin{aligned} \mathsf{F}_{\text{ext}} &= \mathsf{F}_{\text{ext}}\left(t_k,\mathsf{q}\left(t_k\right),\dot{\mathsf{q}}\left(t_k\right)\right) = \left[\mathsf{F}_{\text{ext}}^0,\ldots,\mathsf{F}_{\text{ext}}^{(2n)}\right]^T, \\ \mathsf{F}_{\text{int}} &= \mathsf{F}_{\text{int}}\left(\mathsf{q}\left(t_k\right),\dot{\mathsf{q}}\left(t_k\right)\right) = \left[\mathsf{F}_{\text{int}}^0,\ldots,\mathsf{F}_{\text{int}}^{(2n)}\right]^T. \end{aligned} \tag{6.34}$$

As the discrete elastic rod can be considered as a set of mass particles joined by elastic elements and acted upon by external forces, classical methods, such as those in [57] can be used to show that the equations of motion for the rod can be expressed in the canonical form:

$$\frac{d}{dt}\left(\frac{\partial L}{\partial \dot{q}^J}\right) - \frac{\partial L}{\partial q^J} = Q_J, \qquad (J = 1,\ldots,2n) \tag{6.35}$$

where T denotes the kinetic energy of the rod, U denotes the potential energy associated with elastic energy E_e and externally applied conservative forces, and

$$Q_J = \mathbf{F}_{\text{nc}_0}\cdot\frac{\partial\dot{\mathbf{x}}_0}{\partial\dot{q}^J} + \ldots + \mathbf{F}_{\text{nc}_{n-1}}\cdot\frac{\partial\dot{\mathbf{x}}_{n-1}}{\partial\dot{q}^J}. \tag{6.36}$$

In these representations for the generalized force Q_J, $\mathbf{F}_{\text{nc}_k}$ is the non-conservative force acting on the kth vertex. The equations of motion (6.35) are equivalent to linear combinations of Newton's laws of motion $\mathbf{F}_i = m_i\ddot{\mathbf{x}}_i$ applied to each of the nodes of the rod.

As discussed in Bergou et al. [3], the motion of the rod is determined by using Newton's method to solve the following equations for $\mathsf{q}(t_{k+1})$ and $\dot{\mathsf{q}}(t_{k+1})$:

$$\begin{aligned}(t_{k+1}-t_k)\,\dot{\mathsf{q}}(t_{k+1}) &= \mathsf{q}(t_{k+1})-\mathsf{q}(t_k),\\ \mathsf{M}(\dot{\mathsf{q}}(t_{k+1})-\dot{\mathsf{q}}(t_k)) &= (t_{k+1}-t_k)\,(\mathsf{F}_{\text{ext}}(t_k,\mathsf{q}(t_k),\dot{\mathsf{q}}(t_k))+\mathsf{F}_{\text{int}}(\mathsf{q}(t_{k+1}),\dot{\mathsf{q}}(t_{k+1}))).\end{aligned} \tag{6.37}$$

In these equations, M is a mass matrix discussed in Section 6.2. We shall also present prescriptions for the components of F_{int} in terms of the gradients of elastic energies and viscous damping forces and the components F_{ext} in terms of assigned forces and moments.

6.6 Constraining a Discrete Elastic Rod

There are two common instances where integrable constraints are imposed on the discrete elastic rod. The first case arises when the rod is in contact with a surface. The second case arises when certain edges of the rod are folded onto themselves or (equivalently) edges of a rod are bonded together. Both cases occur when the soft robots shown in Figure 7.2 are modeled using a discrete elastic rod. As we shall demonstrate below, it is straightforward to construct the potential and kinetic energies for the constrained (folded) structure. In addition, because the constraints imposed during the folding process are integrable, deriving the equations of motion follows a standard procedure (see, e.g., [6, 46]). Alternative numerical methods to impose the constraints are discussed in Bergou et al. [4, Section 8].

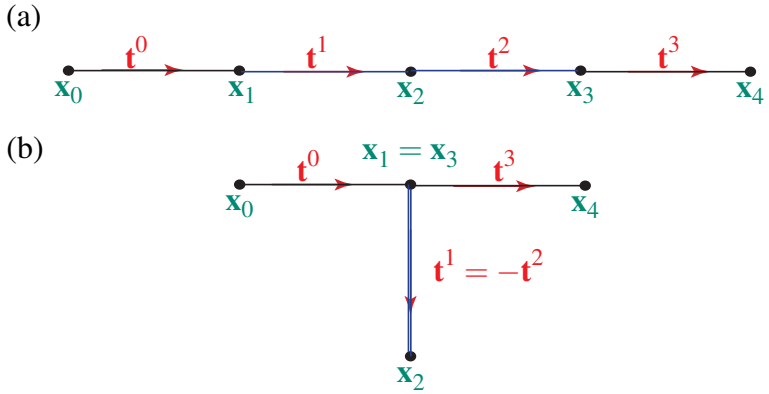

Fig. 6.3 *(a) A discrete elastic rod composed of 4 edges and 5 nodes and (b) the folded discrete elastic rod obtained by permanently joining two of the edges of the rod together.*

6.6.1 Constrained Equations of Motion

After the integrable constraints have been imposed on the discrete elastic rod, a new set of coordinates can be defined by eliminating the redundant coordinates. This new set of

coordinates is denoted by a tilde:

$$\tilde{\mathsf{q}} = \left[\tilde{q}^1, \quad \ldots, \quad \tilde{q}^N\right], \tag{6.38}$$

where N is the number of degrees of freedom of the constrained rod. For instance, for the folded structure shown in Figure 6.3(b), $N = 10-2$. In the sequel, we ornament kinetic and kinematic quantities associated with the constrained system with a tilde.

In the event that the rod is in contact with a rough surface, it is prudent not to impose the constraints associated with the contact until the concomitant normal forces have been computed. In the PDER formulation, the contact of a rod with a surface is enforced through the contact of a node. For the purposes of exposition, suppose the kth node is in contact with a stationary planar surface whose unit normal is $\mathbf{E}_2$. Let $\mathbf{v}_k = \dot{\mathbf{x}}_k$. Then, we prescribe the constraint forces $\mathbf{F}_{k_{\text{con}}}$ acting on the node as follows:

$$\mathbf{F}_{k_{\text{con}}} = \left\{ \begin{array}{cc} N_k\mathbf{E}_2 + F_{f_k}\mathbf{E}_1 & \text{when } \mathbf{v}_k = 0, \qquad |F_{f_k}| \le \mu_s|N_k| \\ N_k\mathbf{E}_2 - \mu_k|N|\frac{\mathbf{v}_k}{\|\mathbf{v_k}\|} & \text{otherwise} \end{array} \right\}. \tag{6.39}$$

The unit vector $\frac{\mathbf{v}_k}{\|\mathbf{v_k}\|}$ is parallel to the slipping direction of the kth node. At the stick-slip transition, $\mathbf{v}_k = 0$, the friction force is static, and we prescribe the slip direction to be antiparallel to the direction of the limiting static friction force.

By imposing the integrable constraints, we can also compute the constrained kinetic energy $\tilde{T}$ of the structure:

$$\tilde{T} = \frac{1}{2}\dot{\tilde{\mathsf{q}}}^T\tilde{\mathsf{M}}\dot{\tilde{\mathsf{q}}}. \tag{6.40}$$

where the $N \times N$ mass matrix $\tilde{\mathsf{M}}$ is computed using the $2n \times 2n$ matrix M by combining the elements associated with the joined nodes. Similarly, for the elastic potential energy, we need to eliminate several terms associated with bending of the pairs of folded edges and possibly introducing new intrinsic curvature terms into the expression for E_e to arrive at $\tilde{E}_e$. Related remarks pertain to the potential energy associated with the applied conservative forces. The pair of energies are then added to define $\tilde{U}$.

Lagrange's equations of motion for the constrained rod are

$$\frac{d}{dt}\left(\frac{\partial\tilde{L}}{\partial\dot{\tilde{q}}^K}\right) - \frac{\partial\tilde{L}}{\partial\tilde{q}^K} = \tilde{Q}_K, \qquad (K = 1,\ldots,N), \tag{6.41}$$

where $\tilde{L} = \tilde{T} - \tilde{U}$. Constraint forces $\mathbf{F}_{\mathrm{c}_k}$ are needed to impose the integrable constraints associated with contact, attachment, or folding. However, in the case where contact is with a smooth surface, it can be shown that these forces do not contribute to several of the forces $\tilde{Q}_K$:

$$\mathbf{F}_{\mathrm{c}_0} \cdot \frac{\partial\dot{\mathbf{x}}_0}{\partial\dot{\tilde{q}}^K} + \ldots + \mathbf{F}_{\mathrm{c}_{n-1}} \cdot \frac{\partial\dot{\mathbf{x}}_{n-1}}{\partial\dot{\tilde{q}}^K} = 0, \qquad (K = 1,\ldots,N). \tag{6.42}$$

Thus (6.41) can be integrated using standard methods.

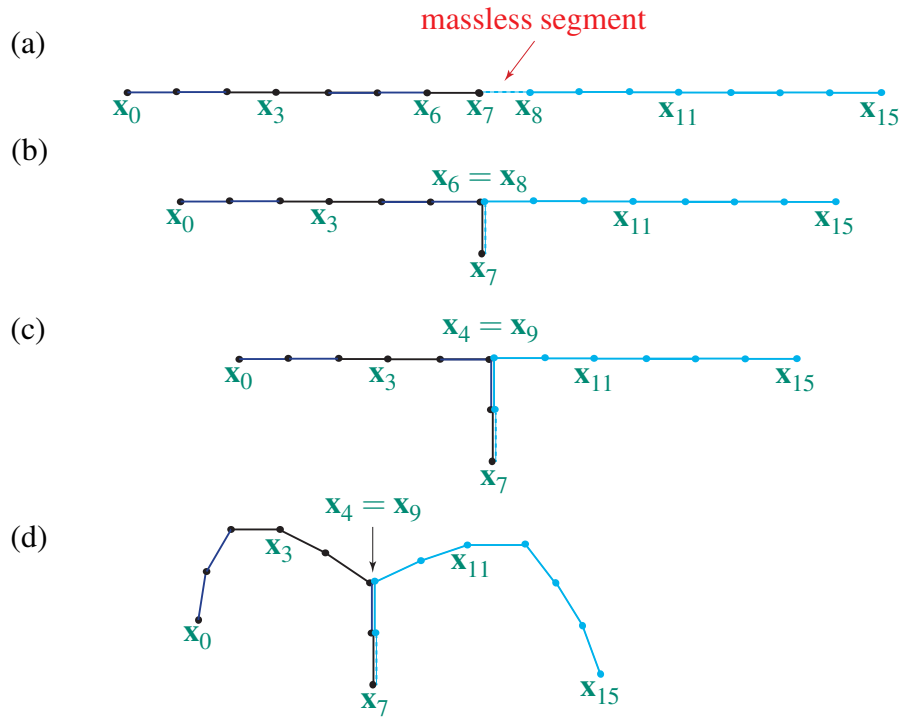

Fig. 6.4 *(a) A discrete elastic rod composed of two segments with 8 nodes and a third massless freely extensible segment with a single edge (dashed line). (b) The folded discrete elastic rod obtained by permanently bonding the third edge to the first segment. (c) The folded discrete elastic rod formed by bonding the 6th edge of the first segment to the first edge of the second segment. (d) Introducing intrinsic curvature into the folded rod.*

6.6.2 Folding a Discrete Elastic Rod

Imagine modeling a T-shaped structure using a discrete elastic rod. The simplest such model will have 4 nodes, however to start the modeling process, we consider a discrete elastic rod with 4 edges (and 5 nodes) (as shown in Figure 6.3). Imagine constraining the positions of nodes $\mathbf{x}_1$ and $\mathbf{x}_3$ to be identical, has the effect of folding the second and third edges onto themselves[1].

To establish the equations of motion for the folded structure, we only need 8 generalized coordinates:

$$\begin{aligned} &\tilde{q}^1 = \mathbf{x}_0 \cdot \mathbf{E}_1, \quad \tilde{q}^2 = \mathbf{x}_0 \cdot \mathbf{E}_2, \quad \tilde{q}^3 = \mathbf{x}_1 \cdot \mathbf{E}_1 = \mathbf{x}_3 \cdot \mathbf{E}_1, \quad \tilde{q}^4 = \mathbf{x}_1 \cdot \mathbf{E}_2 = \mathbf{x}_3 \cdot \mathbf{E}_2, \\ &\tilde{q}^5 = \mathbf{x}_2 \cdot \mathbf{E}_1, \quad \tilde{q}^6 = \mathbf{x}_2 \cdot \mathbf{E}_2, \quad \tilde{q}^7 = \mathbf{x}_4 \cdot \mathbf{E}_1, \quad \tilde{q}^8 = \mathbf{x}_4 \cdot \mathbf{E}_2. \end{aligned} \tag{6.43}$$

[1] For discussion and proof that any discrete rod configuration in Euclidian two dimension space can be reduced into polygonal cycle or a polygonal arc by simple folding motions, we refer the reader to [9, 12, 34].

The mass matrix $\tilde{\mathsf{M}}$ is

$$\tilde{\mathsf{M}} = \begin{bmatrix} M_0 & 0 & 0 & 0 & 0 & 0 & 0 & 0 \\ 0 & M_0 & 0 & 0 & 0 & 0 & 0 & 0 \\ 0 & 0 & M_1+M_3 & 0 & 0 & 0 & 0 & 0 \\ 0 & 0 & 0 & M_1+M_3 & 0 & 0 & 0 & 0 \\ 0 & 0 & 0 & 0 & M_2 & 0 & 0 & 0 \\ 0 & 0 & 0 & 0 & 0 & M_2 & 0 & 0 \\ 0 & 0 & 0 & 0 & 0 & 0 & M_4 & 0 \\ 0 & 0 & 0 & 0 & 0 & 0 & 0 & M_4 \end{bmatrix}. \tag{6.44}$$

The constrained elastic energy $\tilde{E} = \tilde{E}_s + \tilde{E}_b$ can be obtained from Eqn. (6.18):

$$\begin{aligned} \tilde{E}_s &= \frac{1}{2}\left(EA^0 \left(\frac{\left\|\mathbf{e}^0\right\|}{\left\|\bar{\mathbf{e}}^0\right\|} - 1 \right)^2 \left\|\bar{\mathbf{e}}^0\right\| + EA^3 \left(\frac{\left\|\mathbf{e}^3\right\|}{\left\|\bar{\mathbf{e}}^3\right\|} - 1 \right)^2 \left\|\bar{\mathbf{e}}^3\right\| \right) \\ &\quad + \frac{EA^1 + EA^2}{2} \left(\frac{\left\|\mathbf{e}^1\right\|}{\left\|\bar{\mathbf{e}}^1\right\|} - 1 \right)^2 \left\|\bar{\mathbf{e}}^1\right\| \\ \tilde{E}_b &= \frac{1}{2}\left(\frac{E\tilde{I}_1}{\bar{\ell}_1} (\kappa_1 - \bar{\kappa}_1)^2 + \frac{E\tilde{I}_3}{\bar{\ell}_3} (\kappa_3 - \bar{\kappa}_3)^2 \right). \end{aligned} \tag{6.45}$$

The moment of inertia in the bending energy expression is defined as

$$\tilde{I}_1 = \frac{1}{2}\left(I^0 + I^1 + I^2 \right), \qquad \tilde{I}_3 = \frac{1}{2}\left(I^3 + I^1 + I^2 \right). \tag{6.46}$$

The intrinsic curvature at the t-joint is such that the intrinsic turning angle at this point is $\pi/2$, i.e.,

$$\bar{\kappa}_1 = \bar{\kappa}_3 = 2. \tag{6.47}$$

These modifications to the intrinsic curvatures and bending energies are necessary to avoid singularities associated with turning angles of π.

A generalization of this folding procedure that is used to construct the caterpillar-inspired is shown in Figure 6.4. In this construction, we are modeling the bonding of two segments of a discrete elastic rod together by artificially inserting massless freely extensible segments of a rod (i.e., the segment has a Young's modulus of 0). Such a segment is shown as a dashed line in the aforementioned figure.

Chapter 7

Motions of Flexible Shape Memory Alloy Actuator Under Ground Contact

7.1 Introduction

While the mechanics of soft robots is often easily understood from a qualitative perspective, the same cannot be said of a quantitive perspective. To gain the latter perspective, one must develop and analyze models for the soft robot and these models are difficult to develop and analyze. To date, such models include finite-element models and models based on rod theories. However, the analysis of the models in the literature to date is primitive.

The shapes of soft robots range from a soft gripper [15] to bio-inspired worms [54] and caterpillars crawling in forward motion [35] to an octopus [31] with fully functional extending and grabbing tentacles. In order to develop more advanced multi-tasking soft robots, there is a need to develop tractable models for the interaction of a soft robot with its environment.

A model that is quantitatively simple but sophisticated enough to capture the interesting deformation phenomena is called rod theory. This can be used to model uniaxial (long slender) bodies undergoing lateral, longitudinal, and torsional deformations. More advanced variations of the theory can even model deformations of bodies with microstructure, such as muscle fibers embedded in a rod-like matrix. The application of rod theory is not limited to modeling uniaxial animals like caterpillars, worms, etc. and their biomimetic robot counterparts, but also parts of more complex creatures since it is common enough to approximate them as beams.

In this chapter, we will explore how the discrete elastic rod formulation, which was developed to approximate Cosserat rod theories, can be used to model and simulate a caterpillar-inspired soft robot. The design of the soft robot is based on measurements of caterpillar kinematics performed by Trimmer et al. [61], where actuator segments are connected in series to mimic body segments of a caterpillar. These segments are actuated from rear to front resulting in forward locomotion.

7.1.1 Background on Shape Memory Alloy Actuator

A class of soft robots such as those discussed in [31, 35, 54] are made using nickel-titanium (NiTi) shape memory alloy (SMA) wire enclosed in a flexible casing. We refer to the wire and the flexible casing as an SMA actuator. Shape memory alloy is a kind of smart metal that remembers its original shape and deforms back when it is heated. As electric current is passed through the wire, it heats up and transitions from its martensite to austenite state [53]. This transformation bends the actuator and also changes its flexural rigidity. Several deformable configurations can be achieved by strategic arrangement and actuation of the cable. For instance, in the robot described in [35] a single straight SMA wire is placed along the length of a silicone body and the robot is capable of inching locomotion (Figure 7.1 (a)). In Laschi et al.'s robot [31], the SMA wire is arranged in concentric and radial direction to mimic an octopus' tentacle that is capable of extending, bending, and grabbing (Figure 7.1 (b)).

(a) (b)

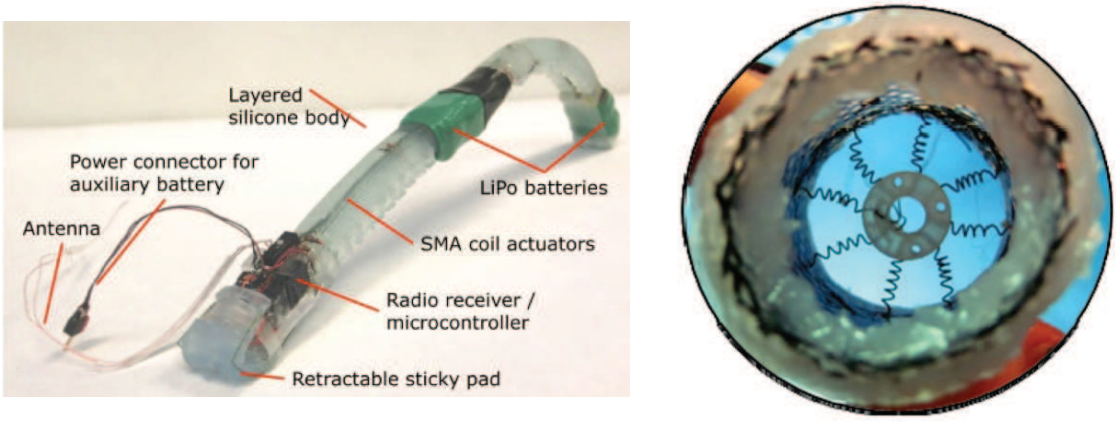

Fig. 7.1 *(a) Trimmer et al.'s soft robot featuring one single SMA wire along its length (image from [35]). (b) Cross section of Laschi et al.'s octopus tentacle arm. SMA wires can be seen in concentric and radial configurations (image from [39]).*

7.1.2 SMA Actuator Fabrication

The actuator is fabricated out of a U-shaped SMA wire (0.3048 mm in diameter, Dynalloy) that is sandwiched by one layer of pre-stretched thermal tape (H48-2, T-Global) and one layer of normal thermal tape (0.5 mm in thickness, H48-2, T-Global). The layers are bonded with a silicone elastomer (Ecoflex 00-30, Smooth-On). The SMA wire is bent into a loop that is 11 mm in width and 34 mm in length.

First, the thermal tape is cut using a CO_2 laser (30 W VLS 3.50; Universal Laser Systems) into two rectangular pieces whose dimensions are 40 $\times$ 18mm and 80 $\times$ 50mm, respectively. Next, the prepolymer part A and part B (Ecoflex 00-30, Smooth-On) are mixed

using a 1:1 mass ratio in a planetary centrifugal mixer (AR-100, THINKY) with 30 seconds mixing and 30 seconds de-gasification. We then apply a 0.2 mm thick uncured Ecoflex on the smaller rectangular thermal tape and make it half-cured at 50°C for 7 minutes. After placing the bent SMA wire on the top side of the half-cured silicone layer, we then apply another layer of the uncured Ecoflex 00-30 silicone with a thickness of 0.4 mm on top. At the same time, we apply a layer of uncured Ecoflex 00-30 silicone with a thickness of 0.1 mm on the upper side of the larger piece of thermal tape that is stretched to 1.5 times of its original length using a linear stretcher (A150602-S1.5, Velmex). Following these procedures, we put both tapes with the uncured Ecoflex 00-30 in the oven and half-cure them at 50°C for 7 minutes and then clamp them together using two binder clips. We then place the final assembly in the oven at 50°C for another 10 minutes so it is fully cured. The final step in the fabrication process is to cut out the actuator using the outline of the smaller piece of thermal tape with a scissors.

7.1.3 Applications

With the actuator described above, it is possible to design modular soft robots that are capable of locomotion. One possible design is to connect the actuators in series and actuate them sequentially in order to mimic the shape of caterpillar segments and prolegs [10] (Figure 7.2 (a)). This design differs from another caterpillar soft robot design done by Trimmer et al. where a single SMA wire is enclosed in rubber-silicon case [35]. Another bio-inspired design based on a starfish is to connect the actuators to form a circle and sequentially actuate the side contacting the ground in order to produce a rolling motion [22] (Figure 7.2 (b)). In the forthcoming section, we will focus on the former design.

(a) (b)

Fig. 7.2 *(a) Caterpillar-inspired robot made out of 4 actuator segments connected in series, with embedded flexible circuit and battery packs on top. (b) Tethered starfish-inspired robot made out of 7 actuator segments that produces a rolling motion when activated. Both pictures are courtesy of the Soft Machines Laboratory at Carnegie Mellon University.*

7.2 Methods

7.2.1 SMA Actuator Parameters

The SMA actuator parameters studied in the following sections are based on the 75% pre-strained sample made by the Soft Machines Laboratory at Carnegie Mellon University. Curvature and flexural rigidity measurements were obtained using the optical method discussed in [10]. For simplicity's sake, the actuator is approximated as a circular arc with constant radius of curvature, leading to uniform pointwise curvature values. The SMA actuator is at its OFF state when there is no electrical current applied to it, and at its ON state when electrical current is being applied. During the OFF state, the radius of curvature of the actuator is 0.0136 m and it has a stiffness modulus of $E = 4.4$ MPa. When the actuator is at its ON state, the radius of curvature is 0.1167 m and it has a stiffness modulus of $E = 11.75$ MPa[1].

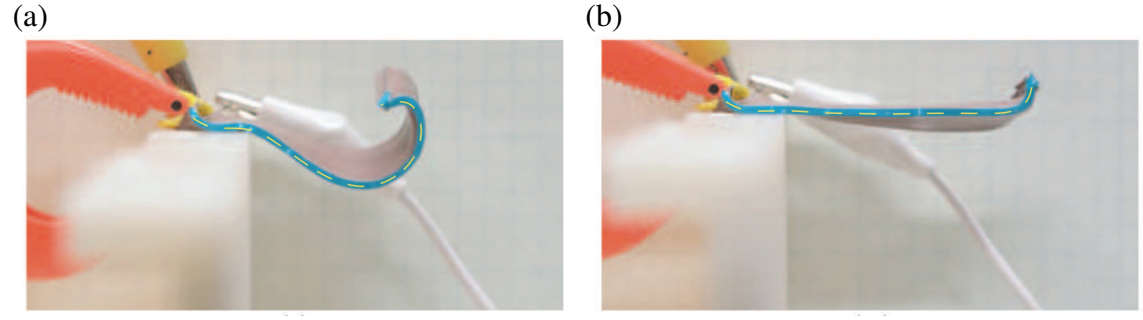

Fig. 7.3 *SMA actuator fabricated by Soft Machine Laboratory at Carnegie Mellon University. (a) shows the unactuated or OFF state and (b) shows the actuated or ON state under electric current.*

7.2.2 Actuation Patterns

The observed time taken for the actuator's curvature value to go from its OFF to ON state is 0.15 s and it takes 1 s for the actuator to cool down to the OFF value. To compensate for our lack of knowledge of $\bar{\kappa}(t)$, we assume two possible manners to model the SMA actuator cycling between two values of flexural rigidity and curvature (Figure 7.4). The first model assumes that curvature and flexural rigidity values decrease slowly together with the cooling of the actuator. This results in a sawtooth shaped actuation pattern. The second model assumes that the ON curvature and flexural rigidity values are maintained for 0.15 s after its actuation, and after that they drop down to their OFF values in the next 0.1 s. It is assumed that the SMA actuator already reaches its OFF values as it cools down for

[1] To convert the measured radius of curvature into pointwise curvature, we multiply the inverse of the radius of curvature with the Voronoi length of each node. Since there are 8 nodes and hence 7 uniform edge lengths, the Voronoi length of each node is 0.007857 m.

Parameter name	Value
Number of vertices	8
Rod length	0.055 m
Rod width	0.008 m
Rod thickness	0.001 m
Radius of curvature (off)	0.0136 m
Radius of curvature (on)	0.1167 m
Young's modulus (off)	4400000 Pa
Young's modulus (on)	11750000 Pa
Volumetric density	758.33 kg m^{-3}
Poisson's ratio	0.5
Coefficient of static friction	0.9
Coefficient of kinetic friction	0.8

Table 7.1 *List of parameters used in the SMA actuator simulation which are kept at constant throughout the simulation.*

the next second. This results in a square wave shaped actuation pattern. In the next section we investigate the effect of different curvature over time patterns on locomotion.

7.2.3 Boundary Conditions

Assume the end points of the SMA actuators are contacting the ground. As the SMA actuator expands from the OFF to ON configuration, there are horizontal surface forces on the contact particles that oppose the expanding motion. Additionally, vertical normal force also varies with the bending. The variation of these forces dictates whether or not the contact point is sticking or slipping according to the static friction criterion, where the static friction force has to be less than the static friction coefficient times the magnitude of surface normal force

$$\left\|\mathbf{F}_f\right\| < \mu_s \left\|\mathbf{N}\right\|. \tag{7.1}$$

When the above condition is met on any nodes contacting the ground, that node remains stationary (thus sticking). However, if this condition is not met, then the node slips horizontally with an opposing friction force value of

$$\mathbf{F}_{f,\text{slip}} = -\mu_k \left\|\mathbf{N}\right\| \frac{\mathbf{v}_{\text{rel}}}{\left\|\mathbf{v}_{\text{rel}}\right\|}. \tag{7.2}$$

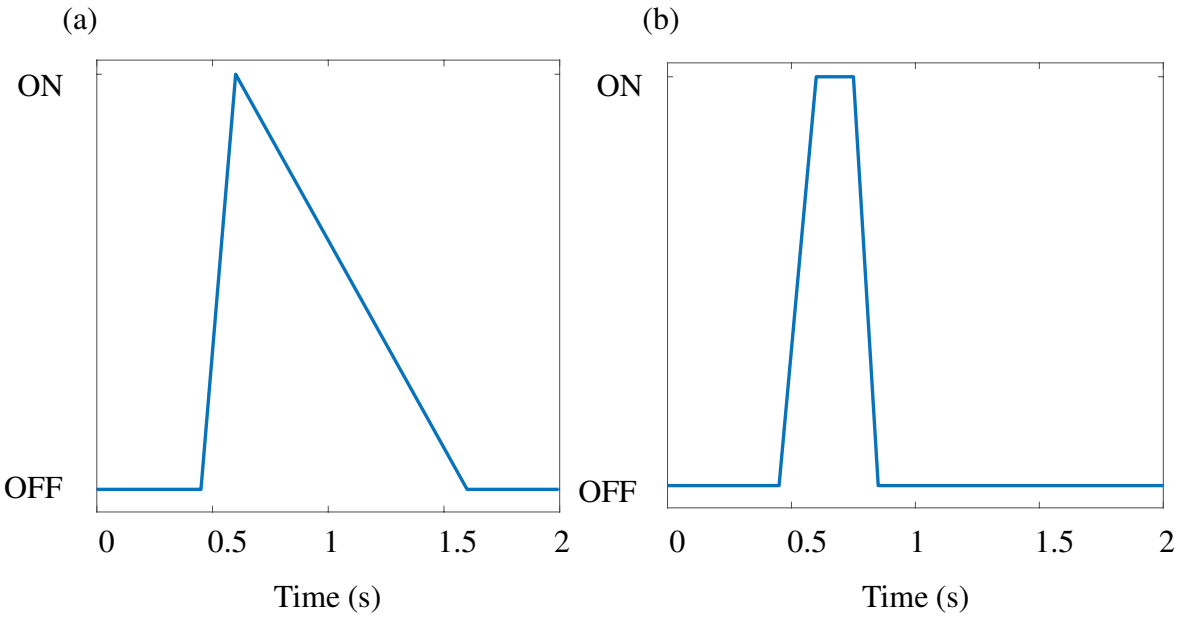

Fig. 7.4 *(a) Sawtooth actuation pattern and (b) square actuation pattern to cycle between two radii of curvature and flexural rigidity values.*

Here, $\mathbf{v}_{\text{rel}}$ is the velocity of the node relative to the surface it is in contact with. In the simulation, we assume a static friction coefficient $\mu_s = 0.9$ and kinetic friction coefficient $\mu_k = 0.8$ based on the value of rubber contacting a smooth pavement [40]. .

7.3 Simulation Results

We postulate that locomotion is produced by a difference of surface forces on the left and right points of contact. Therefore, in the event that the shape of the SMA actuator is a perfectly symmetric circular arc with equal weight distribution, we expect zero net displacement, where displacement is defined as the difference in position of rightmost end point of the actuator over time. of The vertical normal forces at both contact points are found to be identical and the horizontal forces at both contact points are equal and opposite such that no net displacement should occur.

Asymmetry in an actuator can be caused in a variety of ways. First it arises from the fabrication of the SMA actuator itself. After the elastic mold is cured, it is apparent that the actuator does not cure in a perfectly symmetrical manner. If one of the sides is curled more than the other, this leads to asymmetric mass distribution. Secondly, if actuators are connected in series (as for the caterpillar robot), as each segment is activated, it carries the mass of adjacent segments with it. We simulate the second scenario by scaling the mass at the endpoint of an individual actuator by a multiplicative factor so in order to observe how it moves while dragging another actuator. Ultimately, as the scaling factor approaches the

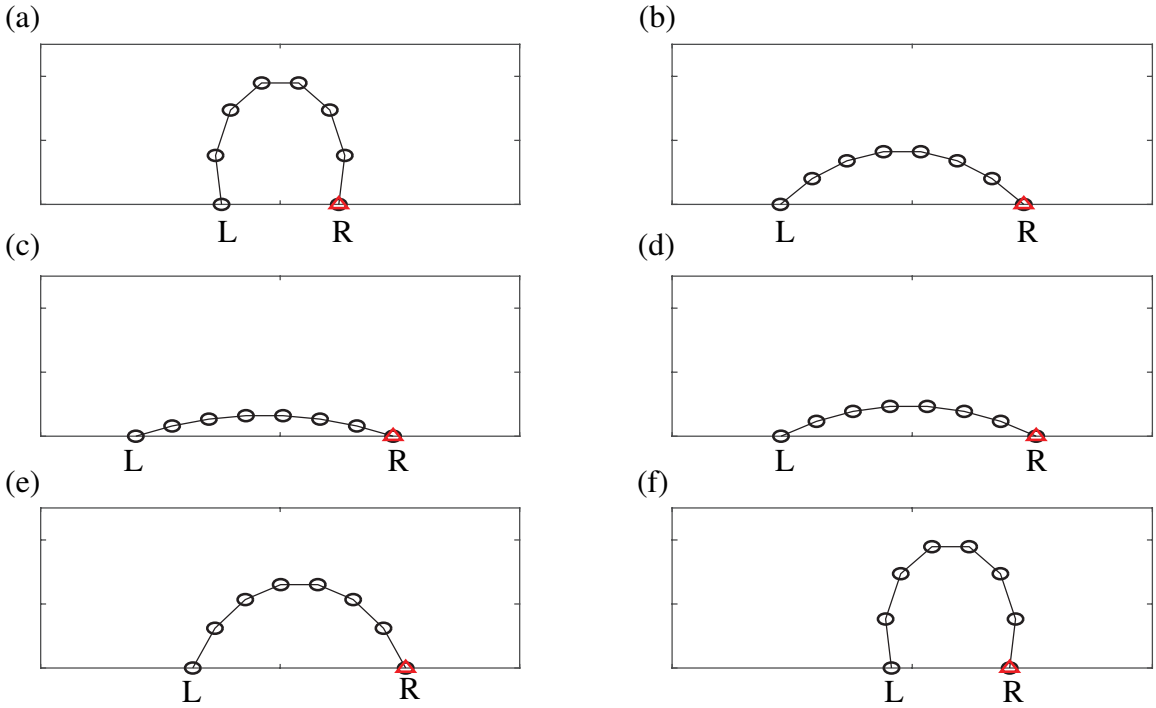

Fig. 7.5 *DER simulation of an asymmetric SMA actuator with 8 nodes under the sawtooth wave activation pattern where the rightmost node (in red) weighs 8 times more than the other remaining nodes at times (a) t = 0 s, (b) t = 0.5 s, (c) t = 0.6 s, (d) t = 1 s, (e) t = 1.5 s, (f) t = 2 s. The width of the box is 10 cm and the height of the box is 2.5 cm. The net displacement is 0.82458 cm or 15% of its body length. Left and right contact points are identified.*

number of vertices in the segment, it approximates the act of dragging an entire adjacent segment.

While the SMA actuator is in motion (from 0.45 s to 1.6 s for the sawtooth wave and from 0.45 s to 1 s for the square wave) it undergoes stick slip motion. The horizontal forces acting on the left and right contact points are opposing the expanding motion (0.45 s to 0.6 s) and the contracting motion (0.6 s to 1.6 s for the sawtooth wave, 0.75 s to 0.85 s for the square wave). The horizontal forces oscillate about zero while the vertical forces oscillate about the fraction of the weight of the SMA actuator. Given that the coefficient of static friction is $\mu_s = 0.9$, it is apparent that the contact points are alternating between sticking and slipping motions as the horizontal forces alternate between zero and nonzero values.

For the sawtooth wave, we observe that while the actuator initially expands symmetrically when going from the OFF to ON position, between 0.6 s to 1.5 s, the actuator slides to the lumped mass side (see Figure 7.8 (a)). Additionally, as the actuator deforms from its ON to OFF position, the side with the lumped mass ends up acting as an anchor such that it remains in its position and drags the rest of the actuator towards that side, resulting in an overall displacement towards the lumped mass side.

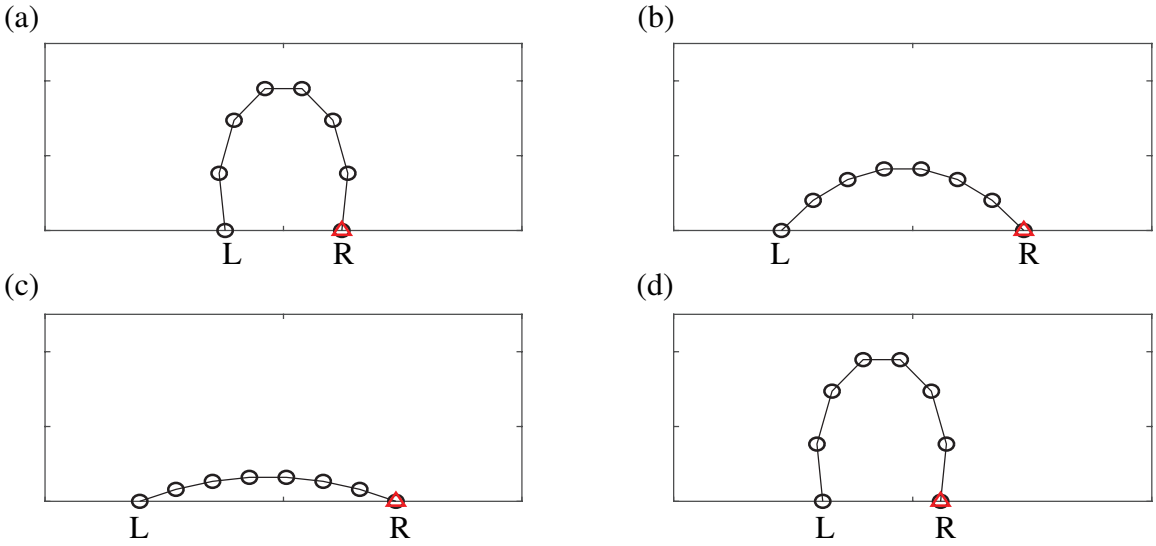

Fig. 7.6 *DER simulation of an asymmetric SMA actuator with 8 nodes under the square wave activation pattern where the rightmost node (in red) weighs 8 times more than the other remaining nodes at times (a) t= 0 s, (b) t = 0.5 s, (c) t = 0.6 s, (d) t = 1 s. The width of the box is 10 cm and the height of the box is 2.5 cm. The net displacement is -0.62077 cm or 11.3% of its body length. Left and right contact points are identified.*

For the square wave, it turns out that the side that weighs more does not expand as much as the other when the actuator deforms from its OFF to ON state, which shifts the geometric center of the actuator to the left. When the actuator returns from the OFF to the ON state, it aligns with the now shifted geometric center. This motion resembles the motion of two masses connected by an asymmetrical spring aided by stick-slip friction in [65].

The following trend in Figure 7.9 is observed as the multiplication factor of the end point mass is increased. Multiplying the mass coefficient of the end point mass by the number of vertices per segment may be used as an approximation for adding an entire segment next to it. It turns out that a significant amount of displacement occurs due to the weight imbalance when the segment is dragging other segment(s). For the sawtooth activation pattern, it seems that to cause an overall displacement to the right, mass should be added to the right side and vice versa. For the square activation pattern, mass should be added to the left in order to move the actuator to the left. It is interesting that these starkly different results are observed with two different kinds of waveforms, and perhaps different modes of locomotion can be observed by varying the input waveforms.

Given that the ground forces always oppose the contacting ends' motion, it is apparent that the work done by the ground forces is negative. Thus, total energy is dissipated through the work done by the ground motion. It is interesting to observe in Figure 7.10 that the work done by the friction force in the left and right ends are not equal; in fact more work is done by the ground forces on the left contact point which is not as heavy as its weighted

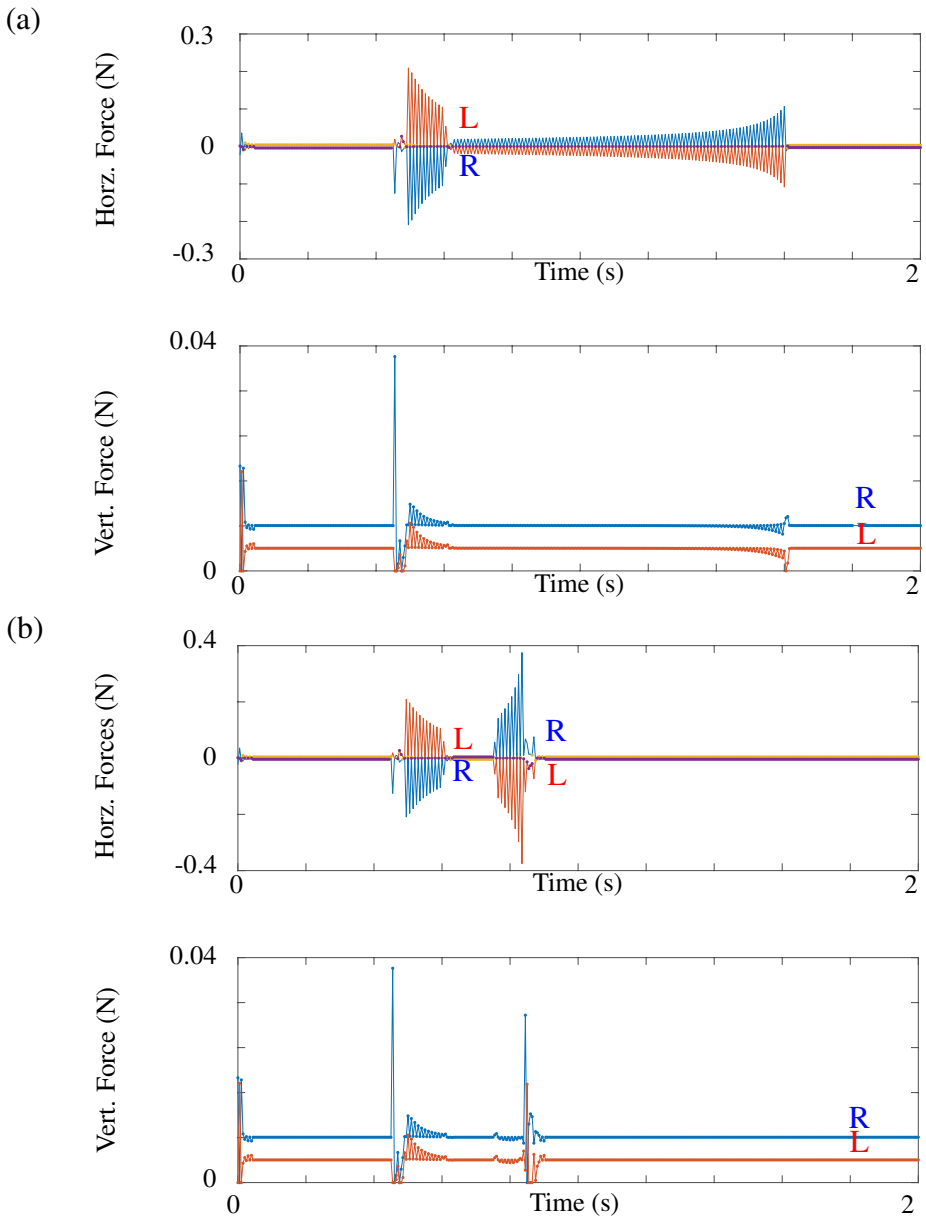

Fig. 7.7 *Stick-slip phenomenon observed on SMA actuator under (a) sawtooth and (b) square activation pattern.*

right counterparts. Since the right endpoint weighs more, it resists motion and undergoes less displacement. We can also compare which actuation pattern results in a more energy efficient motion. It takes less work to move the SMA actuator using the sawtooth wave actuation pattern compared to the square wave actuation pattern. Not only that, but the DER simulation also predicts the sawtooth wave actuation pattern also results in higher displacement compared to the square wave actuation pattern.

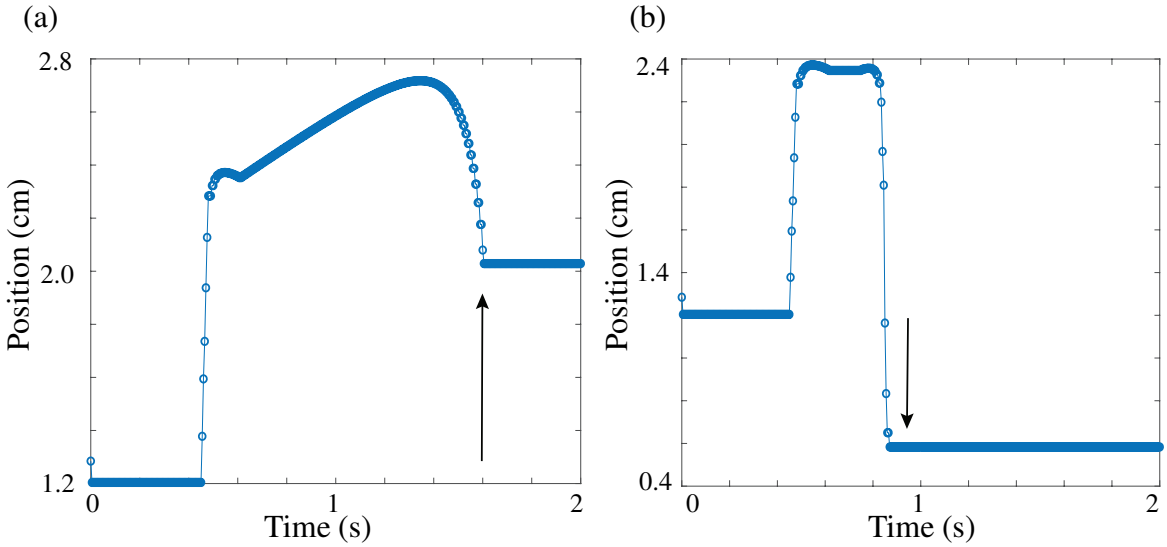

Fig. 7.8 *Horizontal position of the right contact point over time for the SMA actuator activated using (a) sawtooth and (b) square pattern showing displacements of 0.82458 cm and -0.62077 cm respectively. Positive displacement is to the right and negative displacement is to the left. For both figures, the mass of the rightmost endpoint is multiplied by 8. Note how the displacement trends imitate the radius of curvature actuation patterns.*

7.4 Conclusion

With the DER simulation results discussed in this chapter, we have shown that DER can be used as a tool to aid the choice of various design parameters in the development of soft robots. We have shown the various result that come about by changing the input wave parameter, mass distribution, and coefficient of friction. Several of the results are surprising and unpredictable for there is complex dynamic interplay during the deformation and motion. These phenomena would not be noticeable if we were to ignore the quantitative analysis of soft body motion and assume that soft bodies cannot do much interaction to their surroundings compared to their rigid counterparts.

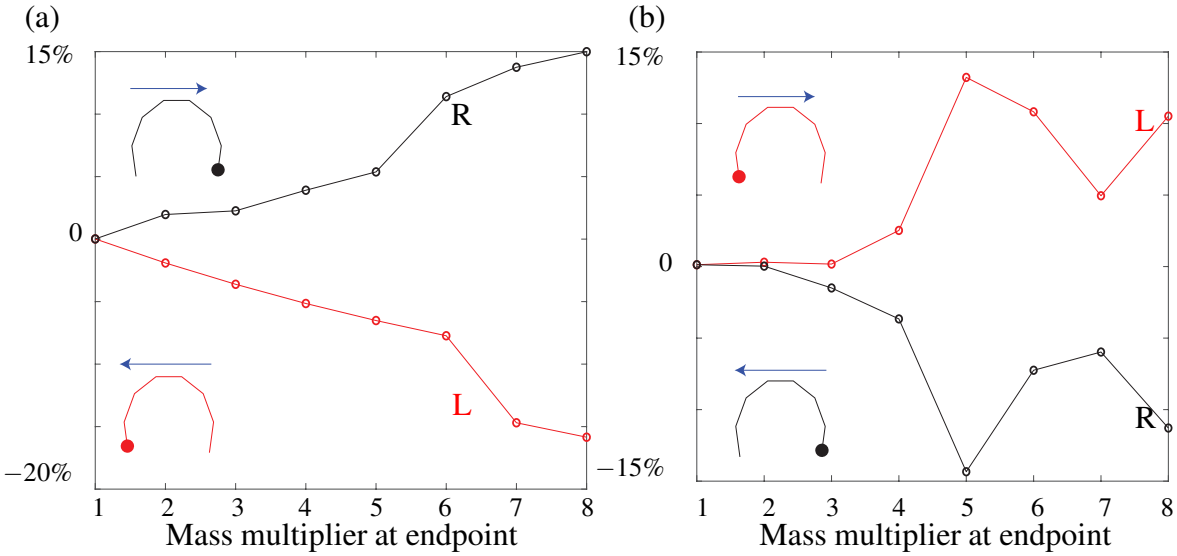

Fig. 7.9 *Plot of net displacement (as a percentage of body length) versus multiplication factor to the weight on the left and right most nodes, (a) is for the sawtooth actuation pattern and (b) is for the square activation pattern. For reference, the length of the SMA actuator is 5.5 cm. Note that positive displacement means displacement towards the right and negative displacement means displacement towards the left. Also shown are cartoons with direction of overall trend (weight on left side will result in displacement to the right and vice versa).*

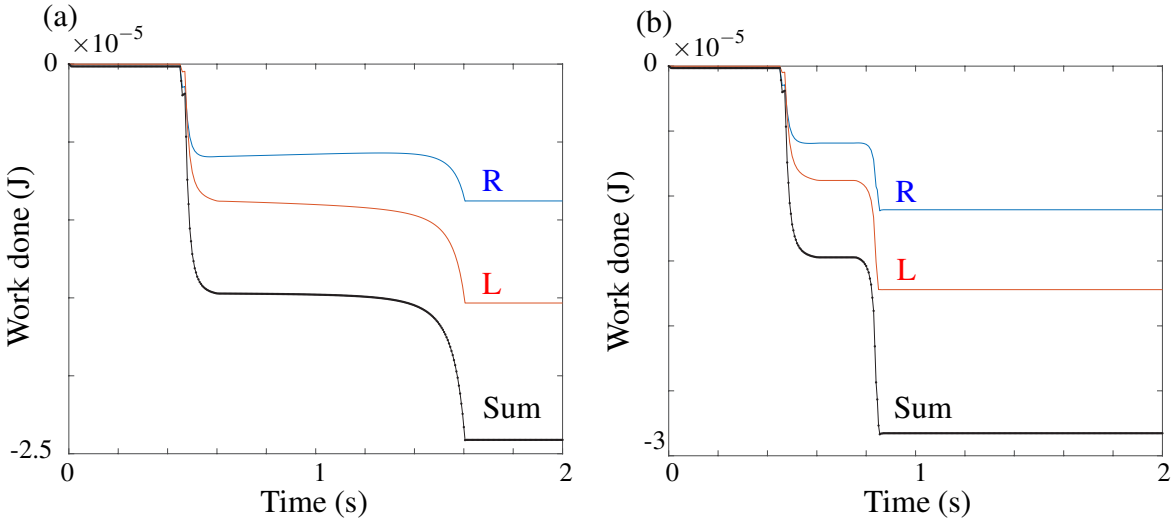

Fig. 7.10 *Work done over time by ground contact forces on each legs and the sum of those for one cycle of the (a) sawtooth and (b) square activation wave. The net work done is negative as the work done by the ground forces dissipate energy. Note that the mass of the rightmost endpoint for both cases are 8 times heavier than the remaining nodes in the simulation.*

Chapter 8

Closing Comments

We have presented a derivation of the Discrete Elastic Rod (DER), which was developed to simulate long and slender objects in computer graphics, for general engineering audiences. This method provides a way to simulate the dynamics of uniaxial deformable objects and capture their bending and twisting motions. The equations of motion (6.37) can be viewed as a $(4n-1)$-degree-of-freedom mechanical system composed of mass particles connected by discrete deformable elements. While the stretching of these elements is easy to accommodate and the bending can be modeled using the vector $\kappa_i \mathbf{b}_i$ at each vertex, the twisting of the rod is challenging to model in a computationally efficient manner.

A planar version (PDER) is developed from the full formulation, where the rod is free to move a plane and torsional deformations are ignored. There is only one kind of strain measure, which is the planar curvature $\kappa_k \mathbf{E}_3$, that is used to measure bending on a plane. The result is a $2n$-degree-of-freedom system which can be put in a canonical form with the help of Lagrange's equations of motion and state space form. Geometrical constraints can easily be incorporated into the system using the system of particles approach due to similarity in their formulations.

The DER method is applied to simulate a single Shape Memory Alloy (SMA) actuator that is a component in a caterpillar inspired soft robot. The locomotion method is by switching the intrinsic curvature and Young's modulus between two values. Simulation results show how stick-slip Coulomb friction acting on the ground contact points of the actuator where the mass is not evenly distributed while the actuator is deforming end up influencing the motion either to the right or the left, depending on the waveform of the intrinsic curvature function over time.

We have shown how the DER and PDER method can be a useful tool to aid the design of soft robots. Currently we are working to compare the simulation results with a benchmark robot manufactured by Soft Machines Lab at Carnegie Mellon University. We hope that DER can eventually be used to predict motion patterns that yield the highest locomotion speed, among other parameters to be optimized.

References

[1] S. S. Antman. Nonlinear Problems of Elasticity, volume 107 of Applied Mathematical Sciences. Springer-Verlag, New York, second edition, 2005.

[2] B. Audoly, N. Clauvelin, P.-T. Brun, M. Bergou, B. Grinspun, and M. Wardetzky. A discrete geometric approach for simulating the dynamics of thin viscous threads. Journal of Computational Physics, 253:18–49, 2013.

[3] M. Bergou, B. Audoly, E. Vouga, M. Wardetzky, and E. Grinspun. Discrete viscous threads. ACM Transactions on Graphics (SIGGRAPH), 29(4):116:1–116:10, 2010.

[4] M. Bergou, M. Wardetzky, S. Robinson, B. Audoly, and E. Grinspun. Discrete elastic rods. ACM Transactions on Graphics (SIGGRAPH), 27(3):63:1–63:12, August 2008.

[5] A. I. Bobenko. Geometry II: Discrete Differential Geometry, 2015.

[6] J. Casey. Geometrical derivation of Lagrange's equations for a system of particles. American Journal of Physics, 62(9):836–847, 1994.

[7] J. Casey and V. C. Lam. On the relative angular velocity tensor. ASME Journal of Mechanisms, Transmissions, and Automation in Design, 108:399–400, 1986.

[8] P. Chadwick. Continuum Mechanics. Dover Publications, New York, second corrected and enlarged edition, 1999.

[9] R. Connelly, E. D. Demaine, and G. Rote. Straightening polygonal arcs and convexifying polygonal cycles. In Foundations of Computer Science, 2000. Proceedings. 41st Annual Symposium on, pages 432–442. IEEE, 2000.

[10] C. A. Daily-Diamond, A. Novelia, and O. M. O'Reilly. Dynamical analysis and development of a biologically inspired SMA caterpillar robot. Bioinspiration & Biomimetics, 12(5):056005, 2017.

[11] K. M. de Payrebrune and O. M. O'Reilly. On constitutive relations for a rod-based model of a pneu-net bending actuator. Extreme Mechanics Letters, 8:38–46, 2016.

[12] E. D. Demaine and J. O'Rourke. A survey of folding and unfolding in computational geometry. In J. E. Goodman, J. Pach, and E. Welzl, editors, Combinatorial and Computational Geometry, volume 52 of Mathematical Sciences Research Institute Publications, pages 167–211. Cambridge University Press, New York, 2005.

[13] D. Evangelista, S. Hotton, and J. Dumais. The mechanics of explosive dispersal and self-burial in the seeds of the filaree, Erodium cicutarium (Geraniaceae). Journal of Experimental Biology, 214(4):521–529, 2011.

[14] F. B. Fuller. Decomposition of the linking number of a closed ribbon: A problem from molecular biology. Proceedings of the National Academy of Sciences of the United States of America, 75(8):3557–3561, 1978.

[15] K. C. Galloway, K. P. Becker, B. Phillips, J. Kirby, S. Licht, D. Tchernov, R. J. Wood, and D. F. Gruber. Soft robotic grippers for biological sampling on deep reefs. Soft robotics, 3(1):23–33, 2016.

[16] L. E. Goodman and A. R. Robinson. Effect of finite rotations on gyroscopic sensing devices. ASME Journal of Applied Mechanics, 25:210–213, 1952.

[17] A. E. Green, P. M. Naghdi, and M. L. Wenner. On the theory of rods. I Derivations from three-dimensional equations. Proceedings of the Royal Society. London. Series A. Mathematical, Physical and Engineering Sciences, 337(1611):451–483, 1974.

[18] M. E. Gurtin. An Introduction to Continuum Mechanics. Academic Press, New York, 1981.

[19] T. J. Healey. Material symmetry and chirality in nonlinearly elastic rods. Mathematics and Mechanics of Solids, 7(4):405–420, 2002.

[20] D. W. Henderson. Differential Geometry: A Geometric Introduction. Prentice Hall, Upper Saddle River, New Jersey, 1998.

[21] T. Hoffmann. Discrete Differential Geometry of Curves and Surfaces. Math-for-Industry (MI) Lecture Notes Series, Faculty of Mathematics, Kyushu University, Japan, 2009.

[22] X. Huang, M. Khalid Jawed, A. Batzorig, and C. Majidi. A versatile and robust soft rolling robot driven by shape memory alloy. Bulletin of the American Physical Society, 2018.

[23] M. K. Jawed, F. Da, J. Joo, E. Grinspun, and P. M. Reis. Coiling of elastic rods on rigid substrates. Proceedings of the National Academy of Sciences of the United States of America, 111(41):14663–14668, 2014.

[24] M. K. Jawed, N. K. Khouri, F. Da, E. Grinspun, and P. M. Reis. Propulsion and instability of a flexible helical rod rotating in a viscous fluid. Physical Review Letters, 115(16):168101, 2015.

[25] M. K. Jawed, A. Novelia, and O. M. O'Reilly. A Primer on the Kinematics of Discrete Elastic Rods. SpringerBriefs in Applied Sciences and Technology. Springer-Verlag, New York, 2018.

[26] J. M. Kaldor, D. L. James, and S. Marschner. Efficient yarn-based cloth with adaptive contact linearization. In ACM SIGGRAPH 2010 Papers, SIGGRAPH '10, pages 105:1–105:10, New York, NY, USA, 2010. ACM.

[27] L. Kelvin and P. G. Tait. A Treatise on Natural Philosophy. Cambridge University Press, Cambridge, Reprinted edition, 1912.

[28] S. Kim, C. Laschi, and B. Trimmer. Soft robotics: a bioinspired evolution in robotics. Trends in Biotechnology, 31(5):287–294, 2013.

[29] G. Kirchhoff. Über des gleichgewicht und die Bewegung eines unendlich dünnen elastichen Stabes. Crelles Journal für die reine und angewandte Mathematik, 56:285–313, 1859.

[30] H. Lang, J. Linn, and M. Arnold. Multi-body dynamics simulation of geometrically exact Cosserat rods. Multibody System Dynamics, 25(3):285–312, 2011.

[31] C. Laschi, M. Cianchetti, B. Mazzolai, L. Margheri, M. Follador, and P. Dario. Soft robot arm inspired by the octopus. Advanced Robotics, 26(7):709–727, 2012.

[32] C. Laschi, B. Mazzolai, and M. Cianchetti. Soft robotics: Technologies and systems pushing the boundaries of robot abilities. Sci. Robot., 1(1):eaah3690, 2016.

[33] T. A. Lauderdale and O. M. O'Reilly. On transverse and rotational symmetries in elastic rods. Journal of Elasticity, 82(1):31–47, 2006.

[34] W. J. Lenhart and S. H. Whitesides. Reconfiguring closed polygonal chains in Euclidean$d$-space. Discrete and Computational Geometry, 13(1):123–140, 1995.

[35] H.-T. Lin, G. G. Leisk, and B. A. Trimmer. Goqbot: a caterpillar-inspired soft-bodied rolling robot. Bioinspiration & Biomimetics, 6(2):026007, 2011.

[36] A. Loock, E. Schömer, and I. Stadtwald. A virtual environment for interactive assembly simulation: From rigid bodies to deformable cables. In 5th World Multiconference on Systemics, Cybernetics and Informatics, pages 325–332, 2001.

[37] N. Lv, J. Liu, X. Ding, J. Liu, H. Lin, and J. Ma. Physically based real-time interactive assembly simulation of cable harness. Journal of Manufacturing Systems, 43(Part 3):385–399, 2017. Special Issue on the 12th International Conference on Frontiers of Design and Manufacturing.

[38] J. E. Marsden and T. S. Ratiu. Introduction to Mechanics and Symmetry: A Basic Exposition of Classical Mechanical Systems, volume 17 of Texts in Applied Mathematics. Springer-Verlag, New York, second edition, 1999.

[39] B. Mazzolai, L. Margheri, M. Cianchetti, P. Dario, and C. Laschi. Soft-robotic arm inspired by the octopus: II. from artificial requirements to innovative technological solutions. Bioinspiration & biomimetics, 7(2):025005, 2012.

[40] J. L. Meriam and L. G. Kraige. Engineering Mechanics: Dynamics, volume 2. John Wiley & Sons, 2012.

[41] R. Montgomery. How much does the rigid body rotate? A Berry's phase from the 18th century. American Journal of Physics, 59(5):394–398, 1991.

[42] P. M. Naghdi. Finite deformation of elastic rods and shells. In D. E. Carlson and R. T. Shield, editors, Proceedings of the IUTAM Symposium on Finite Elasticity: Held at Lehigh University, Bethlehem, PA, USA August 10–15, 1980, pages 47–104. Springer Netherlands, Dordrecht, 1982.

[43] A. Novelia and O. M. O'Reilly. On geodesics of the rotation group SO(3). Regular and Chaotic Dynamics, 20(6):729–738, 2015.

[44] O. M. O'Reilly. On the computation of relative rotations and geometric phases in the motions of rigid bodies. ASME Journal of Applied Mechanics, 64(4):969–974, 1997.

[45] O. M. O'Reilly. On constitutive relations for elastic rods. International Journal of Solids and Structures, 35(11):1009–1024, 1998.

[46] O. M. O'Reilly. Intermediate Engineering Dynamics: A Unified Treatment of Newton-Euler and Lagrangian Mechanics. Cambridge University Press, Cambridge, 2008.

[47] O. M. O'Reilly. Modeling Nonlinear Problems in the Mechanics of Strings and Rods: The Role of the Balance Laws. Interaction of Mechanics and Mathematics. Springer International Publishing, New York, 2017.

[48] D. K. Pai. STRANDS: Interactive simulation of thin solids using Cosserat models. Computer Graphics Forum, 21(3):347–352, 2002.

[49] C. Paul. Morphological computation: A basis for the analysis of morphology and control requirements. Robotics and Autonomous Systems, 54(8):619–630, 2006.

[50] A. Pressley. Elementary Differential Geometry. Springer Undergraduate Mathematics Series. Springer-Verlag London, Ltd., London, second edition, 2010.

[51] M. B. Rubin. Cosserat Theories: Shells, Rods, and Points. Kluwer Academic Press, Dordrecht, 2000.

[52] D. Rus and M. T. Tolley. Design, fabrication and control of soft robots. Nature, 521(7553):467, 2015.

[53] S. Seelecke and I. Muller. Shape memory alloy actuators in smart structures: Modeling and simulation. Applied Mechanics Reviews, 57(1):23–46, 2004.

[54] S. Seok, C. D. Onal, K.-J. Cho, R. J. Wood, D. Rus, and S. Kim. Meshworm: a peristaltic soft robot with antagonistic nickel titanium coil actuators. IEEE/ASME Transactions on mechatronics, 18(5):1485–1497, 2013.

[55] M. D. Shuster. A survey of attitude representations. American Astronautical Society. Journal of the Astronautical Sciences, 41(4):439–517, 1993.

[56] J. C. Simo and L. Vu-Quoc. On the dynamics in space of rods undergoing large motions - a geometrically exact approach. Computer Methods in Applied Mechanics and Engineering, 66(2):125–161, 1988.

[57] J. L. Synge and B. A. Griffith. Principles of Mechanics. McGraw-Hill, New York, third edition, 1959.

[58] J. L. Synge and A. Schild. Tensor Calculus. University of Toronto Press, Toronto, 1949.

[59] W. Thomson and P. G. Tait. Treatise on Natural Philosophy. Oxford University Press, Oxford, 1867.

[60] I. Todhunter. Spherical Trigonometry: For the Use of Colleges and Schools. Macmillan & Co., London, U. K., 1886.

[61] B. A. Trimmer and J. Issberner. Kinematics of soft-bodied, legged locomotion in *manduca sexta* larvae. The Biological Bulletin, 212(2):130–142, 2007.

[62] D. Trivedi, C. D. Rahn, W. M. Kier, and I. D. Walker. Soft robotics: Biological inspiration, state of the art, and future research. Applied Bionics and Biomechanics, 5(3):99–117, 2008.

[63] N. Umetani, R. Schmidt, and J. Stam. Position-based elastic rods. In Proceedings of the ACM SIGGRAPH/Eurographics Symposium on Computer Animation, pages 21–30. Eurographics Association, 2014.

[64] E. Vouga. Personal communication by email, November 2016.

[65] X. Zhou, C. Majidi, and O. M. O'Reilly. Energy efficiency in friction-based locomotion mechanisms for soft and hard robots: slower can be faster. Nonlinear Dynamics, 78(4):2811–2821, 2014.

[66] V. F. Zhuravlev. The solid angle theorem in rigid body dynamics. Journal of Applied Mathematics and Mechanics (PMM), 60(2):319–322, 1996.